Molecular dynamics free energy simulations of ATP:Mg^{2+} and ADP:Mg^{2+} using the polarizable force field AMOEBA.

Brandon Walker, Zhifeng Jing, Pengyu Ren

Department of Biomedical Engineering at The University of Texas at Austin, Austin, Texas 78712, United States

* Corresponding Author: E-mail: pren@mail.utexas.edu. Phone: (512) 232-1832.

Abstract

ATPases and GTPases are two important classes of protein that play critical roles in energy transduction, cellular signaling, gene regulation and catalysis. These proteins use cofactors such as nucleoside di and tri-phosphates (NTP, NDP) and can detect the difference between NDP and NTP which then induce different protein conformations. Mechanisms that drive proteins into the NTP or NDP conformation may depend on factors such as ligand structure and how Mg^{2+} coordinates with the ligand, amino acids in the pocket and water molecules. Here, we have used the advanced electrostatic and polarizable force field AMOEBA and molecular dynamics free energy simulations (MDFE) to examine the various binding mechanisms of ATP:Mg^{2+} and ADP:Mg^{2+}.We compared the ATP:Mg^{2+} binding with previous studies using non-polarizable force fields and experimental data on the binding affinity. It was found that the total free energy of binding for ATP:Mg^{2+} (-7.00 $\pm$ 2.13 kcal/mol) is in good agreement with experimental values (-8.6 $\pm$ .2 kcal/mol)[1]. In addition, parameters for relevant protonation states of ATP, ADP, GTP and GDP have been derived. These parameters will allow for researchers to investigate biochemical phenomena involving NTP's and NDP's with greater accuracy than previous studies involving non-polarizable force fields.

Keywords
AMOEBA, ATP, ADP, GTP, GDP, Mg, Free Energy Simulations

Introduction

Essential biochemical processes such as energy transduction, cellular signaling, gene regulation and catalysis rely on nucleotide ligand induced conformational changes to control the active states of protein populations. Changing nucleotides in protein active binding sites induces conformational conversion arising from alterations in electrostatic interactions of the protein system with the new or absent phosphate group. Additionally, different intra-ligand binding modes between the phosphate chain and Mg^{2+} are expected to play an important role in driving protein conformational changes. More specifically, interactions between the nucleotide's phosphate chain and Mg^{2+} can be different for a single nucleotide: Mg^{2+} system (**Figure 1** top panel) and between different nucleotides in the unbound protein:nucleotide:Mg^{2+} state (**Figure 1** bottom panel) and various possible bound protein:nucleotide:Mg^{2+} states[2-8]. Moreover, the terminal phosphates have two relevant protonation states, where interactions with Mg^{2+} will tend to prefer the deprotonated terminal phosphate oxygens[9]. This begs the question of how Mg^{2+} ions

prefer to bind in these systems. Previous studies investigating these issues have tended to focus on the differences between NDP and NTP using alchemical MDFE simulations, usually with non-polarizable force fields[2, 10-13] . However, many studies on bound and unbound protein conformations with non-polarizable force fields are expected to rely heavily on error cancelation, which may not work for all properties[14].

Insert Figure 1

To understand the specific binding of ATP:Mg^{2+} , ADP:Mg^{2+} and their dependence on Mg^{2+} coordination, MDFE simulations are the ideal tool and have previously been applied to similar systems[1, 7, 15]. However, the validity of resulting free energies depends on the quality of the force field model, the parameters used, as well as adequate sampling. ATP:Mg^{2+} and ADP:Mg^{2+} are both highly charged systems that require rigorous treatment of electrostatic polarizability. It has been previously shown that accurate modeling of charged systems is important for precisely computing thermodynamic quantities such as binding free energy or binding affinity[16-32] . The AMOEBA force field has consistently been shown to improve upon electrostatics vs. its non-polarizable force field counterparts, thus AMOEBA is the ideal choice of force field for this study.

Besides using an accurate force field model that captures the relevant physics and parameters, adequate sampling including identification of the most relevant binding mode conformations is critical for correctly computing the free energy of binding. Binding mode conformations can consist of the ligand conformation, ion position relative to ligand and any coordinating waters. Here we assume that multiple Mg^{2+} ion binding to NTP/NDP occurs much less frequently than single Mg^{2+} binding. In NTP, a Mg^{2+} ion can be coordinated by one, two or three phosphate groups at a time. Additionally, the oxygens on each phosphate group may coordinate with Mg^{2+} in a monodentate, bidentate or tridentate fashion. The γ phosphate for ATP^{-4}:Mg^{2+} or β phosphate for ADP^{-3}:Mg^{2+}can form a tridentate binding mode. There also exist ligand conformations with the phosphate chain wrapped around the Mg^{2+} to bind in a tridentate manner.

A PDB survey has found bidentate modes between two oxygens on different phosphates to be most common and about a third of structures found coordinate only one oxygen from a single phosphate group[14]. The PDB survey used a coordination sphere of 3 angstroms to define coordination type. Only one of the dominant ATP binding modes in this study was bidentate for 13% of the trajectory. It is noted however, that there will be differences in ATP:Mg^{2+} conformations in protein pockets vs bulk solution due to steric clashes and electrostatic forces exerted by protein pocket.

Thomas Simonson and Priyadarshi Satpati explored the differences between direct or Inner Sphere Mg^{2+} coordination by one or more oxygens from phosphate groups (example **Fig 1**) and indirect, Outer Sphere coordination involving one or more bridging waters between the phosphate group(s) and Mg^{2+}, using a fixed charge force field and thermodynamic integration to alchemically transform binding modes. The GTP:Mg^{2+} complex was shown to be predominately IS[1], hence we do not need to include contributions from OS binding modes for the computing binding free energy. **Table 1** shows experimental data on five experimental techniques that are

more or less sensitive to OS binding modes depending on experimental methodology, which provides a benchmark for our MDFE computations.

Insert Table 1

In this work, we use the advanced electrostatic and polarizable force field AMOEBA and the double decoupling method[33] to examine the various binding modes of ATP^{-4}:Mg^{2+}, ATP^{-3}:Mg^{2+}, ADP^{-3}:Mg^{2+}, ADP^{-2}:Mg^{2+}. We first parameterized the molecules, then identified possible binding modes and ran MDFE simulations for each binding mode and protonation states, and then computed the binding free energy by combining the results of all binding mode.

Results

Binding modes of ATP:Mg^{2+}, ADP:Mg^{2+}

First, we explore the potential binding sites of Mg^{2+} around ATP and ADP phosphate chains. Mg^{2+} was placed systematically at sites near the oxygen atoms within the ATP, ADP phosphate chain and initially using harmonic spring restraints. Binding modes were named according to the where they cluster during production dynamics simulations with no restraints in **Fig. S2** and **S3** using nomenclature seen in **Fig 2.** Dominant binding modes (lowest ΔG) are depicted in **Fig 3**. After equilibrating and MDFE simulations, a long simulation was used to characterize each binding mode. Where a mode is characterized with images such as **Figure 3**. 100 evenly spaced frames were sampled from the simulated trajectory with the phosphate chains superposed to show where Mg^{2+} prefers to bind along the chain. This of course assumes we have sampled all relevant areas and have found the most dominant mode for each ATP, ADP species. By observing all binding modes in **Fig. S2, S3** qualitatively, it can be seen that although each simulation starts with a different spring configuration and hence different free energy path, each molecule essentially has only one binding mode shown by where the Mg^{2+} tends to cluster without restraints.

A more quantitative approach for characterizing the binding modes is to count the frequency of all atoms to be within a certain distance (3 Å) of Mg^{2+} over the MD trajectory. Additionally, the minimum, mean, maximum and standard deviation of distance for nearby atoms (defined by any atom close enough to be within the coordination sphere for at least one snapshot of the trajectory) are reported in **Table 2**. The mean distances for most modes tend to be around 2 Å and are overwhelmingly monodentate (single atom in Atom column), where there is a case of bidentate and tridentate that occur for < 15% of corresponding trajectories. Additionally, the radial distribution function was computed between Mg^{2+} and oxygen in water and shown for the dominant binding modes in **Fig. 4** (**Fig. S4** for all modes). All RDF's behave roughly the same with the first shell lying around 2 Å and a second shell at about 4 Å. All of the binding modes have an average first-shell water number of about 5, except for $ADP^{-3}_{OP^{\alpha},3}$ which has 6.0. For

comparison, the expected first shell water number for Mg^{2+} and oxygen in water in bulk water is 6.00. So typically about one water molecule is lost between aqueous Mg^{2+} and ATP/ADP-bound Mg^{2+}. Additionally, **Table S1** shows average first-shell water number vs. binding free energy and enthalpy for each binding mode. RDFs between water oxygen and the oxygen on ATP that coordinates with and without Mg^{2+} are computed as well as first shell waters (**Fig. S5, S6**, **Table S2, S3**). Without Mg^{2+} bound, these phosphate oxygen atoms on average coordinate between 2.5-3.6 water molecules in the first shell. With Mg^{2+} coordinated there is between 3.5-5.6 water molecules in the first shell. ATP/ADP oxygen gains about one water molecule when coordinating Mg^{2+}. The increase in first-shell water molecules is due to the strong interaction between water oxygen and Mg^{2+}. No correlation is found between the hydration structure of ATP/ADP:Mg^{2+} and binding free energies or enthalpies. However, there is apparent correlation between the hydration of unbound ATP/ADP and the binding free energy. The oxygen atoms with few first-shell water molecules have stronger binding free energy, possibly because of the smaller solvation penalty.

Insert Figure 2

Insert Figure 3

Insert Table 2

Insert Figure 3

Binding thermodynamics

We found the total binding free energy for binding modes of ATP^{-4}:Mg^{2+} to be -7.20 $\pm$ 1.78 kcal/mol, where we use **Eq. 6** and **7** to combine individual binding mode free energy and errors. Considering all ATP^{-4}:Mg^{2+} binding modes and the single ATP^{-3}:Mg^{2+} binding mode, the total binding energy of ATP:Mg^{2+} is 7.00 $\pm$ 2.13 kcal/mol. The ATP^{-3}:Mg^{2+} binding mode did not contribute much to the total free energy since it is much less favorable than for ATP^{-4}:Mg^{2+}. For ADP^{-3}: Mg^{2+} we found the total binding free energy combining all modes to be -2.94 kcal/mol. Combining with the single ADP^{-2}: Mg^{2+} binding mode gives -3.09 $\pm$ 1.78 kcal/mol. **Tables 2** and **3** show the binding free energy ΔG for various modes that were tested. The total binding free energy for ATP:Mg^{2+} was within statistical error of the total experimental binding free energy. For ADP:Mg^{2+}, however, the simulation result is significantly different from the experimental target of -6.5$\pm$ .2 kcal/mol. This could be due to insufficient sampling of the ADP phosphate chain or issues involving parameterization.

Insert Table 3

We further examined the enthalpic and entropic contributions to the binding free energy for each binding mode**.** The typical error in ΔH^{bind} and $T\Delta S^{bind}$ is about ~40-45$\frac{kcal}{mol}$ respectively. **Table 4** tabulates the results for ΔH^{bind} and $T\Delta S^{bind}$, which is also summarized in **Figures 5** and **6**. All binding modes have a favorable enthalpic ΔH^{bind} and an unfavorable $T\Delta S^{bind}$ which agrees with

intuition. As Mg^{2+} changes from unbound to bound, it gains more favorable and negative interactions with ATP, ADP. Additionally, the phosphate chain will have less degrees of freedom to move when in bound vs unbound state, explaining the unfavorable $T\Delta S^{bind}$ for all modes. For Mg^{2+} binding to ATP/ADP there is an apparent enthalpy-entropy compensation, i.e. a larger ΔH^{bmd} such as in $ATP^{-4}_{OP^{\alpha}OP^{\gamma},2}$ and $ADP^{-3}_{OP^{\alpha},1}$ is accompanied by larger $T\Delta S^{bind}$. This can be explained by stronger interactions between ATP, ADP and Mg^{2+} causing the phosphate in that region to become more rigid and hence a larger magnitude of $T\Delta S^{bind}$.

Insert Table 4

Insert Figure 5

Insert Figure 6

Effect of Neutralizing Ligand System

When computing electrostatics via Ewald under PBC the energy per box becomes infinite except for an electrically neutral system. So conventionally a neutralizing charge density is added that is spread uniformly over the periodic box. For a single charge q, inserted into a neutral periodic box, a charge density of $\frac{-q}{V}$ is added to the box, where V is the box volume. The charge q will experience a potential shift $\phi' = \phi - \bar{\phi}$. Where $\phi(\vec{r})$is a function of all coordinates and $\bar{\phi}$ is the spatial average over all coordinates. Additionally, there is a smaller secondary effect due to polarization being constrained to be periodic at all times. Both of these effects change the electrostatic potential ϕ and hence can affect estimates for ΔG^{bind}. In the simplest case of a spherical ion centralized in a large finite box, an expression has been derived previously in **Eq. 1.** [35]

Thomas Simonson & Benoît Roux[35] reviewed several systems and analyze their free energy corrections. In Mg^{2+} phosphate binding, a simulation box length of 25Å was used and a correction of 1.22 kcal/mol was computed via **Eq. 1**, where the leading term due to Ewald correction for solvation is -.96 kcal/mol and the second term due to reaction field PBC artifacts is -.26 kcal/mol. The complexation corrections canceled out due to the end states being 1 and -1 respectively.

In order to quantify the effect of including $2Cl^-$ in our ligand we ran 4ns of MDFE simulations with and without $2Cl^-$ in our ligand and tabulated the results in **Table 5**. For comparison we also used **Eq. 1** to compute the analytical correction. Using the formula in **Eq. 1** to correct for solvation and complexation end states, we obtain a correction value of ΔG=-1.35 kcal/mol, which would give $ATP^{-4}_{OP^{\alpha}P^{\gamma},2}$ **:**Mg^{2+} a value of -6.27 $\pm$ 0.31 kcal/mol, assuming no uncertainty in ϵ_W . This correction gives a value closer to the result with $2Cl^-$ -6.46 kcal/mol.

Insert Table 5

$$\Delta G(L \to \infty) - \Delta G(L) = \frac{1}{4\pi\epsilon_0}\frac{q^2|\xi|}{2\epsilon_W L} + \frac{1}{4\pi\epsilon_0}\frac{2\pi q^2 R^2}{3L^3}\frac{\epsilon_W - 1}{\epsilon_W} + O(R^2 L^{-3}\,\epsilon_W{}^{-3}) \qquad \textbf{Eq. 1}$$

where $|\xi| = 2.837297$, $\epsilon_W = 80$, q is the integer charge, L is the box length and R is the Van der Waals radius over which the spherically symmetric charge is distributed. For Mg^{2+} we use R=1.2Å [36].

NTP, NDP Conformation

To characterize ATP and ADP conformation, we constructed a free energy map (**Fig 2**) of the most important backbone phosphate chain dihedral angles (**Fig. 7**) and dihedral angles characterizing the phosphate chain relative to the sugar and base, and the base relative to the sugar on a 12x12 grid of 30° bins (**Fig. 8**), where the trajectories used for analysis were taken from gas phase to prevent Mg^{2+} from biasing the conformational flexibility. A value of 0 on the free energy map indicates that the corresponding dihedral angle pair was not observed in the trajectory. As can be seen from the top panel of **Fig. 8**, the ADP^{-3} phosphate chain seems to be much more flexible then ATP^{-4}. A study done on ATP conformation in bulk solution and PDB used a free energy plot of χ and γ to compare PDB statistics to data obtained from simulations using the GROMACS force field[35]. The study did capture the PDB hot spot (χ, γ) = (-170:-90:,40:70) or (190:270,40:70) in their simulated free energy plot, our plot is also able to capture this hot spot. However, we should not expect the PDB plot and simulated plots to be exactly the same due to differences in the chemical environment between bulk solution and protein pockets. Our simulated free energy plot did not capture the hot spots from the previous study's simulated plot, due to differences in force field model and parameters between AMOEBA and GROMACS. The study also found C2′ exo and C2′ endo sugar puckering conformations was highly dominated in water (using GROMACS) followed by O4′ endo[35]. In the PDB survey they found C2′ exo and C2′ endo to be populated roughly the same but O4′ endo to be less populated. In this study we observed C3'endo, C4'exo and C2'exo to be the most frequent conformations (see **Sugar Puckering** in **SI**).

Insert Figure 7

Insert Figure 8

Conclusion

Although we began simulations with Mg^{2+} in many different configurations, each molecule has only one binding mode depicted by where Mg^{2+} tends to cluster without restraints. The calculated ATP:Mg^{2+} binding free energy (-7.00 $\pm$ 2.13) kcal/mol is within statistical error to the experimental target of -8.6 $\pm$ .2 kcal/mol, so we expect that all ATP^{-4}: Mg^{2+}, ATP^{-3}: Mg^{2+}, GTP^{-4}:Mg^{2+}, GTP^{-3}:Mg^{2+} parameters are sufficiently able to model the correct electrostatics and give reasonable results for the binding free energy since they used the same valence and Van der Waals parameters for the phosphate chains. The binding free energy results for ADP:Mg^{2+} (-3.09

$\pm$ 1.78) was not within statistical error of the experimental target of -6.5$\pm$ .2 kcal/mol. This either indicates an underlying issue with the AMOEBA model, parameters or a sampling problem. Since AMOEBA is able to reproduce ATP experimental free energy results, it is more likely to be a parameterization or sampling problem.

There is an apparent enthalpy-entropy compensation because of stronger binding mode interactions (greater binding enthalpy) causing the phosphate chain in the binding region to lose degrees of freedom and hence have a greater binding entropy as a result.

Free energy corrections due to Ewald corrections have significant effects and we compared ΔG^{bind} to $ATP^{-4}_{OP\alpha OP\gamma,2}$:$Mg^{2+}$,$ATP^{-4}_{OP\alpha P\gamma,2}$**:**$Mg^{2+}2Cl^-$ where one had 2Cl^- included in the system to keep the total charge of the periodic system 0 for all perturbations, and another with a net charge for all perturbations. We observed a large correction of -1.346 kcal/mol for the system with net charge, bringing the ΔG^{bind} without 2Cl^- (-4.92 $\pm$.31 kcal/mol) to a value of -6.266 $\pm$ 0.31, which is very similar to the results of the neutral system -6.46 $\pm$.54 kcal/mol. Future studies can always include extra ions in such binding reactions to avoid needing such corrections.

According to our free energy plots the ADP^{-3} phosphate chain seems to be much more flexible then ATP^{-4}. Our plot is also able to capture a PDB hot spot of ATP for the χ and γ dihedral angles. However, we did not capture the hot spots from the previous study's simulated plot, due to differences in force field model and parameters between AMOEBA and GROMACS. The study also found C2′ exo and C2′ endo sugar puckering conformations was highly dominated in water (using GROMACS) followed by O4′ endo[35]. In the PDB survey they found C2′ exo and C2′ endo to be populated roughly the same but O4′ endo to be less populated. In this study we observed C3'endo, C4'exo and C2'exo to be the most frequent conformations.

Computational Methods

Parametrization

Ab initio quantum mechanics calculations (QM) were performed using Gaussian 09. All molecular mechanics (MM) force field-based calculations were performed using TINKER 8 Software[37].

Valence

First the sugar and base valence parameters for GTP, GDP, ATP and ADP were taken from previously derived nucleic acid parameters[38]. Next torsion parameters for the various phosphate chain model compounds, were derived by using the automatic parametrization software POLTYPE program[39] (**Fig S8**). Torsional parameters for various phosphate chain model structures were optimized at MP2/cc-pVTZ level and the single point energy was calculated at the MP2/6-311++G(2d,2p) level, see Torsion Parametrization in SI. The molecular mechanics energy was fit to reproduce the QM conformational energy profile. Then optimized Van der Waals parameters were then obtained by probing specific oxygen types using ATP^{-3} water-model compound dimers to reproduce the QM energy vs distance profile (see Van der Waal Parameterization SI) at an

MP2/6-311++G** level of theory with Gaussian counterpoise, this enables the intermolecular energy to be computed. The valence parameter transfer scheme between fragments and parent molecules are depicted in (**Fig S9**).

Electrostatics

Since it is known from PDB surveys and MD simulations of bulk solution that phosphate chains on systems like ATP tend to be extended[35], restraints were used during initial QM optimization of the whole NTP/NDP molecules to prevent the chain from interacting with the sugar or base too closely during gas phase optimization. Atomic multipole moments were initially assigned from QM electron density calculated at the MP2/6-311G** level via Stone's distributed multipole analysis [39]. After transferring the model compound parameters and sugar/base parameters to each whole molecule (ATP^{-4}, ATP^{-3}, ADP^{-3}, ADP^{-2}, GTP^{-4}, GTP^{-3}, GDP^{-3}, GDP^{-2} **Fig. S9**) the electrostatic optimizations were done with Tinker's POTENTIAL program to fit electrostatic potentials around all molecules, where only the phosphate chain and the neighboring CH2 were allowed to optimize dipoles and quadrupoles. AMOEBA's polarization scheme and how polarizable groups are defined are described in detail in a previous paper describing the POLTYPE protocol [39].

It is noted that in the case of the deprotonated terminal phosphate, which is expected to be dominant over the protonated form[34], there may be issues in accurately computing the free energy from QM. Priyadarshi Satpati and coworkers used various water configurations around Mg^{2+} and phosphate to compute the ΔG_{bind} of Mg^{2+}:phosphate complex via a solvent continuum model, normal mode analysis and using B3LYP-D/aug-cc-pVDZ level of QM theory. They found that the QM results had a binding free energy of −10.8 kcal/mol, significantly larger than the experimental value of −3.7 kcal/mol [7]. Either the QM level of theory (incorrect electron density), the reaction field approximation of solvent continuum model, normal mode approximation or a combination thereof is causing this error. The normal mode analysis however, is a reasonable approximation for rigid systems like phosphate. For this study, we are only concerned if the QM electron density is not accurate since we do not use normal mode analysis to compute the free energy.

Molecular Dynamics

All molecular dynamics simulations (MD) were run using the Tinker-OpenMM package with a RESPA integrator, Bussi thermostat, Monte Carlo barostat, and 3.0 fs time step with hydrogen-mass repartition on GPUs. The van der Waals (vdW) iterations used a 12.0 Å cutoff, while the electrostatic interactions used PME with a real-space cutoff of 7.0 Å cutoff. An overview of the molecular dynamics scheme is shown in **Fig S21**.

Each binding mode was solvated with $70Å^3$ periodic box and K and Cl ions were added to model the physiological salt concentration [KCl]=100 mM in a cell[39]. Additional ions were added to keep the net charge of the box neutral to eliminate the effects of adding a uniform electrostatic potential everywhere during Ewald computation[40-41]. Initial structure minimization is done to get an initial starting structure for water-water, ligand-water interactions. We used a total 3 ns NVT to equilibrate and then 1 ns of NPT to obtain the average box size. For each binding mode a harmonic spring restraint of 15 kcal/mol was used to initially keep the ion bound where the ideal

distance for the given spring constant was determined from initial gas phase structure. The spring restraint strength was perturbed off during Equilibration according to **Table S6**, in order to allow the Mg^{2+} to relax to where it naturally tends to bind. With the intention of using the double-decoupling method (**Figure 9**), for each perturbation production dynamics simulation we used a total of 10 ns in NVT to ensure adequate sampling within a region of the phosphate chain. The electrostatics was first perturbed to zero and then Van der Waals interactions were perturbed to zero according to the perturbation scheme in **Fig S20** according to **Eq. 2**. BAR is used to compute free energy changes denoted by ΔG between pairs of consecutive lambdas, **Eq. 3**.

Insert Figure 9

$$P_{final} = P_{initial}\lambda \qquad \textbf{Eq. 2}$$

$$\sum_{i=1}^{n_i} \frac{1}{1+e^{ln\frac{n_i}{n_j}+\beta\Delta U_{ij}-\beta\Delta G}} - \sum_{i=1}^{n_j} \frac{1}{1+e^{ln\frac{n_j}{n_i}+\beta\Delta U_{ji}-\beta\Delta G}} = 0 \qquad \textbf{Eq. 3}$$

Free Energy

The absolute Helmholtz binding free energy (ΔG_{bind}) for individual binding modes was calculated via the double decoupling method[33], perturbation schedules are shown in **Fig.S16**. Initial simulations for ATP^{-4} began from the last structure of the equilibrated trajectory with the $2Cl^{-}Mg^{2+}$ as the system. First electrostatics of the system were decoupled from the environment while the Van der Waals interaction strength was held constant, then Van der Waals was decoupled after electrostatic interactions were completely removed according to the perturbation schedules in **Fig. S22**. An ion restraint was also used to keep the ion near its initial position, where the restraint strength was slowly turned on as electrostatics and Van der Waals were decoupled from the system and environment (λ_{res} in **Fig. S22**). In this study total of 22 alchemical states were chosen to ensure a smooth transition between the two ends states. According to the thermodynamic cycle (**Fig. S23**), we can use **Eq. 4** to compute the absolute binding free energy ΔG_{bind}. Due to there being a harmonic restraint when Van der Waals and electrostatics are completely decoupled between the system and the surrounding environment on the right hand side of the cycle, but not the left side, an analytical correction ΔG_{cor} is used to account for the artificial entropy effects of the restraint according to **Eq. 5**[33]

$$\Delta G_{bind} = \Delta G_{comp} - \Delta G_{solv} + \Delta G_{cor} \qquad \textbf{Eq. 4}$$

$$\Delta\, G_{cor} = RTln(C^{\circ}\left(\frac{2\pi RT}{k}\right)^{\frac{3}{2}}) \qquad \textbf{Eq. 5}$$

Due to the time scale of conversion between these various modes being larger than the production MD simulation time we computed a method to combine free energy results for various binding modes and protonation states for a molecule, shown in **Eq. 6** and **7**.

$$\Delta G_{species}^{total} = -RTln\frac{\sum_{i=1}^{i=l} e^{-\frac{\Delta G_i^{p_1}}{RT}} + \sum_{j=p_1+1}^{j=p_f} \omega^j \sum_{i=1}^{i=l} e^{-\frac{\Delta G_i^j}{RT}}}{1+\sum_{j=p_1+1}^{j=p_f} \omega^j} \quad \textbf{Eq. 6}$$

where $\omega^j = \frac{[X^{p_1+c}]}{[X^{p_1}]} = c10^{pH+pK_a^j}$, $c = j - p_1$ for the reaction $[X^{p_1}] + cH^+ \rightarrow [X^{p_1+c}]$

$$\delta\,\Delta G^{total} = \sqrt{\sum_{j=p_1+1}^{j=p_f}(\frac{\partial \Delta G}{\partial \omega^j}\delta\omega^j)^2 + \sum_{j=p_1}^{j=p_f}\sum_{i=1}^{i=l}(\delta\Delta G_i^j)^2} \quad \textbf{Eq. 7}$$

where species refers to ATP or ADP, the ith subscript refers to binding mode and the superscript (j index) indicates the terminal phosphates protonation state see **Total Binding Free Energy** in SI. We obtain $\Delta G_{ATP} = (-7.00 \pm 2.13)$ kcal/mol and $\Delta G_{ADP} = (-3.09 \pm 1.80.)$ kcal/mol . See ***Deriving $\delta\Delta G^{total}$*** for obtaining the error $\delta\Delta G^{total}$.

Acknowledgements

The authors are grateful for support by the Robert A. Welch Foundation (F-1691), National Institutes of Health (R01GM106137 and R01GM114237) and National Science Foundation (CHE-1856173).

References

1. Simonson, T.Satpati, P., Simulating gtp:Mg and gdp:Mg with a simple force field: A structural and thermodynamic analysis. *Journal of Computational Chemistry* **2013,** *34* (10), 836-846.
2. Tewari, Y. B., Goldberg, R. N., & Advani, J. V. (1991). Thermodynamics of the disproportionation of adenosine 5′-diphosphate to adenosine 5′-triphosphate and adenosine 5′-monophosphate. Biophysical Chemistry, 40(3), 263–276. doi: 10.1016/0301-4622(91)80025-m3.
Koch, O.;Cappel, D.;Nocker, M.;Jager, T.;Flohe, L.;Sotriffer, C. A.Selzer, P. M., Molecular dynamics reveal binding mode of glutathionylspermidine by trypanothione synthetase. *Plos One* **2013,** *8* (2).
4. Pfaendtner, J.;Branduardi, D.;Parrinello, M.;Pollard, T. D.Voth, G. A., Nucleotide-dependent conformational states of actin. *Proceedings of the National Academy of Sciences of the United States of America* **2009,** *106* (31), 12723-12728.
5. Yang, W.;Gao, Y. Q.;Cui, Q.;Ma, J.Karplus, M., The missing link between thermodynamics and structure in f1-atpase. *P Natl Acad Sci USA* **2003,** *100* (3), 874-9.
6. Gao, Y. Q.;Yang, W.Karplus, M., A structure-based model for the synthesis and hydrolysis of atp by f-1-atpase. *Cell* **2005,** *123* (2), 195-205.
7. Satpati, P.;Clavaguera, C.;Ohanessian, G.Simonson, T., Free energy simulations of a gtpase: Gtp and gdp binding to archaeal initiation factor 2. *J Phys Chem B* **2011,** *115* (20), 6749-63.
8. Satpati, P.Simonson, T., Conformational selection through electrostatics: Free energy simulations of gtp and gdp binding to archaeal initiation factor 2. *Proteins* **2012,** *80* (5), 1264-82.

9. Bax, B.;Chung, C. W.Edge, C., Getting the chemistry right: Protonation, tautomers and the importance of h atoms in biological chemistry. *Acta Crystallogr D Struct Biol* **2017,** *73* (Pt 2), 131-140.
10. Priess, M.;Goddeke, H.;Groenhof, G.Schafer, L. V., Molecular mechanism of atp hydrolysis in an abc transporter. *Acs Central Sci* **2018,** *4* (10), 1334-1343.
11. Harrison, C. B.Schulten, K., Quantum and classical dynamics simulations of atp hydrolysis in solution. *Journal of Chemical Theory and Computation* **2012,** *8* (7), 2328-2335.
12. Ito, Y.Ikeguchi, M., Mechanism of the alphabeta conformational change in f1-atpase after atp hydrolysis: Free-energy simulations. *Biophys J* **2015,** *108* (1), 85-97.
13. Nam, K.;Pu, J.Karplus, M., Trapping the atp binding state leads to a detailed understanding of the f1-atpase mechanism. *P Natl Acad Sci USA* **2014,** *111* (50), 17851-6.
14. Faver, J. C.;Yang, W.Merz, K. M., Jr., The effects of computational modeling errors on the estimation of statistical mechanical variables. *J Chem Theory Comput* **2012,** *8* (10), 3769-3776.
15. Thompson, D.Simonson, T., Molecular dynamics simulations show that bound mg2+ contributes to amino acid and aminoacyl adenylate binding specificity in aspartyl-trna synthetase through long range electrostatic interactions. *J Biol Chem* **2006,** *281* (33), 23792-803.
16. Savelyev, A.MacKerell, A. D., Competition among li+, na+, k+, and rb+ monovalent ions for DNA in molecular dynamics simulations using the additive charmm36 and drude polarizable force fields. *Journal of Physical Chemistry B* **2015,** *119* (12), 4428-4440.
17. Jiao, D.;Golubkov, P. A.;Darden, T. A.Ren, P., Calculation of protein-ligand binding free energy by using a polarizable potential. *P Natl Acad Sci USA* **2008,** *105* (17), 6290-5.
18. Jiao, D.;Zhang, J. J.;Duke, R. E.;Li, G. H.;Schnieders, M. J.Ren, P. Y., Trypsin-ligand binding free energies from explicit and implicit solvent simulations with polarizable potential. *Journal of Computational Chemistry* **2009,** *30* (11), 1701-1711.
19. Ponder, J. W.;Wu, C. J.;Ren, P. Y.;Pande, V. S.;Chodera, J. D.;Schnieders, M. J.;Haque, I.;Mobley, D. L.;Lambrecht, D. S.;DiStasio, R. A., et al., Current status of the amoeba polarizable force field. *Journal of Physical Chemistry B* **2010,** *114* (8), 2549-2564.
20. Wu, J. C.;Piquemal, J. P.;Chaudret, R.;Reinhardt, P.Ren, P. Y., Polarizable molecular dynamics simulation of zn(ii) in water using the amoeba force field. *Journal of Chemical Theory and Computation* **2010,** *6* (7), 2059-2070.
21. Zhang, J. J.;Yang, W.;Piquemal, J. P.Ren, P. Y., Modeling structural coordination and ligand binding in zinc proteins with a polarizable potential. *Journal of Chemical Theory and Computation* **2012,** *8* (4), 1314-1324.
22. Huang, J.;Lopes, P. E. M.;Roux, B.MacKerell, A. D., Recent advances in polarizable force fields for macromolecules: Microsecond simulations of proteins using the classical drude oscillator model. *Journal of Physical Chemistry Letters* **2014,** *5* (18), 3144-3150.
23. Mu, X. J.;Wang, Q. T.;Wang, L. P.;Fried, S. D.;Piquemal, J. P.;Dalby, K. N.Ren, P. Y., Modeling organochlorine compounds and the sigma-hole effect using a polarizable multipole force field. *Journal of Physical Chemistry B* **2014,** *118* (24), 6456-6465.
24. Shi, Y.;Ren, P. Y.;Schnieders, M.Piquemal, J. P., Polarizable force fields for biomolecular modeling. *Rev Comp Ch* **2015,** *28*, 51-86.
25. Bell, D. R.;Qi, R.;Jing, Z.;Xiang, J. Y.;Mejias, C.;Schnieders, M. J.;Ponder, J. W.Ren, P., Calculating binding free energies of host-guest systems using the amoeba polarizable force field. *Phys Chem Chem Phys* **2016,** *18* (44), 30261-30269.

26. Harger, M.;Li, D.;Wang, Z.;Dalby, K.;Lagardere, L.;Piquemal, J. P.;Ponder, J.Ren, P., Tinker-openmm: Absolute and relative alchemical free energies using amoeba on gpus. *J Comput Chem* **2017,** *38* (23), 2047-2055.
27. Jing, Z. F.;Qi, R.;Liu, C. W.Ren, P. Y., Study of interactions between metal ions and protein model compounds by energy decomposition analyses and the amoeba force field. *Journal of Chemical Physics* **2017,** *147* (16).
28. Mackerell, A. D., Jr., Empirical force fields for biological macromolecules: Overview and issues. *J Comput Chem* **2004,** *25* (13), 1584-604.
29. Patel, S.Brooks, C. L., 3rd, Charmm fluctuating charge force field for proteins: I parameterization and application to bulk organic liquid simulations. *J Comput Chem* **2004,** *25* (1), 1-15.
30. Patel, S.;Mackerell, A. D.Brooks, C. L., Charmm fluctuating charge force field for proteins: Ii - protein/solvent properties from molecular dynamics simulations using a nonadditive electrostatic model. *Journal of Computational Chemistry* **2004,** *25* (12), 1504-1514.
31. Baker, C. M.;Anisimov, V. M.MacKerell, A. D., Development of charmm polarizable force field for nucleic acid bases based on the classical drude oscillator model. *Journal of Physical Chemistry B* **2011,** *115* (3), 580-596.
32. Savelyev, A.MacKerell, A. D., Balancing the interactions of ions, water, and DNA in the drude polarizable force field. *Journal of Physical Chemistry B* **2014,** *118* (24), 6742-6757.
33. Hamelberg, D.McCammon, J. A., Standard free energy of releasing a localized water molecule from the binding pockets of proteins: Double-decoupling method. *Journal of the American Chemical Society* **2004,** *126* (24), 7683-7689.
34. Swartz, M. A.;Tubergen, P. J.;Tatko, C. D.Baker, R. A., Experimental determination of pk(a) values and metal binding for biomolecular compounds using p-31 nmr spectroscopy. *J Chem Educ* **2018,** *95* (1), 182-185.
35. Kobayashi, E.;Yura, K.Nagai, Y., Distinct conformation of atp molecule in solution and on protein. *Biophysics (Nagoya-shi)* **2013,** *9*, 1-12.
36. Simonson, T.Roux, B., Concepts and protocols for electrostatic free energies. *Mol Simulat* **2016,** *42* (13), 1090-1101.
37. Rackers, J. A.;Wang, Z.;Lu, C.;Laury, M. L.;Lagardere, L.;Schnieders, M. J.;Piquemal, J. P.;Ren, P.Ponder, J. W., Tinker 8: Software tools for molecular design. *J Chem Theory Comput* **2018,** *14* (10), 5273-5289.
38. Zhang, C.;Lu, C.;Jing, Z.;Wu, C.;Piquemal, J. P.;Ponder, J. W.Ren, P., Amoeba polarizable atomic multipole force field for nucleic acids. *J Chem Theory Comput* **2018,** *14* (4), 2084-2108.
39. Wu, J. C.;Chattree, G.Ren, P., Automation of amoeba polarizable force field parameterization for small molecules. *Theor Chem Acc* **2012,** *131* (3), 1138.
40. Bogusz, S.;Cheatham, T. E.Brooks, B. R., Removal of pressure and free energy artifacts in charged periodic systems via net charge corrections to the ewald potential. *Journal of Chemical Physics* **1998,** *108* (17), 7070-7084.
41. Lin, Y. L.;Aleksandrov, A.;Simonson, T.Roux, B., An overview of electrostatic free energy computations for solutions and proteins. *J Chem Theory Comput* **2014,** *10* (7), 2690-709.

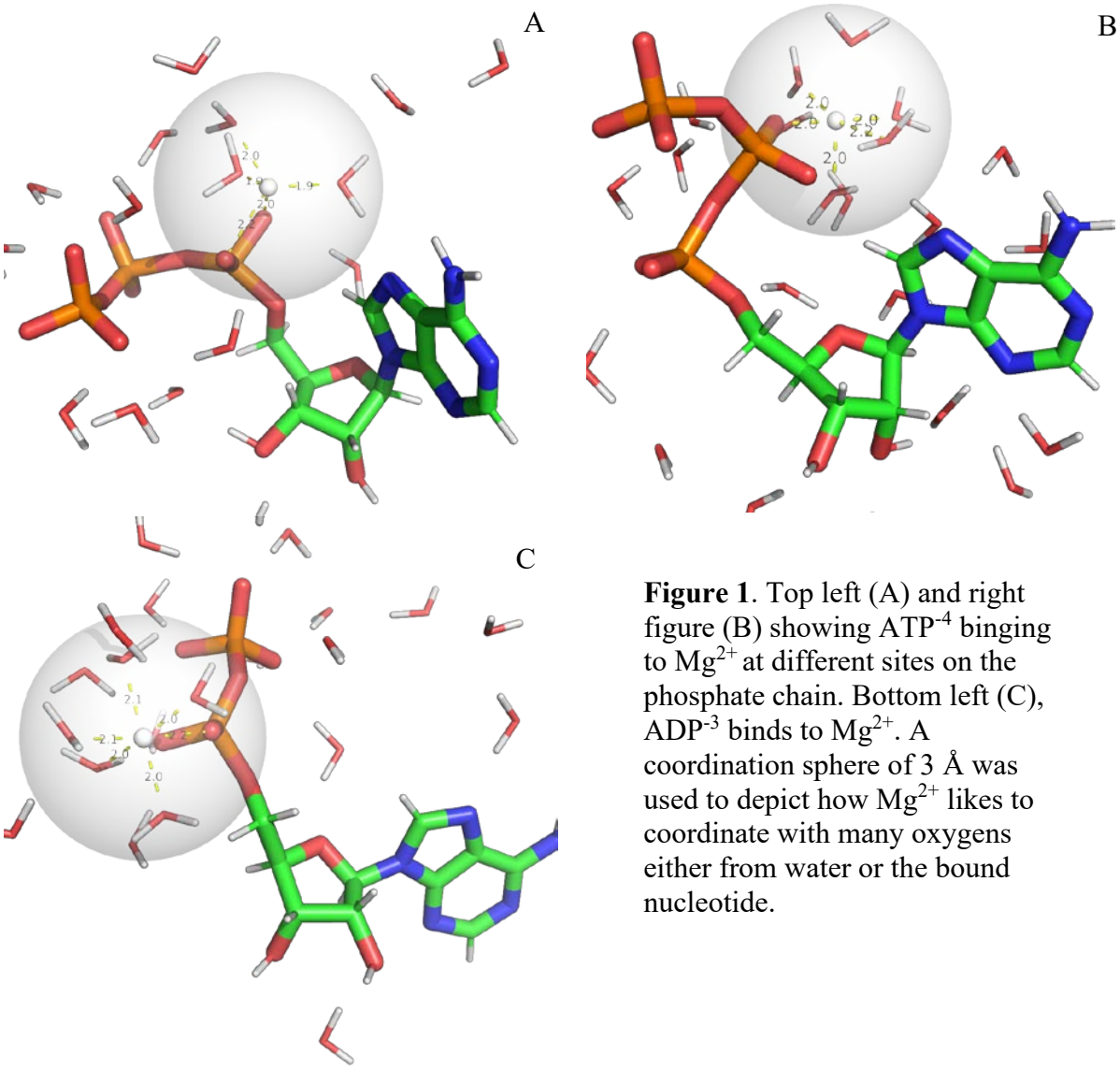

Figure 1. Top left (A) and right figure (B) showing ATP^{-4} binging to Mg^{2+} at different sites on the phosphate chain. Bottom left (C), ADP^{-3} binds to Mg^{2+}. A coordination sphere of 3 Å was used to depict how Mg^{2+} likes to coordinate with many oxygens either from water or the bound nucleotide.

Technique	ΔG_{bind}^{ATP}	ΔG_{bind}^{ADP}
All	-8.6±.2	-6.5±.2
p^{31}	-8.9	-7.3
pH titration	-7.8	-6.2
Resin competition	-8.0	-6.5
Calorimetry	-9.4	-7.3
Spectrophotometry	-9.0	-6.6

Table 1. Binding free energies of Mg^{2+} to ATP and ADP in kcal/mol. Results are summarized by Thomas Simonson and Priyadarshi Satpati[1] and originally compiled by Goldberg and Tewari[2].

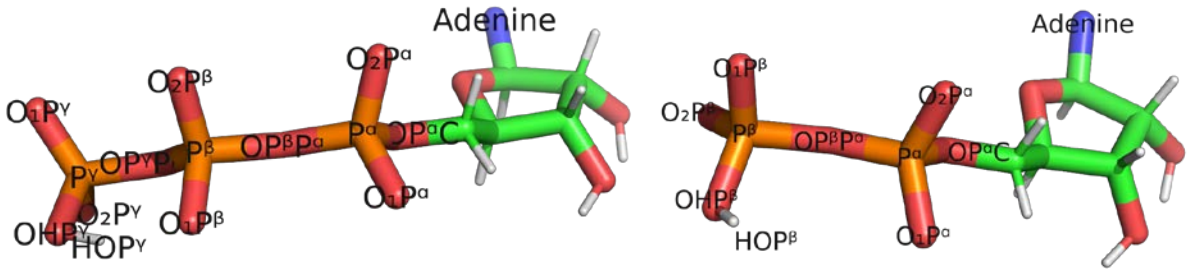

Figure 2. Nomenclature for phosphate chain atoms of ATP, ADP, GTP, GDP. Where the deprotonated terminal phosphate oxygens (not shown above) are denoted OP^{γ} and OP^{β} for NTP and NDP respectively

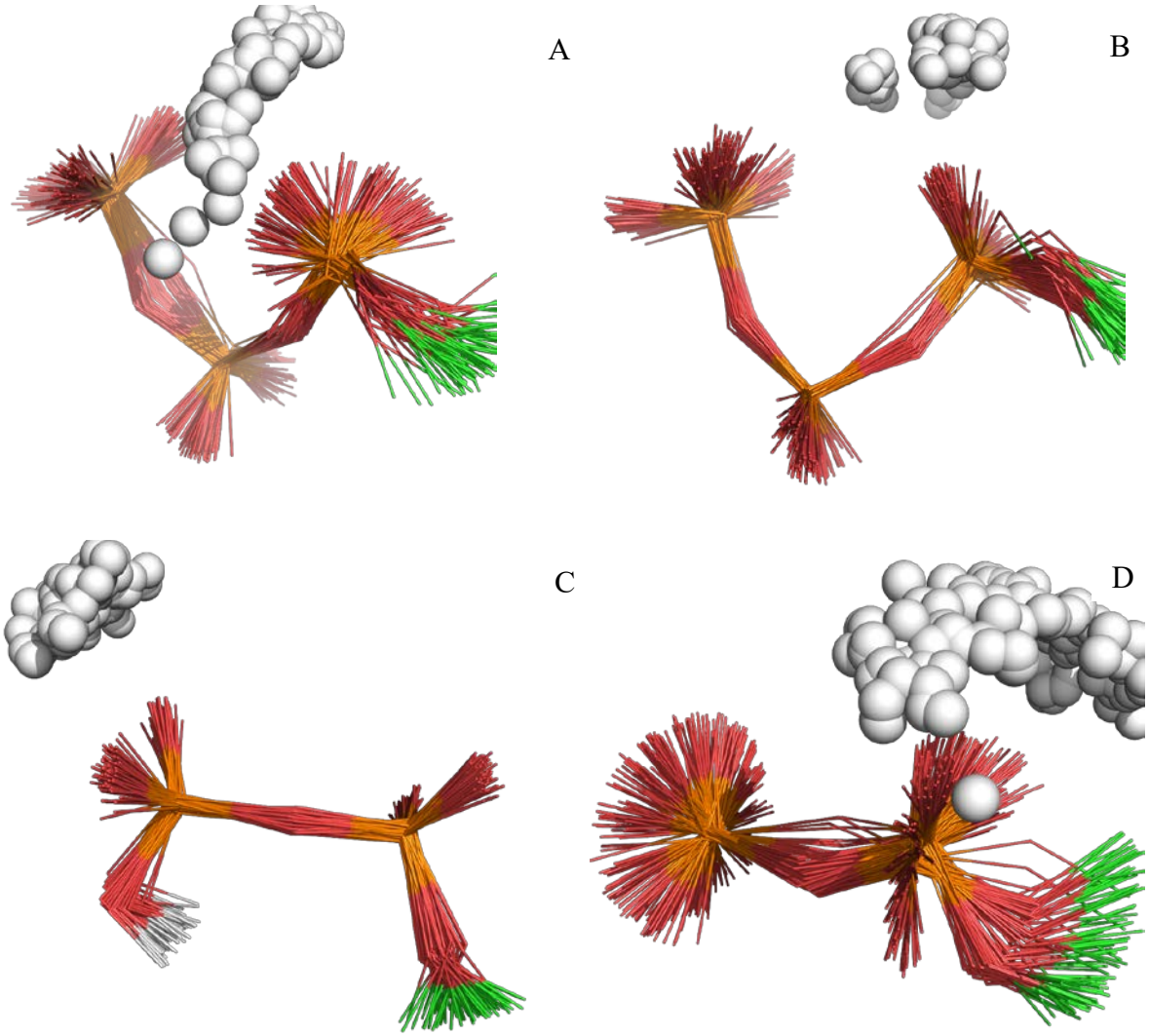

Figure 3. The dominant ATP mode on the top left (A) $ATP^{-4}_{OP^{\alpha}P^{\gamma},1}$ and dominant ADP mode on the bottom left (C) $ADP^{-2}_{OP^{\beta},1}$ is shown with binding free energies of -7.67 and -3.15 kcal/mol respectively. The next most favorable modes are $ATP^{-4}_{OP^{\alpha}P^{\gamma},2}$ top right (B) and $ADP^{-3}_{OP^{\alpha},3}$ on the bottom right (D) with binding free energy of -7.08 and -2.29 kcal/mol respectively.

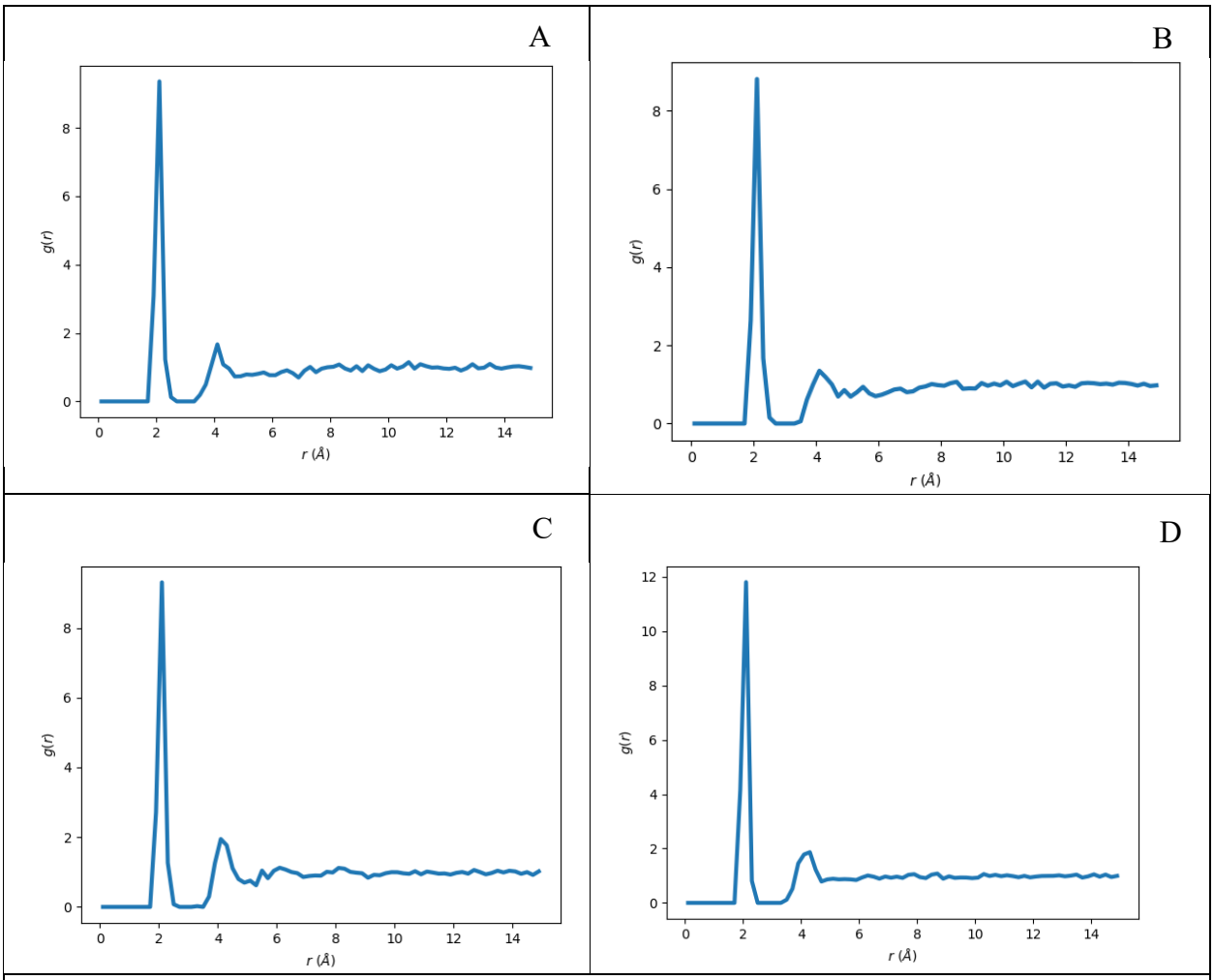

Figure 4. The radial distribution functions for Mg^{2+} and oxygen in water are shown for dominant ATP mode on the top left (A) $ATP^{-4}_{OP^{\alpha}P^{\gamma},1}$ and dominant ADP mode on the bottom left (C) $ADP^{-2}_{OP^{\beta},1}$ is shown. The next most favorable modes are $ATP^{-4}_{OP^{\alpha}P^{\beta},2}$ top right (B) and $ADP^{-3}_{OP^{\alpha},3}$ on the bottom right (D).

Table 2. Statistics for atom-Mg^{2+} distances relevant to each binding mode.

Binding Mode	Atom	% Occurrence	Min	Mean	Max	Std
$ATP^{-4}_{OP^{\alpha}OP^{\gamma},2}$	OP^{γ}	99.94	2.82	3.75	4.9	0.36
$ATP^{-4}_{OP^{\alpha}OP^{\gamma},3}$	O_1P^{α}	86.66	1.82	2.01	2.43	0.07
$ATP^{-4}_{OP^{\alpha}OP^{\gamma},3}$	OP^{γ},O_1P^{α}	13.18	-	-	-	-
$ATP^{-3}_{OP^{\alpha},1}$	O_1P^{α}	99.92	1.89	2.12	2.54	0.09
$ADP^{-3}_{OP^{\alpha},1}$	O_2P^{α}	99.74	1.83	2.04	2.43	0.07
$ADP^{-3}_{OP^{\alpha},2}$	O_2P^{α}	99.52	1.83	2.04	2.4	0.08
$ADP^{-3}_{OP^{\alpha},3}$		99.98				
$ADP^{-2}_{OP^{\beta},1}$	O_2P^{β}	84.8	1.84	2.04	2.63	0.09
$ADP^{-2}_{OP^{\beta},1}$	P^{β},O_2P^{β},O_1P^{β}	14.42	-	-	-	-

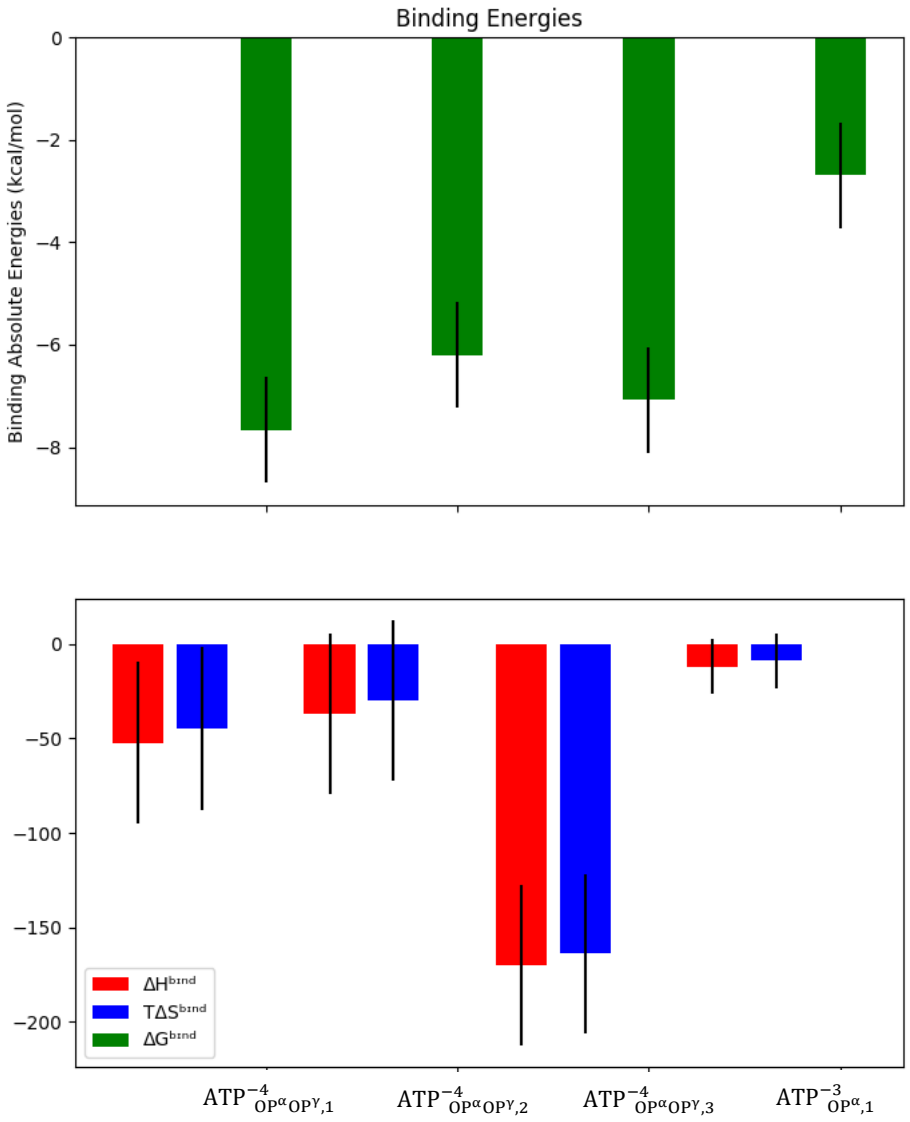

Figure 5. Enthalpy and entropy contributions to ATP:Mg binding free energy. ΔG^{bind} is shown in the top panel, ΔH^{bind} is the first bar on the bottom panel and $T\Delta S^{bind}$ is the second bar on the bottom panel, where each group of bars corresponds to the binding mode labeled on the x-axis.

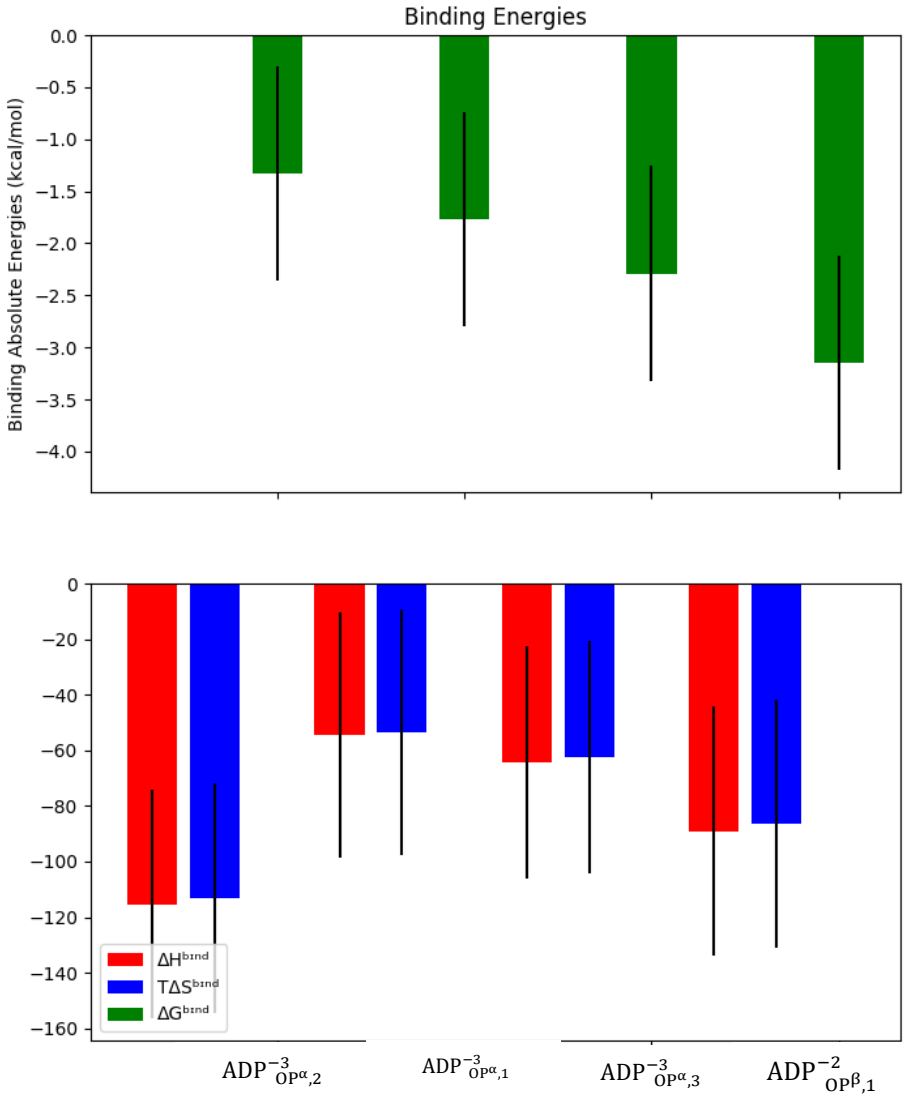

Figure 6. Enthalpy and entropy contributions to ADP:Mg binding free energy. ΔG^{bind} is shown in the top panel, ΔH^{bind} is the first bar on the bottom panel and $T\,\Delta S^{bind}$ is the second bar on the bottom panel, where each group of bars corresponds to the binding mode labeled on the x-axis.

Table 3. Binding free energies of ATP^{-4}:Mg^{2+}, ATP^{-3}:Mg^{2+} , ADP^{-3}: Mg^{2+} and ADP^{-2}: Mg^{2+} in kcal/mol for all binding modes. Using an analytical restraint correction of 1.53 kcal/mol. ΔG^{solv} is the change of solvation free energy, ΔG^{comp} is change of complexation free energy, $\Delta G^{bindcorr}$ is the change of binding free energy and $\delta\Delta G^{bind}$ is the error in ΔG^{bind}.

Name	ΔG^{solv}	ΔG^{comp}	ΔG^{bind}	$\delta\Delta G^{bind}$
$ATP^{-4}_{OP^{\alpha}OP^{\gamma},1}$	-606.42	-614.09	-7.67	1.03
$ATP^{-4}_{OP^{\alpha}OP^{\gamma},2}$	-606.42	-612.63	-6.21	1.03
$ATP^{-4}_{OP^{\alpha}OP^{\gamma},3}$	-606.42	-613.5	-7.08	1.03
$ATP^{-3}_{OP^{\alpha},1}$	-606.42	-608.91	-2.49	1.08
$ADP^{-3}_{OP^{\alpha},1}$	-606.42	-607.75	-1.33	1.03
$ADP^{-3}_{OP^{\alpha},2}$	-606.42	-608.19	-1.77	1.03
$ADP^{-3}_{OP^{\alpha},3}$	-606.42	-608.71	-2.29	1.03
$ADP^{-2}_{OP^{\beta},1}$	-606.42	-609.57	-3.15	1.03

Table 4. Binding enthalpies and entropies of ATP^{-4}:Mg^{2+} , ATP^{-3}:Mg^{2+}, ADP^{-3}:Mg^{2+} and ADP^{-2}:Mg^{2+} in kcal/mol for all binding modes. ΔH^{solv} is the change of solvation free energy, ΔH^{comp} is change of complexation enthalpy, ΔH^{bind} is the change of binding enthalpy and ΔH^{bind} is the error in $\delta\Delta H^{bind}$. ΔS^{solv} is the change of solvation free entropy, ΔS^{comp} is the change of complexation free entropy, ΔS^{bind} is the change of binding free entropy and ΔS^{bind} is the error in $\delta\Delta S^{bind}$.

Name	ΔH^{solv}	ΔH^{comp}	ΔH^{bind}	$\delta\Delta H^{bind}$	$T\Delta S^{solv}$	$T\Delta S^{comp}$	$T\Delta S^{bind}$	$\delta T\Delta S^{bind}$
$ATP^{-4}_{OP^{\alpha}OP^{\gamma},1}$	-542.23	-594.49	-52.26	43.02	65.56	20.86	-44.7	43.02
$ATP^{-4}_{OP^{\alpha}OP^{\gamma},2}$	-542.23	-579.38	-37.15	42.41	65.56	35.76	-29.8	42.41
$ATP^{-4}_{OP^{\alpha}OP^{\gamma},3}$	-542.23	-712.37	-170.14	42.34	65.56	-98.34	-163.9	42.34
$ATP^{-3}_{OP^{\alpha},1}$	-542.23	-554.38	-12.15	14.46	65.56	56.62	-8.94	14.46
$ADP^{-3}_{OP^{\alpha},1}$	-542.23	-657.56	-115.33	41.22	65.56	-47.68	-113.24	41.22
$ADP^{-3}_{OP^{\alpha},2}$	-542.23	-596.69	-54.46	44.03	65.56	11.92	-53.64	44.03
$ADP^{-3}_{OP^{\alpha},3}$	-542.23	-606.63	-64.4	41.74	65.56	2.98	-62.58	41.74
$ADP^{-2}_{OP^{\beta},1}$	-542.23	-631.3	-89.07	44.7	65.56	-20.86	-86.42	44.69

Table 5. Comparison of ΔG^{bind} for mode $ATP^{-4}O_1P^{\alpha}$: with and without $2Cl^-$ in the ligand environment. $\Delta\Delta G^{bind}$ is the relative change of ΔG^{bind} and $\delta\Delta\Delta G^{bind}$ is the error in the relative change.

Name	$\Delta G^{bind}(MD)$	$\Delta G^{bind}(corrected)$	$\delta\Delta G^{bind}$
$ATP^{-4}_{OP^{\alpha}OP^{\gamma},2}$:$Mg^{2+}$	-4.92	-6.27	0.31
$ATP^{-4}_{OP^{\alpha}OP^{\gamma},2}$:$Mg^{2+}2Cl^-$	-6.46	-6.46	0.54

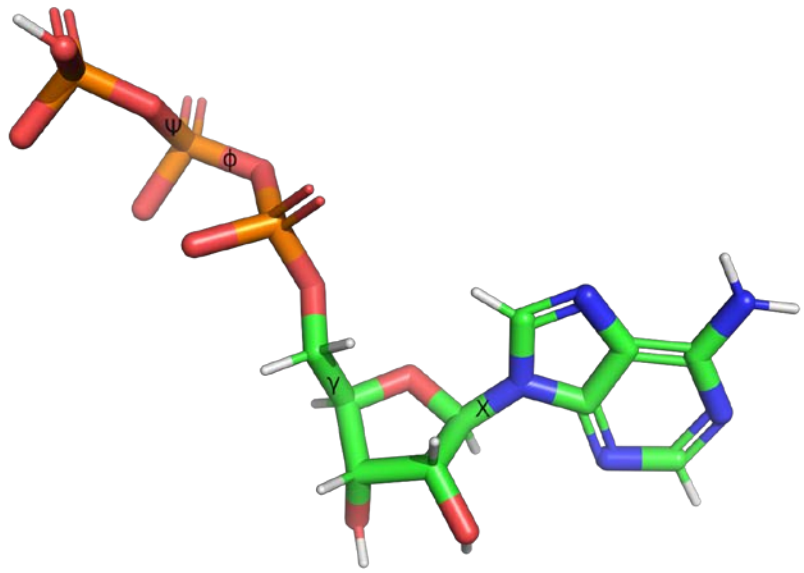

Figure 7. The most important dihedral angles for characterizing NDP/NTP conformation. Two dihedrals alone the backbone of the phosphate chain, ψ, ϕ. The dihedral γ dictates how the phosphate chain is oriented relative to the sugar. Finally, the dihedral χ determines how the base is oriented relative to the sugar.

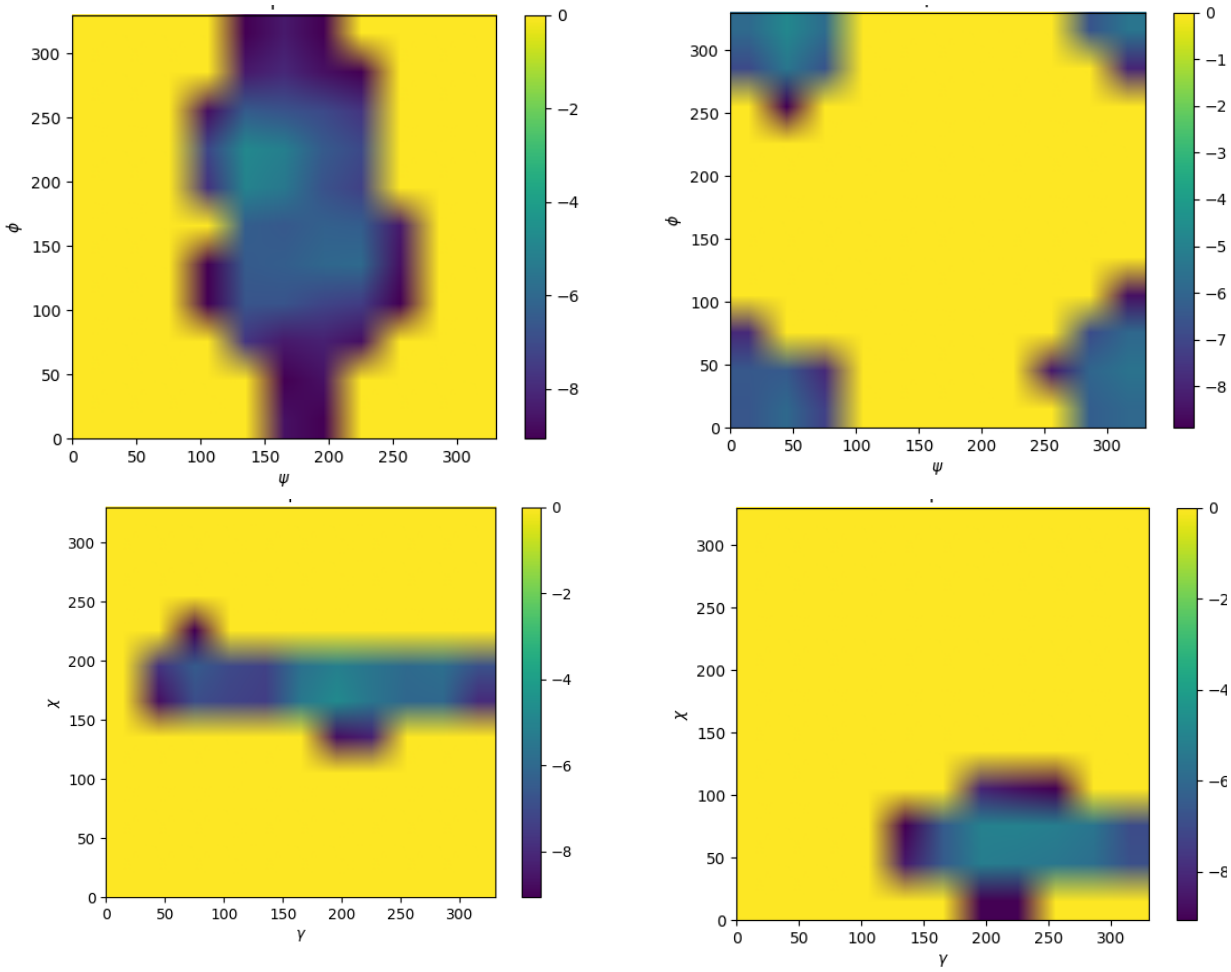

Figure 8. Free energy of backbone dihedral angles ψ, φ , χ and γ for ATP^{-4} and ADP^{-3} in gas phase. Left panel, ADP^{-3} in gas phase, right panel ATP^{-4} in gas phase.

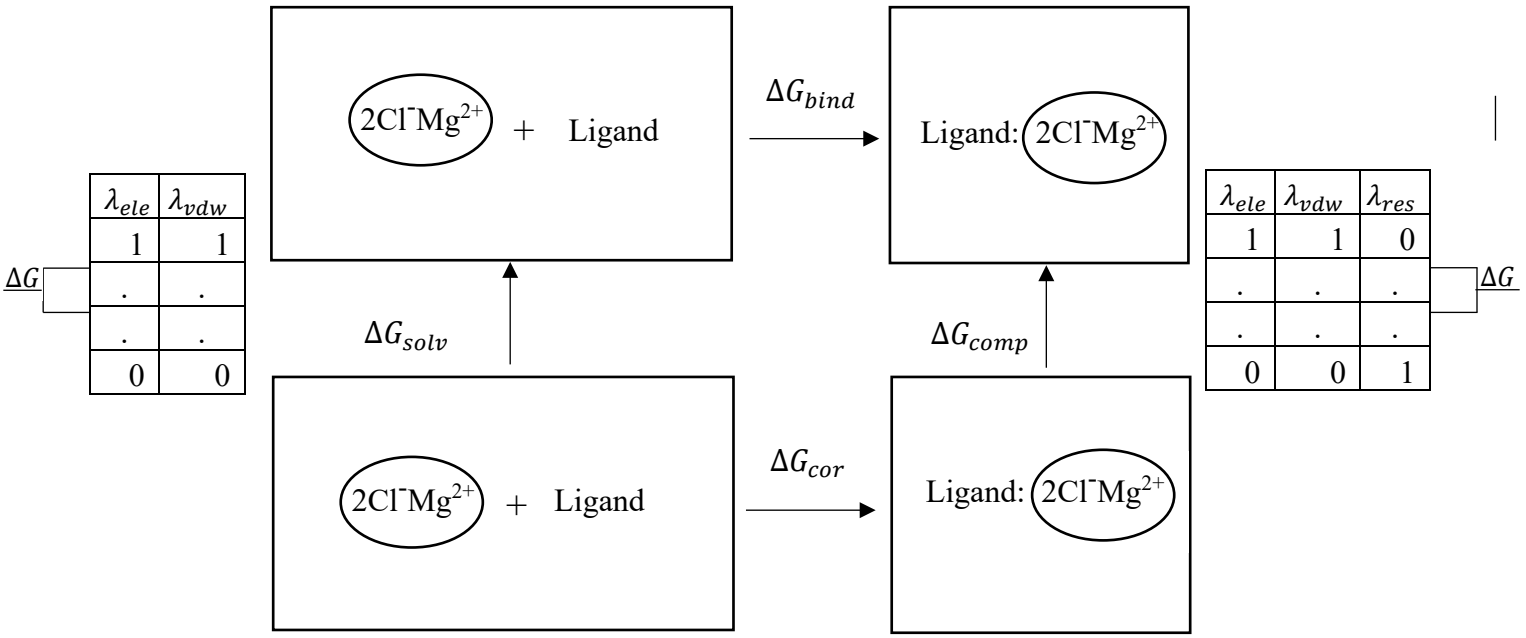

Figure 9. Thermodynamic cycle for calculating the binding free energy ΔG_{bind} for individual modes of ATP^{-4}:Mg^{2+},ATP^{-3}:Mg^{2+},ADP^{-3}: Mg^{2+} and ADP^{-2}: Mg^{2+}. The rectangle represents the periodic box and the oval represents the system, while everything else in the rectangle represents the surrounding environment. The + indicates the species are both free in solution, while the : indicates the bound complex state. The perturbation schedules for electrostatic interactions, Van der Waals interactions and the harmonic spring restraint strength ($\lambda_{ele}, \lambda_{vdw}, \lambda_{res}$) are shown on the left and right (Full schedule **S21**) for computing solvation and complexation free energy respectively (ΔG_{solv} and ΔG_{comp}). Each combination of $\lambda_{ele}, \lambda_{vdw}, \lambda_{res}$ represents an individual dynamic simulation with perturbation lambdas according to equation 1. BAR is used to compute free energy changes denoted by ΔG between pairs of consecutive lambdas (**Eq. 3**).

Supplementary Information for Molecular dynamic free energy simulations of ATP:Mg^{2+} and ADP:Mg^{2+} using the polarizable force field AMOEBA.

Brandon Walker, Zhifeng Jing, Pengyu Ren
Department of Biomedical Engineering, The University of Texas at Austin, Austin, TX, 78712, United
* Corresponding Author: E-mail: pren@mail.utexas.edu. Phone: (512) 232-1832.

Table of Contents

Characterization of Binding Modes

On the left side of figure S2 and S3, initial binding mode structures are shown, where harmonic springs were used between Mg^{2+} and the atoms with distances shown. Harmonic spring restraint perturbation schedules are discussed in the Molecular Dynamics section. On the right-hand side of figure S2 and S3, are figures characterizing the binding location of Mg^{2+} over the course of dynamics simulation. The entire dynamics trajectory at full electrostatics and Van der Waals interaction strength was used to evenly sample 100 frames which were then superposed using Tinkers superpose program (citation). At the end of equilibration (see section), the Mg^{2+} remained relatively close to the initial restrained region of the molecule, however we chose to have a spring restraint strength of zero for this analysis to let the Mg^{2+} explore where it naturally prefers to bind. As a result, many of the initial guesses for where Mg^{2+} should bind are not correct.

Figure S1. See Figure 2 in main text for nomenclature for phosphate chain atoms of ATP, ADP, GTP, GDP.

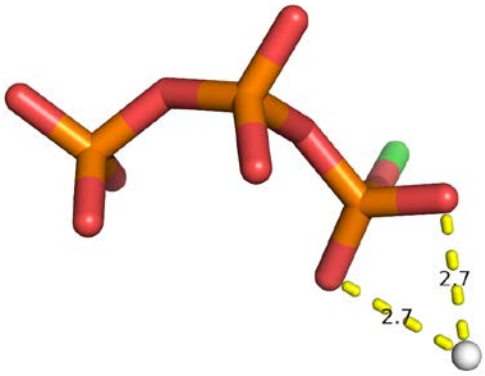

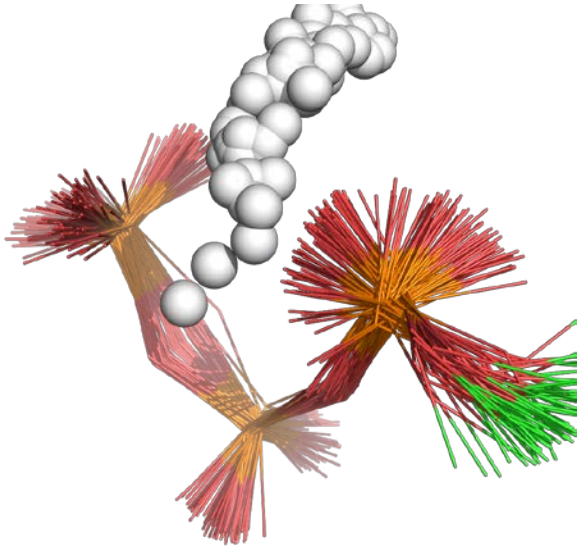

$ATP^{-4}_{OP^{\alpha}OP^{\gamma},1}$

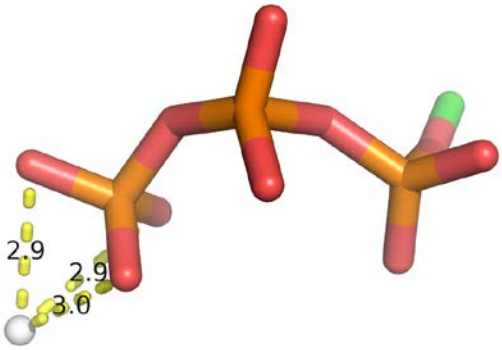

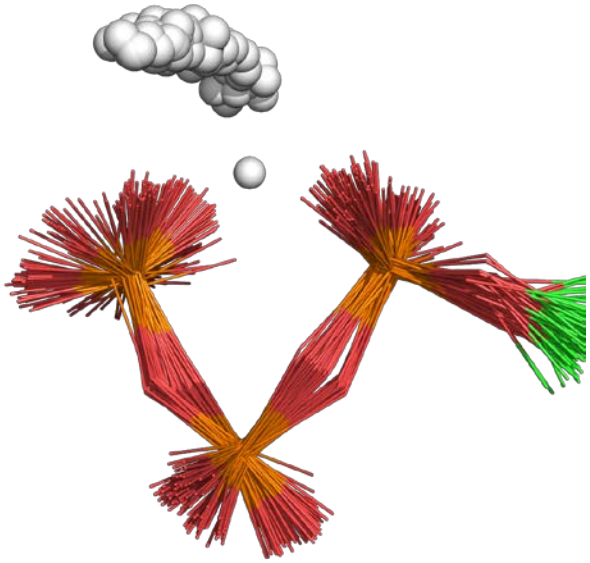

$ATP^{-4}_{OP^{\alpha}OP^{\gamma},2}$

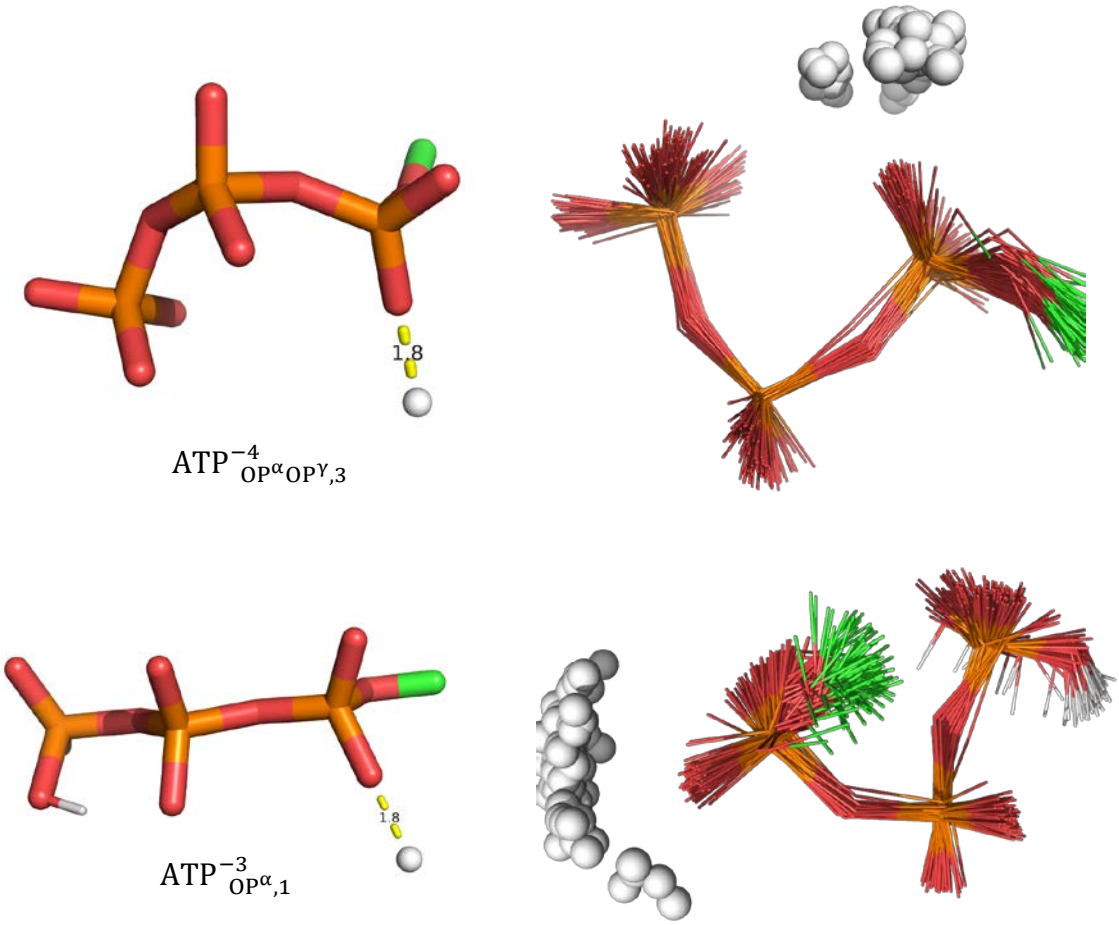

Figure S2. The initial binding mode structures and final superposed phosphate chain structures for ATP^{-4}:Mg^{2+} and ATP^{-3}:Mg^{2+}.

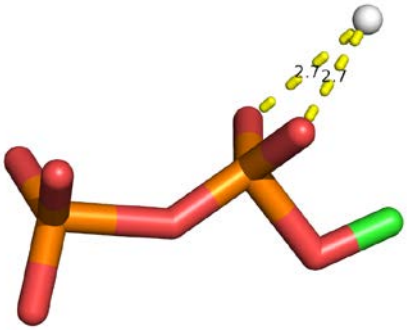

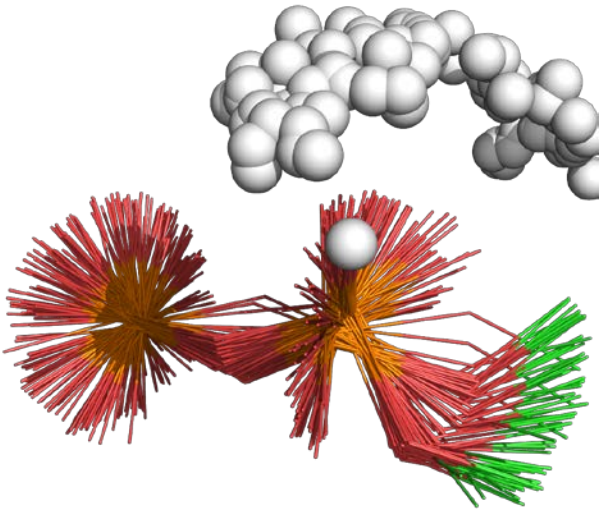

$ADP^{-3}_{OP^{\alpha},1}$

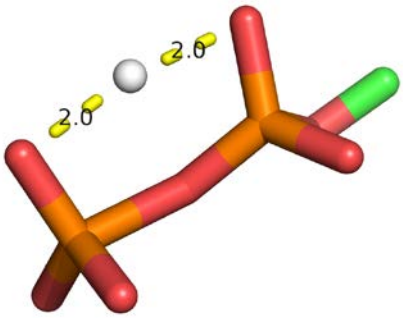

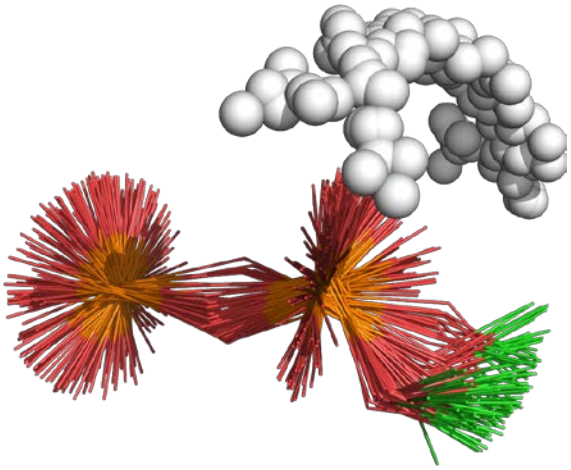

$ADP^{-3}_{OP^{\alpha},2}$

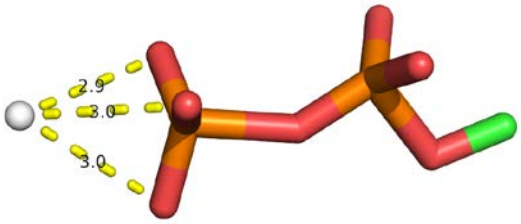

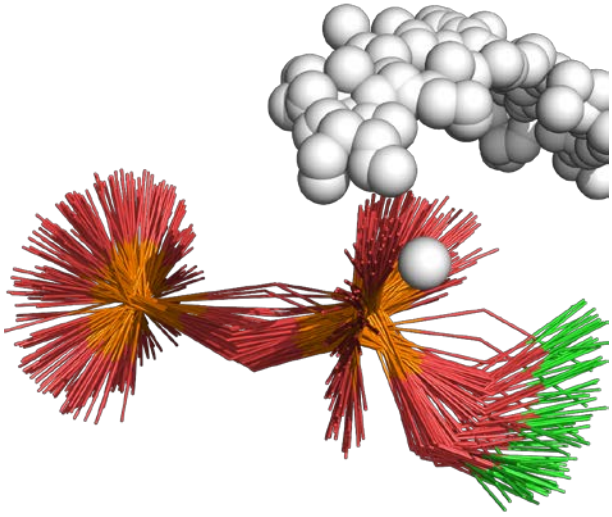

$ADP^{-3}_{OP^{\alpha},3}$

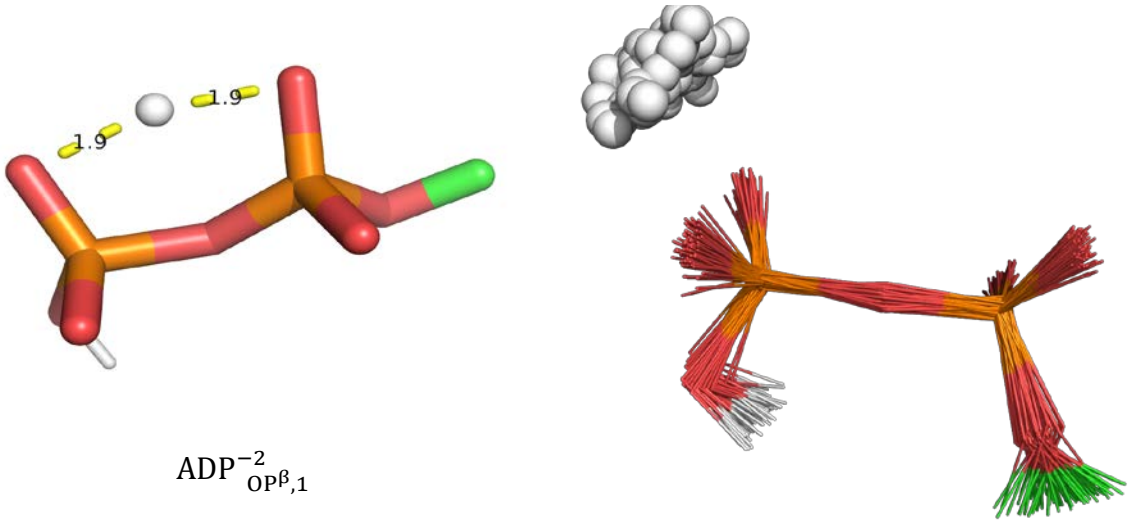

Figure S3. The initial binding mode structures and final superposed phosphate chain structures for ADP^{-3}:Mg^{2+} and ADP^{-2}:Mg^{2+}.

Radial Distribution Functions

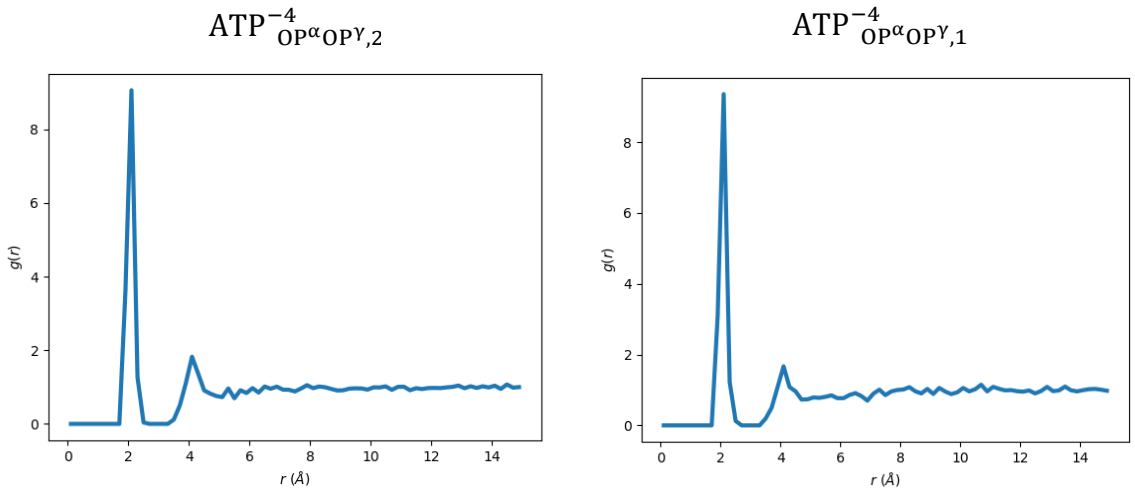

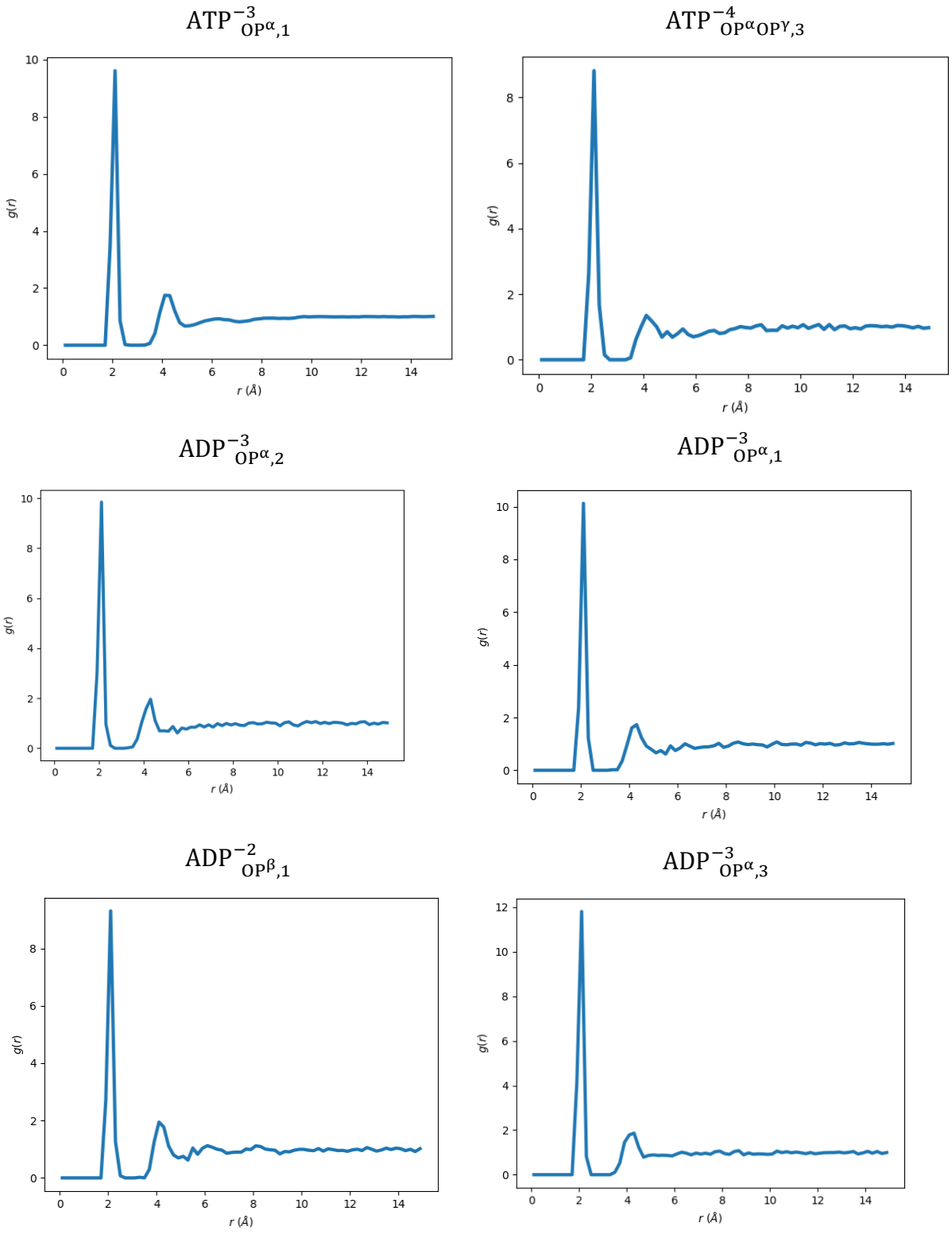

Figure S4. Radial distribution functions (RDFs) for pairs of Mg^{2+} and oxygen in water.

$ATP^{-4}_{OP^{\alpha}OP^{\gamma},2}$

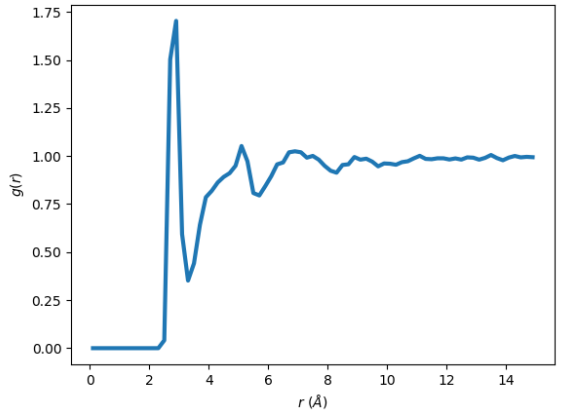

$ATP^{-4}_{OP^{\alpha}OP^{\gamma},1}$

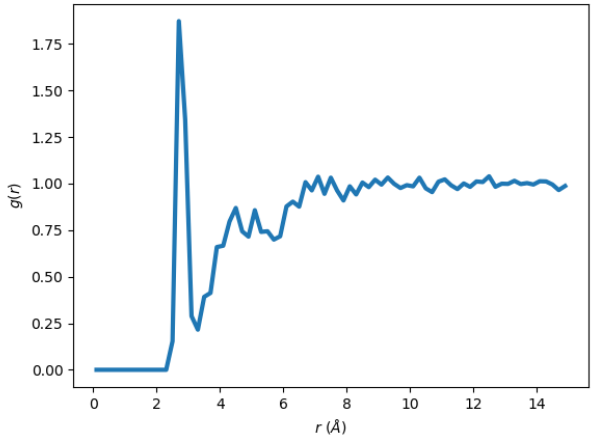

$ATP^{-3}_{OP^{\alpha},1}$

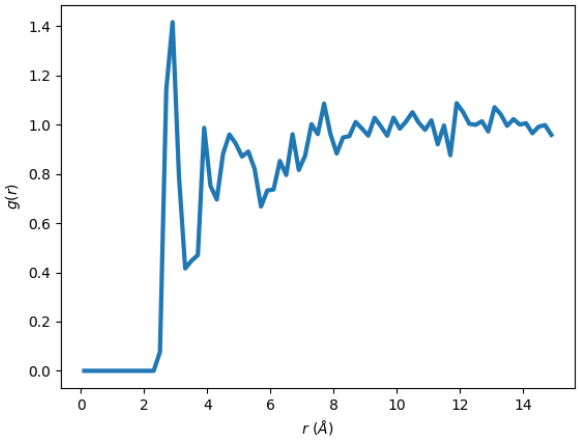

$ATP^{-4}_{OP^{\alpha}OP^{\gamma},3}$

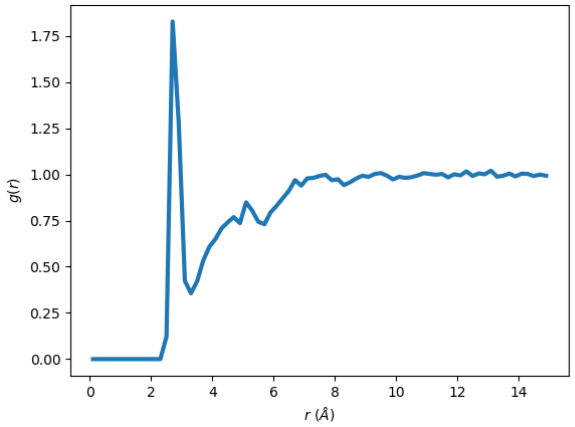

$ADP^{-3}_{OP^{\alpha},2}$

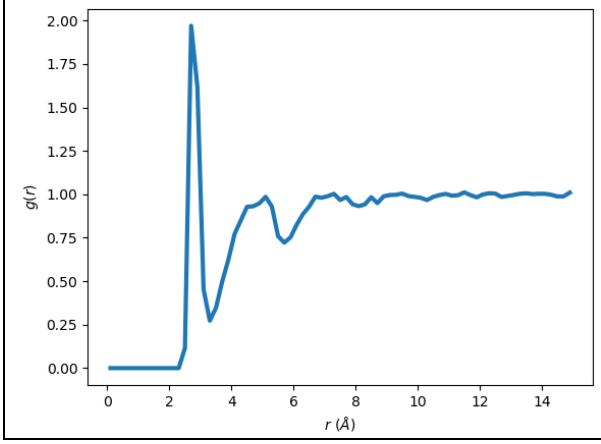

$ADP^{-3}_{OP^{\alpha},1}$

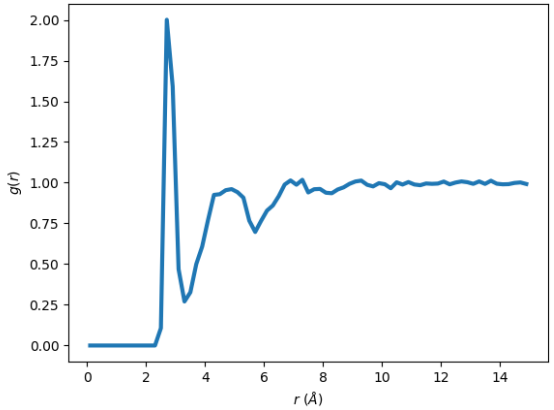

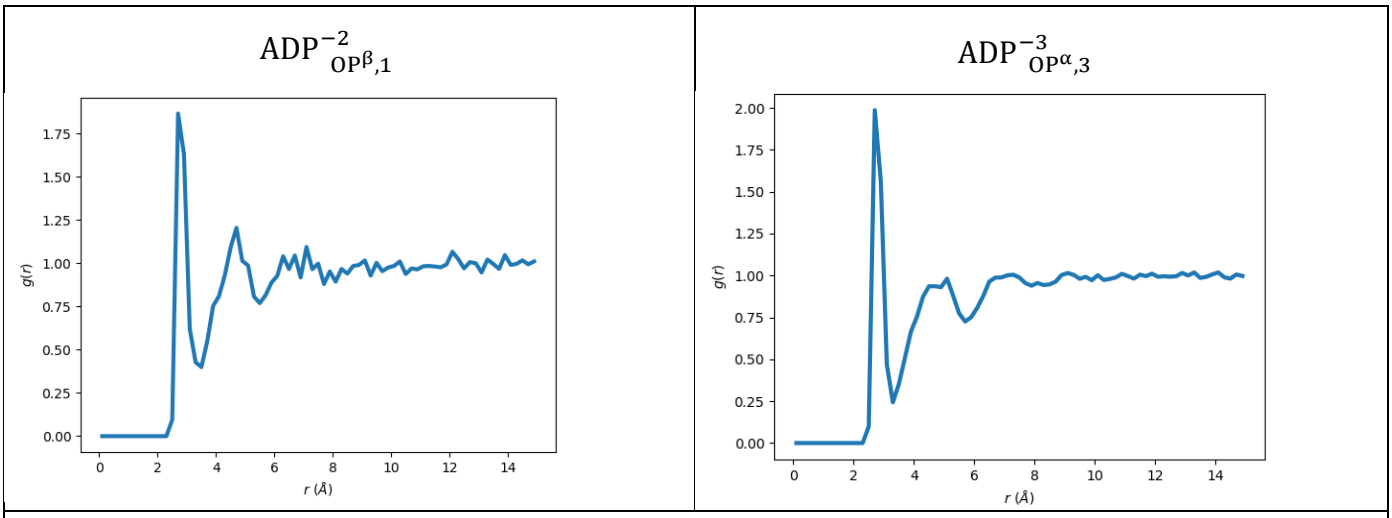

Figure S5. Radial distribution functions (RDFs) for ATP oxygen and oxygen in water.

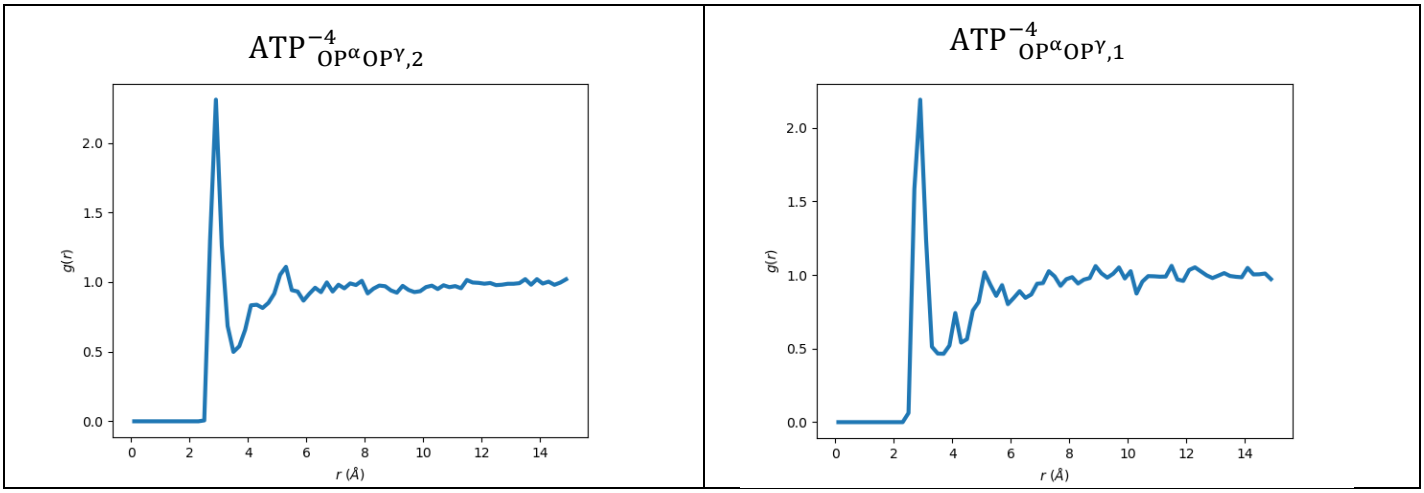

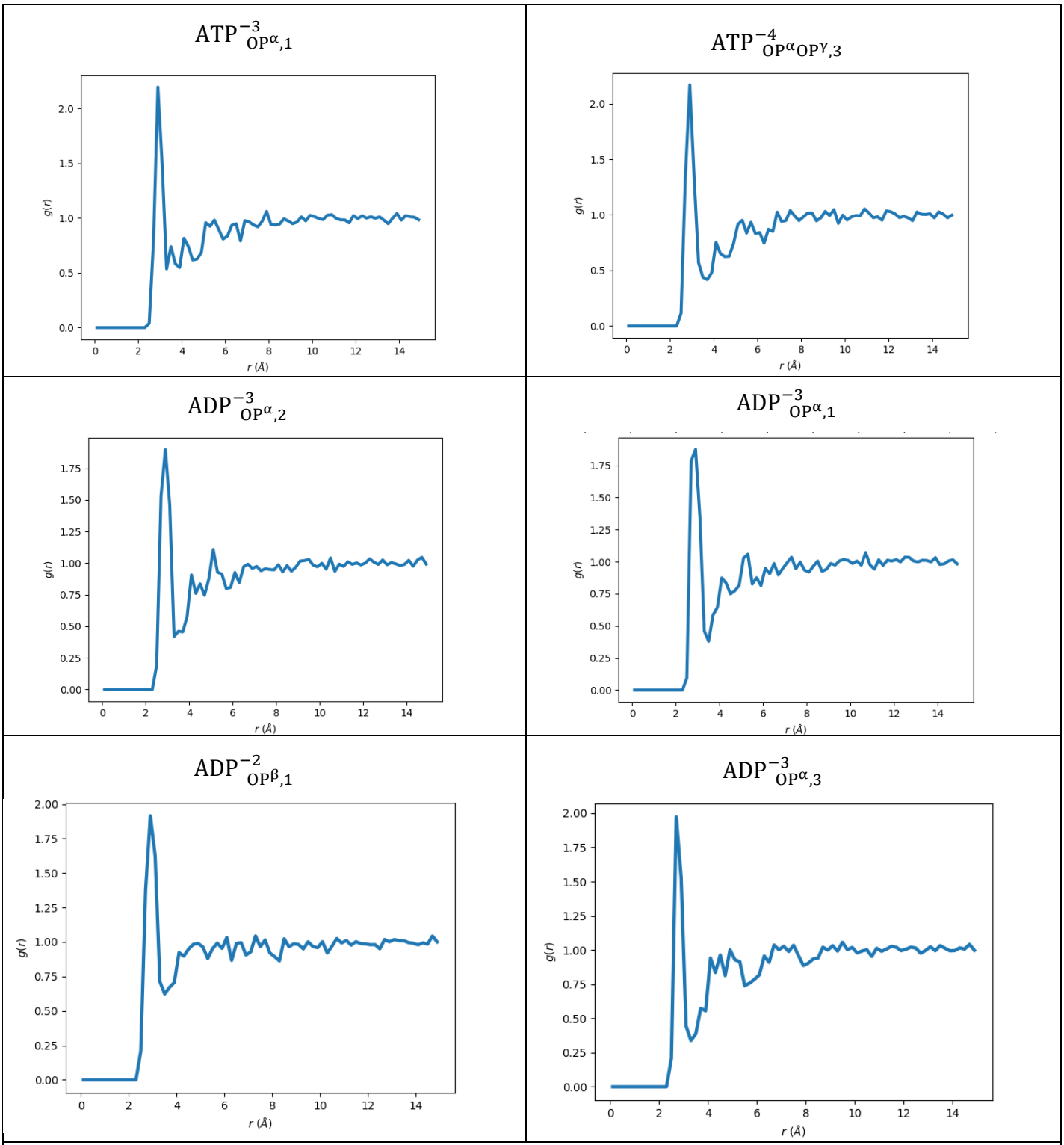

Figure S6. Radial distribution functions (RDFs) for ATP oxygen coordinating Mg^{2+} and oxygen in water.

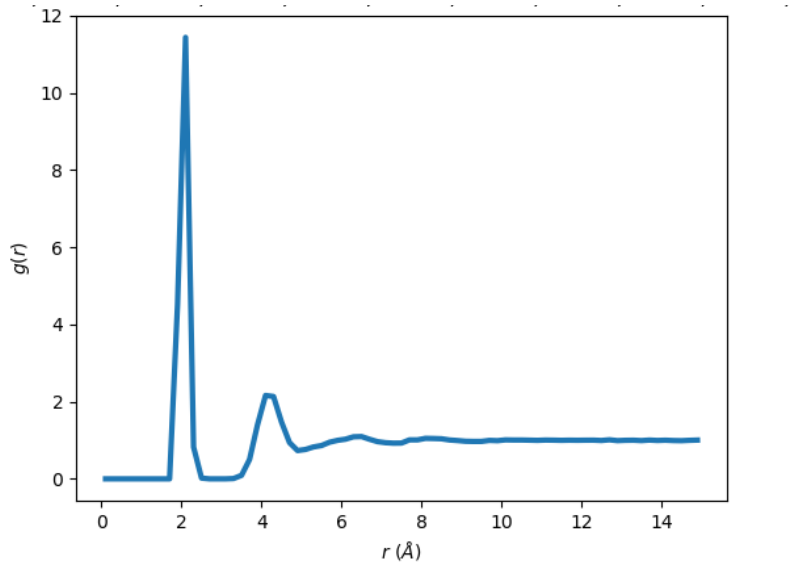

Figure S7. Radial distribution function of $Mg2^{+}$ and oxygen in water for bulk solvent.

Expected First Shell Water Number

Binding Mode	First Shell Waters	ΔG^{bind}	ΔH^{bind}	$\delta\Delta H^{bind}$
$ATP^{-4}_{OP^{\alpha}OP^{\gamma},2}$	5.0	-6.21	-37.15	42.41
$ATP^{-4}_{OP^{\alpha}OP^{\gamma},1}$	4.98	-7.67	-52.26	43.02
$ATP^{-4}_{OP^{\alpha}OP^{\gamma},3}$	4.86	-7.08	-170.14	42.34
$ATP^{-3}_{OP^{\alpha},1}$	5.0	-2.49	-12.15	14.46
$ADP^{-3}_{OP^{\alpha},2}$	4.96	-1.77	-54.46	44.03

$ADP^{-3}_{OP^{\alpha},1}$	5.0	-1.33	-115.33	41.22
$ADP^{-3}_{OP^{\alpha},3}$	6.0	-2.29	-64.4	41.74
$ADP^{-2}_{OP^{\beta},1}$	4.86	-3.15	-89.07	44.7

Table S1. Table showing expected first shell water number for pairs of Mg^{2+} and oxygen in water.

Binding Mode	First Shell Waters	ΔG^{bind}	ΔH^{bind}	$\delta\Delta H^{bind}$
$ATP^{-4}_{OP^{\alpha}OP^{\gamma},2}$	3.38	-6.21	-37.15	42.41
$ATP^{-4}_{OP^{\alpha}OP^{\gamma},1}$	2.60	-7.67	-52.26	43.02
$ATP^{-4}_{OP^{\alpha}OP^{\gamma},3}$	2.76	-7.08	-170.14	42.34
$ATP^{-3}_{OP^{\alpha},1}$	3.21	-2.49	-12.15	14.46
$ADP^{-3}_{OP^{\alpha},2}$	3.01	-1.77	-54.46	44.03
$ADP^{-3}_{OP^{\alpha},1}$	3.03	-1.33	-115.33	41.22
$ADP^{-3}_{OP^{\alpha},3}$	2.93	-2.29	-64.4	41.74
$ADP^{-2}_{OP^{\beta},1}$	3.64	-3.15	-89.07	44.7

Table S2. Table showing expected first shell water number for ATP oxygen coordinating Mg^{2+} (without Mg^{2+}) interactions and oxygen in water.

Binding Mode	First Shell Waters	ΔG^{bind}	ΔH^{bind}	$\delta\Delta H^{bind}$
$ATP^{-4}_{OP^{\alpha}OP^{\gamma},2}$	4.06	-6.21	-37.15	42.41

$ATP^{-4}_{OP^{\alpha}OP^{\gamma},1}$	4.49	-7.67	-52.26	43.02
$ATP^{-4}_{OP^{\alpha}OP^{\gamma},3}$	5.55	-7.08	-170.14	42.34
$ATP^{-3}_{OP^{\alpha},1}$	3.74	-2.49	-12.15	14.46
$ADP^{-3}_{OP^{\alpha},2}$	4.38	-1.77	-54.46	44.03
$ADP^{-3}_{OP^{\alpha},1}$	4.35	-1.33	-115.33	41.22
$ADP^{-3}_{OP^{\alpha},3}$	3.47	-2.29	-64.4	41.74
$ADP^{-2}_{OP^{\beta},1}$	4.26	-3.15	-89.07	44.7

Table S3. Table showing expected first shell water number for ATP oxygen coordinating Mg^{2+} and oxygen in water.

Sugar Puckering Statistics

For each binding mode, we used the trajectory with full electrostatics and Van der Waals to analyze the pseudo angle of the ribose sugar. Where the Pseudo angle[2] P is defined in **Eq. S6**. P was computed for every frame of each binding modes trajectory and the puckering conformation was probability is tabulated in **Table S1**, where the conformation is defined according to **Eq. S7**. From the table it can be seen that across all modes, C3'endo, C4'exo and C2'exo are the most frequent. A previous study on ATP conformation in PDB vs bulk solution found C2′ exo and C2′ endo conformations was highly dominated in water (using GROMACS) followed by O4′ endo[3]. In the PDB survey they found C2′ exo and C2′ endo to be populated roughly the same but O4′ endo to be less populated.

$$\tau_i = \begin{Bmatrix} C4' - O4' - C1' - C2' \text{for } \tau_0 \\ O4' - C1' - C2' - C3' \text{for } \tau_1 \\ C1' - C2' - C3' - C4' \text{for } \tau_2 \\ C2' - C3' - C4' - O4' \text{for } \tau_3 \\ C3' - C4' - O4' - C1' \text{for } \tau_4 \end{Bmatrix}$$

$$A = .4 \sum_{i=0}^{i=4} \tau_i \cos(.8\pi i) \qquad \textbf{Eq. S1}$$

where the τ_i are torsion angles on the sugar shown above

$$B = -.4\sum_{i=0}^{i=4}\tau_i \sin(.8\pi i) \quad \textbf{Eq. S2}$$

$$T_m = \sqrt{A^2 + B^2} \quad \textbf{Eq. S3}$$

$$\theta = \arctan\left(\frac{y}{x}\right) \quad \textbf{Eq. S4}$$

$$\operatorname{atan2}(y,x) = \begin{Bmatrix} \theta \text{ if } x > 0 \\ \theta + \pi \text{ if } x < 0\,, \frac{y}{x} < 0 \\ \theta - \pi \text{ if } x < 0\,, \frac{y}{x} > 0 \end{Bmatrix} \quad \textbf{Eq. S5}$$

$$P = \operatorname{atan2}\left(\frac{B}{T_m}, \frac{A}{T_m}\right)\frac{180}{\pi} \quad \textbf{Eq. S6}$$

$$\text{Conformation} = \begin{Bmatrix} C3'\text{endo if } 0 < P \leq 36 \\ C4'\text{exo if } 36 < P \leq 72 \\ O4'\text{endo if } 72 < P \leq 108 \\ C1'\text{exo if } 108 < P \leq 144 \\ C2'\text{endo if } 144 < P \leq 180 \\ C3'\text{exo if } 180 < P \leq 216 \\ C4'\text{endo if } 216 < P \leq 252 \\ O4'\text{exo if } 252 < P \leq 288 \\ C1'\text{endo if } 288 < P \leq 324 \\ C2'\text{exo if } 324 < P \leq 360 \end{Bmatrix} \quad \textbf{Eq. S7}$$

Table S4. Table showing statistics for sugar puckering.

Binding Mode	C3'endo	C4'exo	O4'endo	C1'exo	C2'endo	C3'exo	C4'endo	O4'exo	C1'endo	C2'exo
$ATP^{-4}_{OP^{\alpha}OP^{\gamma},3}$	36.14	5.28	0.04	0	0	0	0.3	3.26	23.88	31.1
$ATP^{-4}_{OP^{\alpha}OP^{\gamma},1}$	29.5	3.94	0	0.26	19.44	8.6	4.38	0.12	10.82	22.94
$ATP^{-3}_{OP^{\alpha},1}$	10.6	6.38	0.68	11.06	25.46	27.68	3.44	0.64	3.46	10.6
$ADP^{-3}_{OP^{\alpha},1}$	29.12	27.28	3.24	3.08	2.64	3.12	0.34	0.3	5.02	25.86
$ADP^{-3}_{OP^{\alpha},2}$	27.44	34.14	2.68	0.36	0.52	0.26	0.22	0.34	4.88	29.16
$ADP^{-3}_{OP^{\alpha},3}$	30.04	21.24	2.86	1.56	1.42	1.44	0.08	1.02	8.92	31.42
$ADP^{-2}_{OP^{\beta},1}$	26.86	16.52	1.16	5.54	6.14	6	0.72	0.44	8.62	28

Parameterization

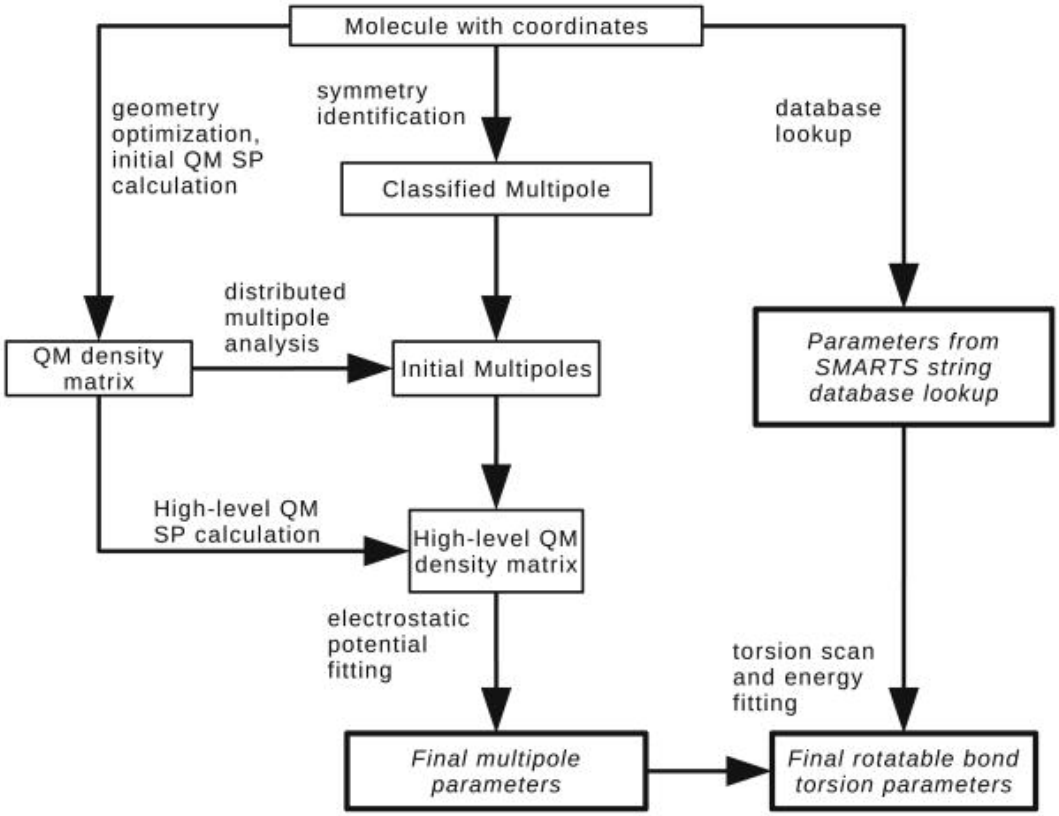

Figure S8. Overview of parameterization procedure for poltype[1]

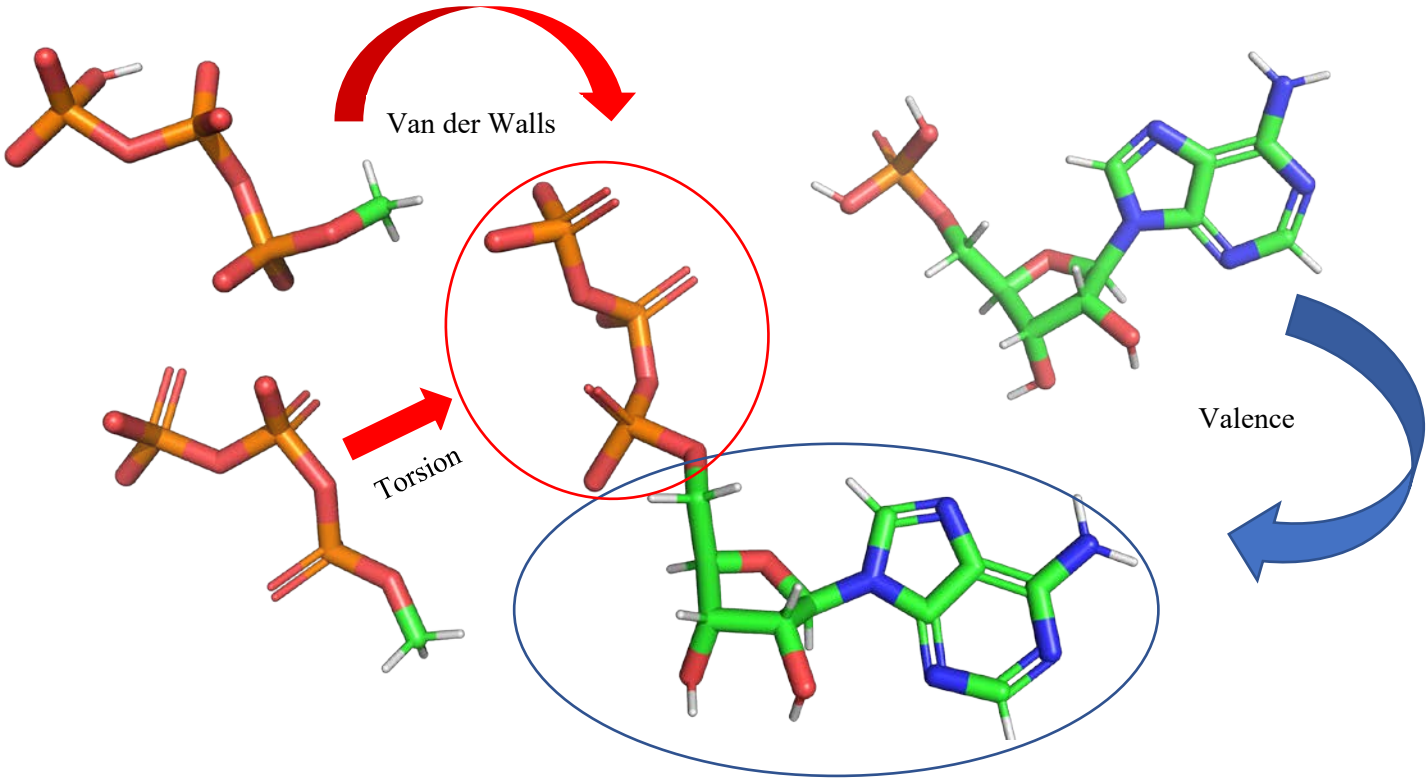

Figure S9. Overview of parameter transfer scheme for NTP, NDP. In this example AMP, ATP and an ATP^{-4} phosphate chain model compound are used. Valence parameters are transferred from AMP, GMP, Van der Waals parameters are transferred from an ATP^{-3} model compound, torsion is transferred from a model compound of the phosphate chain for each NTP/NDP and protonation state. Where polytype was used on each model compound[1] (**Fig S8**).

Van der Waal Parameterization

Water probes were places on various oxygens and then optimized with PCM at a UB3LYP/6-31+g(d)level of theory with Gaussian 09. Then several structures were generated by shifting the water probe about the optimized equilibrium water molecule position. A Gaussian counterpoise was then computed for each structure at a MP2/6-311++G** level of theory to generate the QM energy vs distance curves in **Fig S9**. A range of 3.5-3.8 was used for each oxygen Van der Waals radius and a range of .03-.14 was used for each oxygen Van der Waals depth. The minimum RMSD between the QM and MM curves was kept as the final parameters. After comparing the dominant ΔG (mode $ATP^{-4}_{OP^{\alpha},2}$) for ATP^{-4}, the free energy of (-4.92) did not match the experimental target of -8.6 (see **Table 1**) we adjusted the parameters to make the free energy more favorable as observed from experiment. Finally, linear interpolation was used to generate the final parameters which gives us the binding free energy within statistical uncertainty of the experimental value. These final parameters were then transferred to ATP^{-3}, GTP^{-4}, GTP^{-3}, ADP^{-3}, ADP^{-2}, GDP^{-3}, GDP^{-2}.

Table S5. Table used to generate final parameters for oxygen type 411, see **Fig S9**. Where R is the Van der Waals radius, ε is the Van der Waals depth and ΔG is the binding free energy.

	R	ε	ΔG
From Vdw Probe	3.63	0.112	-4.92
Linear Interpolated	3.5534	0.09315	-8.7974
Guessed Parameters	3.5	0.08	-11.17

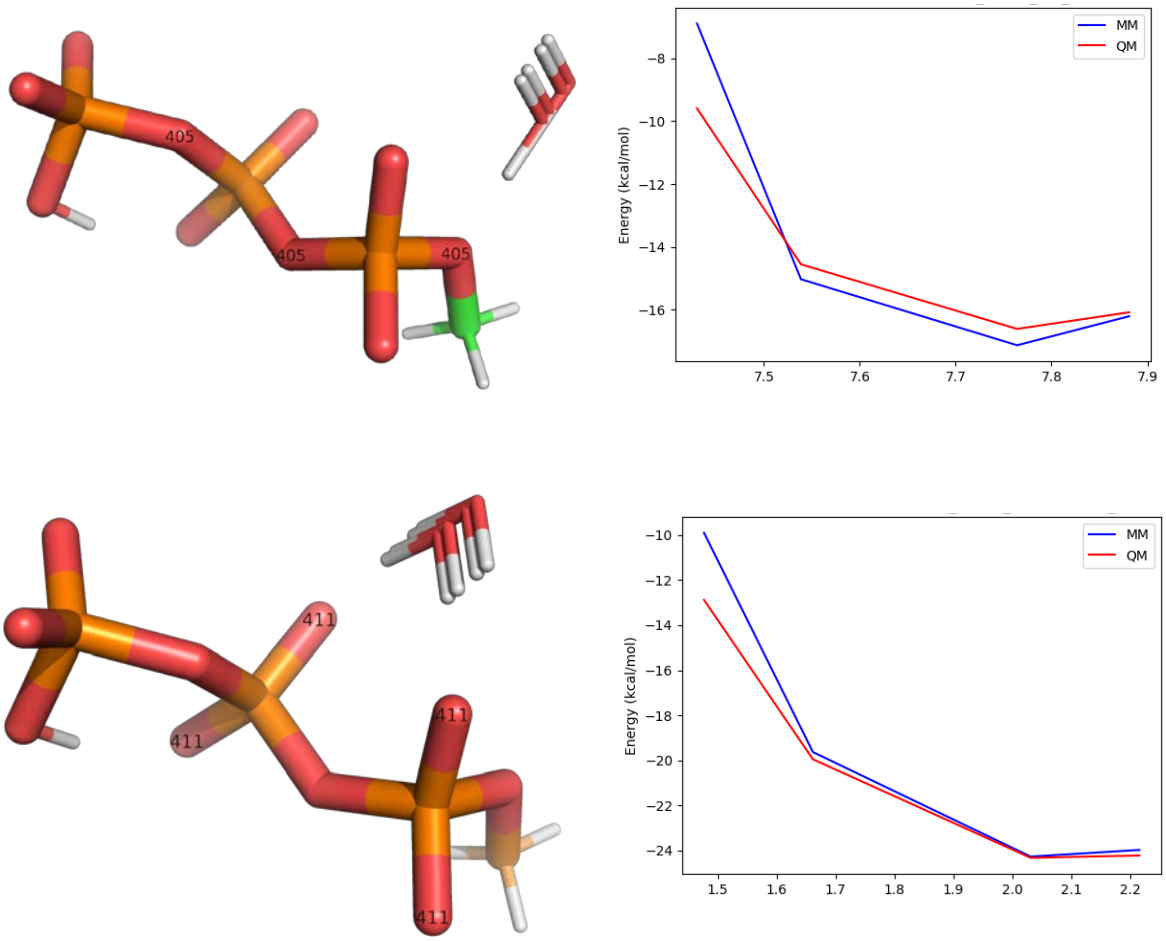

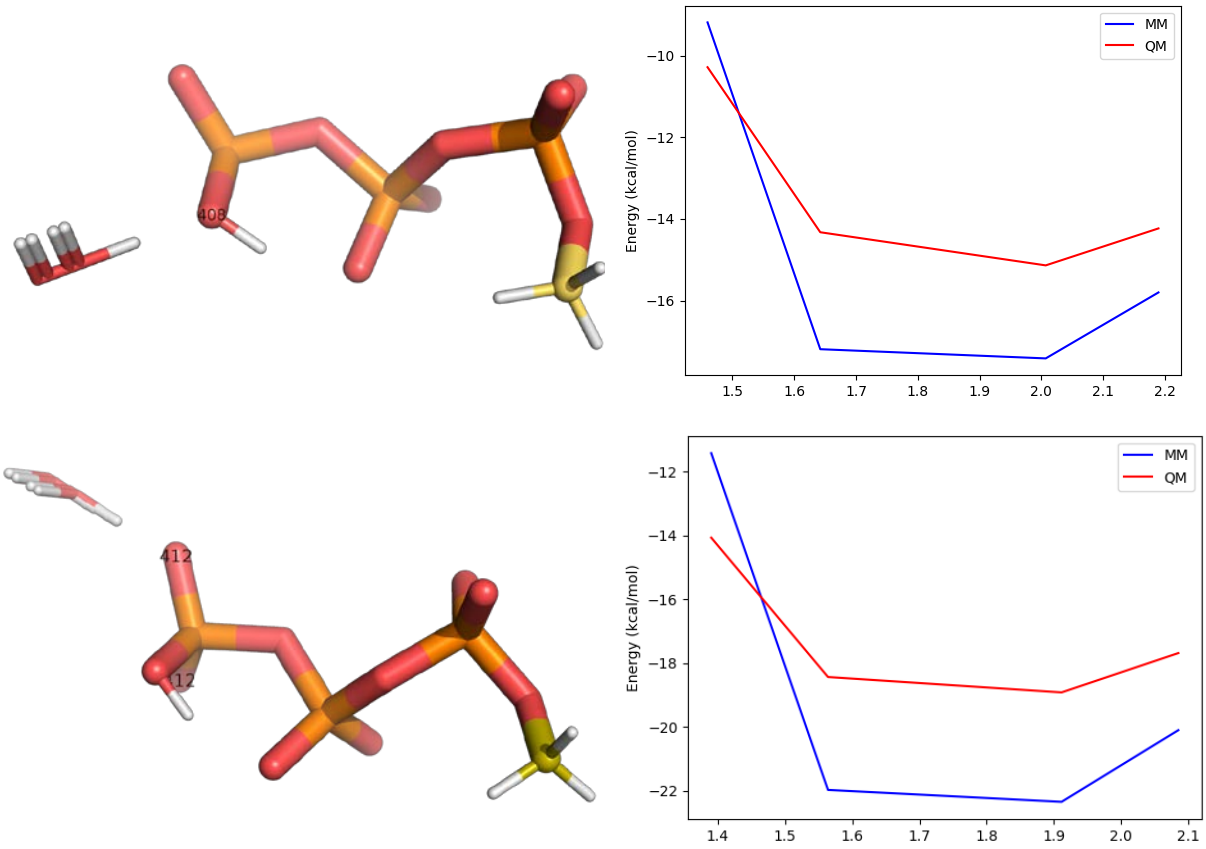

Figure S9. Left all Van der Waals probes used to obtain Van der Waals parameters from Quantum Mechanics (QM) and Molecular Mechanics (MM) best fit Energy vs distance in Å.

Torsion Parametrization

Torsional parameters for the phosphate chain model were fit to reproduce the QM conformational energy profile at MP2/6-311++G** level. The structures were optimized at MP2/cc-pVTZ level and the single point energy was calculated at the MP2/6-311++G(2d,2p) level, see **Fig S14, Fig S16, Fig S18, Fig S20**. Where the MM1 is the MM energy curve without the fitted torsion parameters, MM2 is the MM energy curve with the fitted parameters, QM is the single point energy using MP2/6-311++G(2d,2p) curve and MM1+fit is MM1 + the curve obtained from fitting to the difference between the target and our model (QM-MM1). MM1+fit serves as an additional check to make sure that the final parameters are reasonable, where MM1+fit should be similar in shape to the fitted parameter energy curve (MM2).

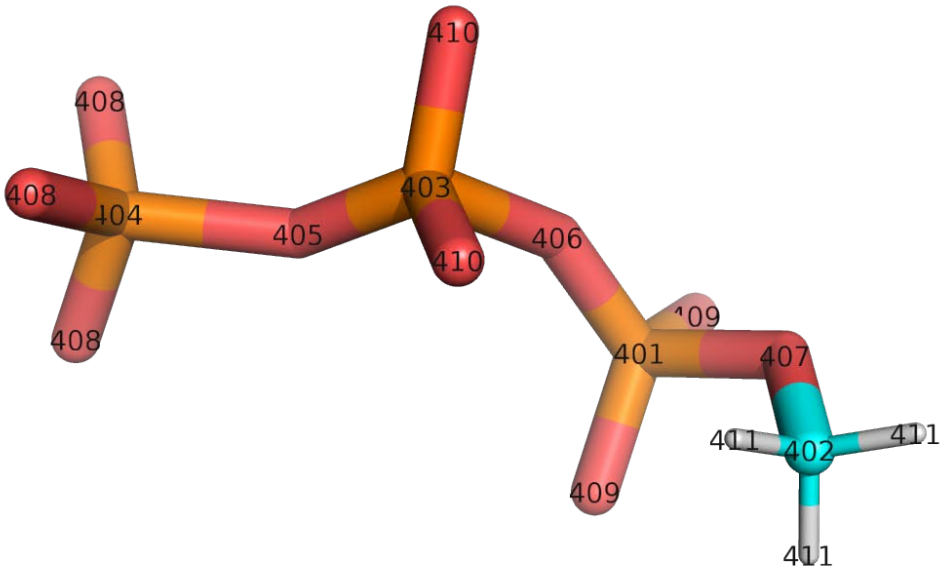

Figure S13. Model compound of ATP^{-4}, GTP^{-4} phosphate chain to obtain torsion parameters.

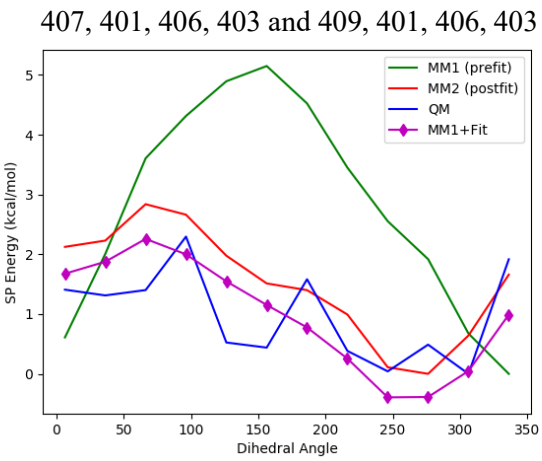

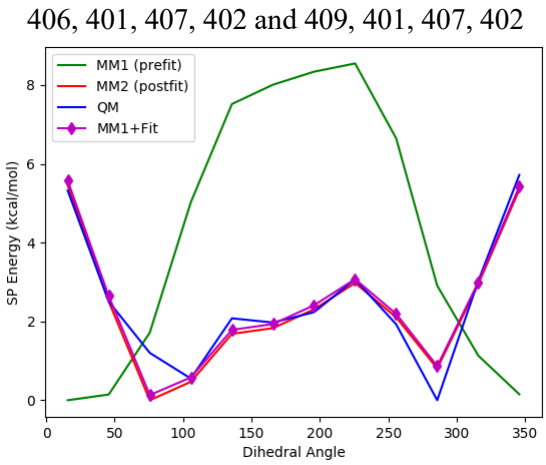

406, 403, 405, 404 and 410 , 403 , 405, 404

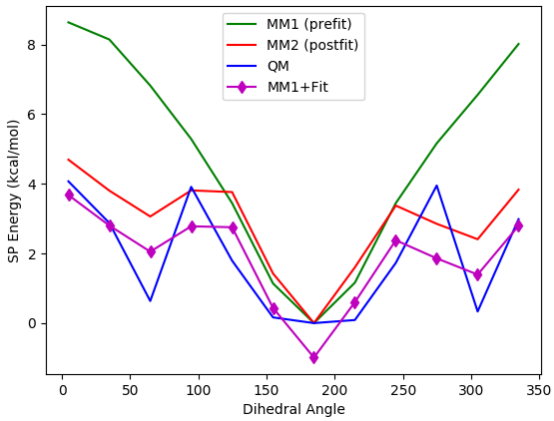

410, 403, 406, 401 and 405, 403, 406, 401

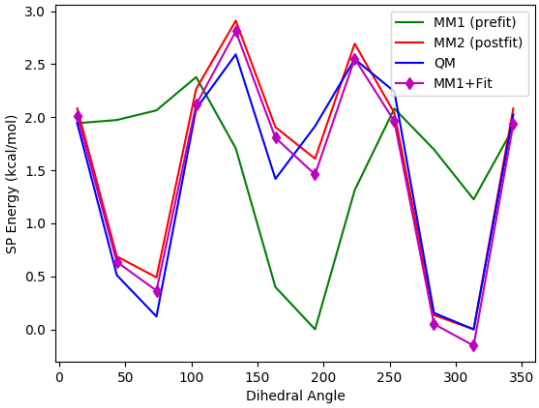

408 , 404 , 405, 403

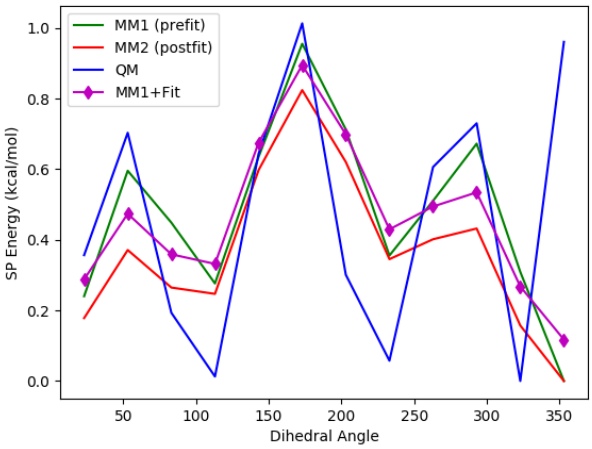

Figure S14. Plots of SP energy vs dihedral angle for ATP^{-4}, GTP^{-4} phosphate chain torsions.

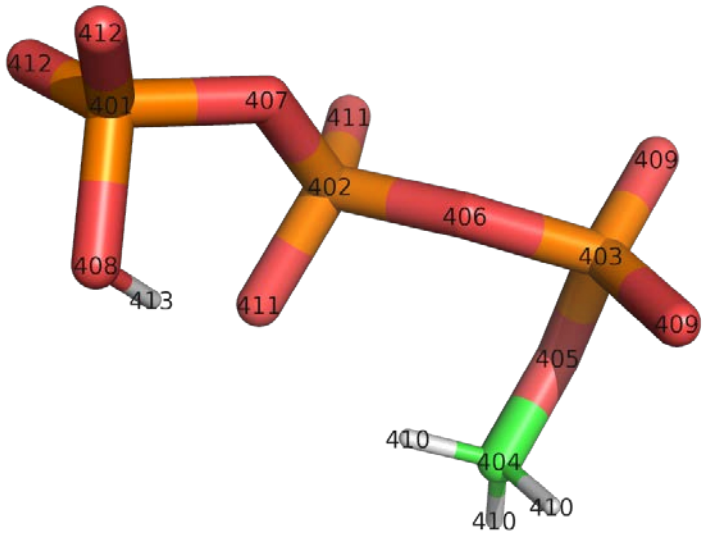

Figure S15. Model compound of phosphate chain for ATP^{-3}, GTP^{-3} torsion parameters.

409, 403, 406, 402 and 405, 403, 406, 402

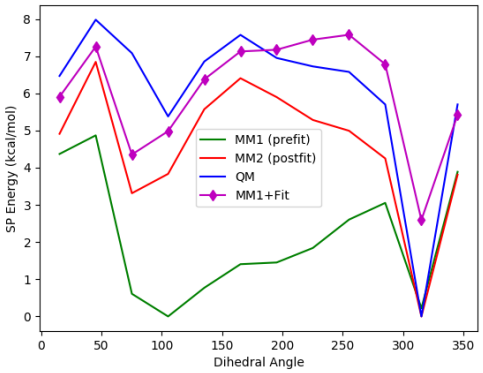

406, 403, 405, 404 and 409, 403, 405, 404

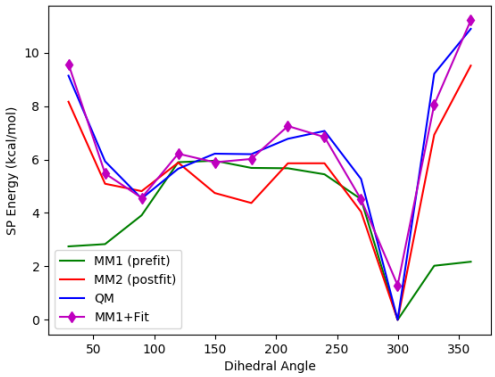

411, 402, 406, 403 and 407, 402, 406, 403

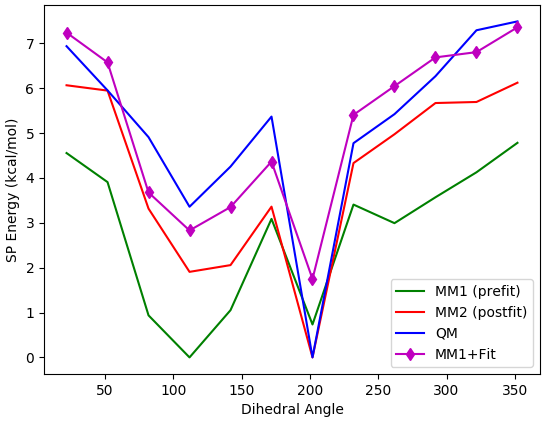

411, 402, 407, 401 and 406, 402, 407, 401

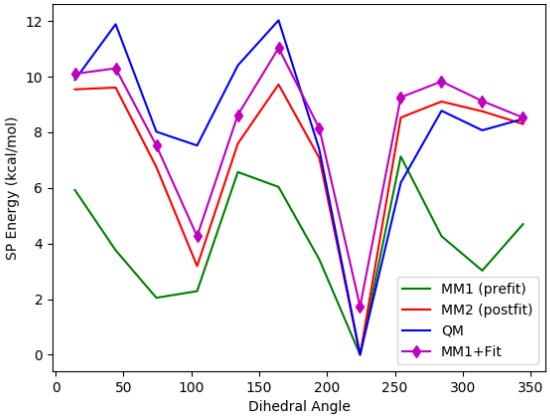

412, 401, 407, 402 and 408, 401, 407, 402

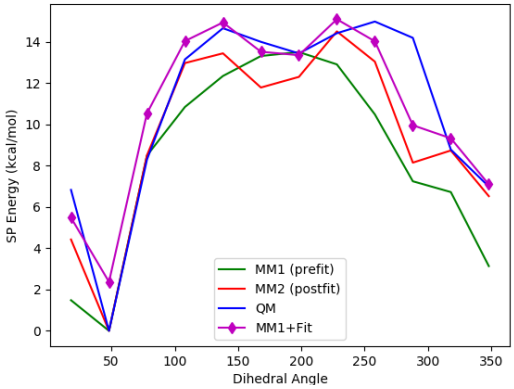

Figure S16. Plots of SP energy vs dihedral angle for ATP^{-3}, GTP^{-3} phosphate chain torsions.

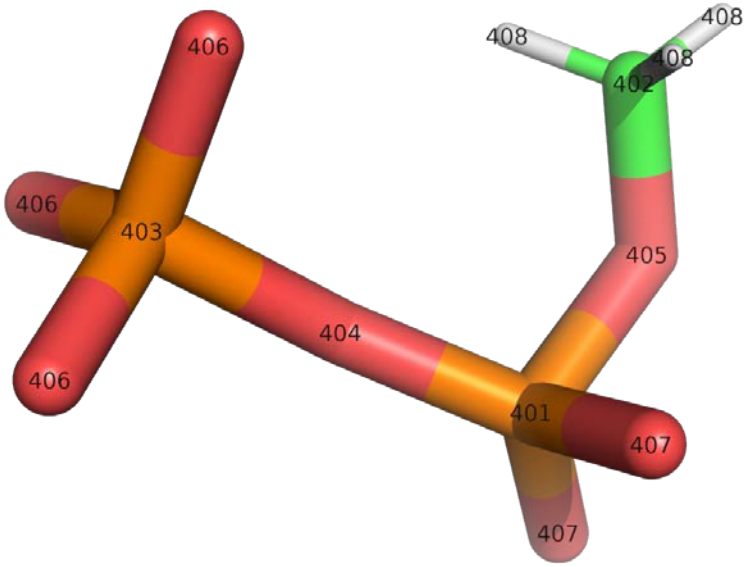

Figure S17. Model compound of phosphate chain for ADP^{-3}/GDP^{-3} torsion parameters.

404, 401, 405, 402 and 407, 401, 405, 402

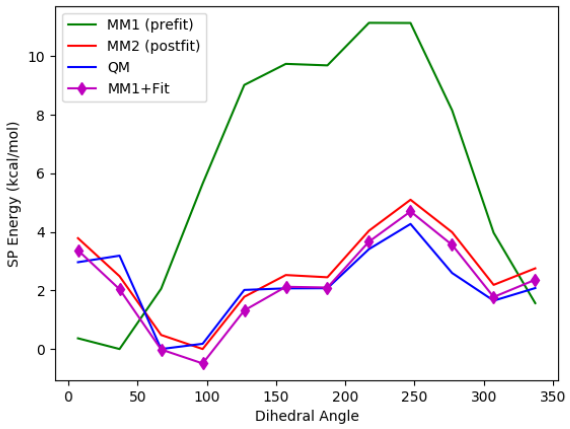

405, 401, 404, 403 and 407, 401, 404, 403

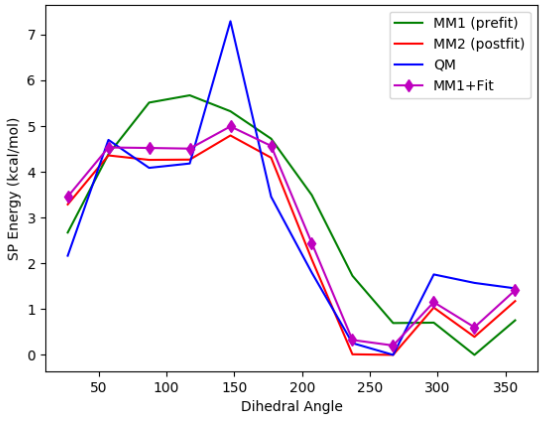

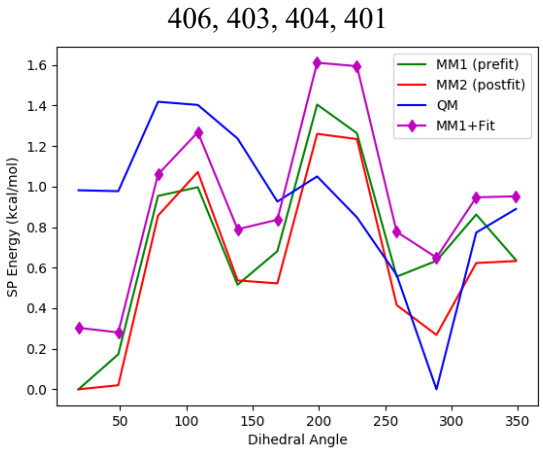

Figure S18. Plots of SP energy vs dihedral angle for ADP^{-3}/GDP^{-3} phosphate chain torsions.

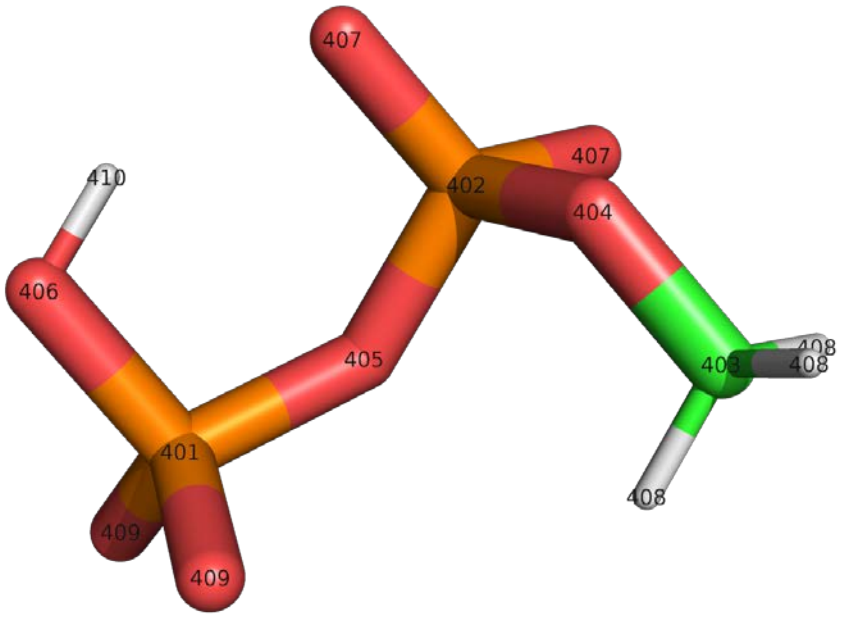

Figure S19. Model compound of phosphate chain for ADP^{-2}, GDP^{-2} torsion parameters.

409,401,405,402 and 406,401,405,402

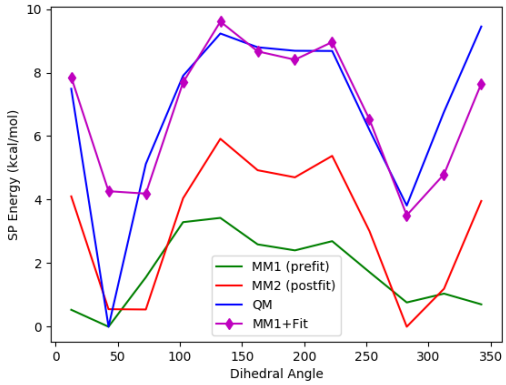

409, 401, 405, 402 and 406, 401, 405, 402

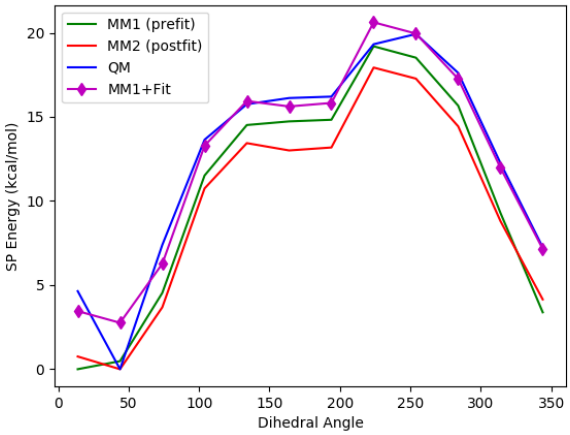

404, 402, 405, 401 and 407, 402, 405, 401

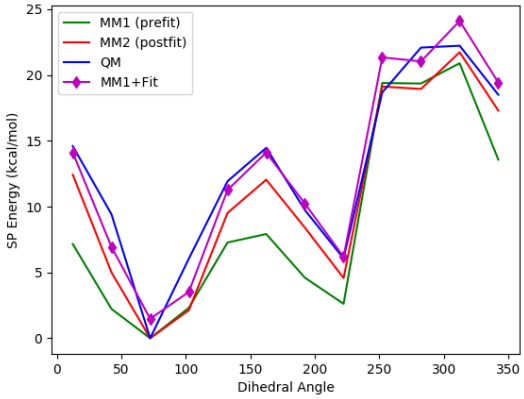

Figure S20. Plots of SP energy vs dihedral angle for ADP^{-2}, GDP^{-2} phosphate chain torsions.

Molecular Dynamics

Equilibration

Table S6. Table describing equilibration scheme, including the harmonic spring restraint perturbation schedule.

Time (ns)	0.33	0.33	0.33	0.33	0.33	0.33	0.33	0.33	0.33	0.33	0.33	0.33	3
Ensemble	NVT	NVT	NVT	NVT	NVT	NVT	NVT	NVT	NVT	NVT	NVT	NVT	NPT
Temp	25	50	75	100	125	150	175	200	225	250	275	298	298
λ_{res}	1	0.92	0.84	0.76	0.68	0.6	0.52	0.44	0.36	0.28	0.2	0.12	0

Production Dynamics

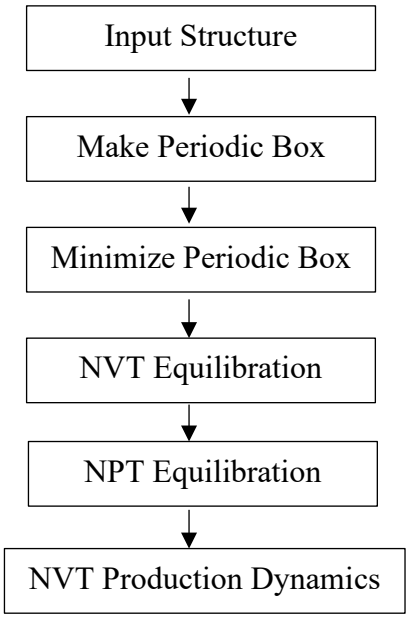

Figure S21. Overview of molecular dynamics scheme.

λ_{ele}	λ_{vdw}
1	1
0.9	1
0.8	1
0.7	1
0.6	1
0.5	1
0.4	1
0.3	1
0.2	1
0.1	1
0	1
0	0.9
0	0.8
0	0.75
0	0.7
0	0.65
0	0.62
0	0.6
0	0.55
0	0.5
0	0.4
0	0

λ_{ele}	λ_{vdw}	λ_{res}
1	1	0
0.9	1	0.1
0.8	1	0.2
0.7	1	0.3
0.6	1	0.4
0.5	1	0.5
0.4	1	0.6
0.3	1	0.7
0.2	1	0.8
0.1	1	0.9
0	1	1
0	0.9	1
0	0.8	1
0	0.75	1
0	0.7	1
0	0.65	1
0	0.62	1
0	0.6	1
0	0.55	1
0	0.5	1
0	0.4	1
0	0	1

Figure S22. Left perturbation scheme for solvation production dynamics, right perturbation scheme for complexation dynamics. Every row in either table represents an individual simulation with the corresponding lambda.

Absolute Binding Free Energy Calculations

The absolute Helmholtz binding free energy (ΔG_{bind}) for individual binding modes was calculated via the double decoupling method[4], shown in **Figure S22**. Initial simulations began from the last structure of the equilibrated trajectory with the $2Cl^{-}Mg^{2+}$ as the system. First electrostatics were decoupled from the environment while the Van der Waals interaction strength was held constant, then Van der Waals was decoupled after electrostatic interactions were completely removed according to the perturbation schedules in **Figure S22**. An ion restraint was also used to keep the ion near its initial position, where the restraint strength was slowly turned on as electrostatics and Van der Waals were decoupled from the system and environment (λ_{res} in **Fig. S22**). In this study total of 22 alchemical states were chosen to ensure a smooth transition between the two ends states. According to the thermodynamic cycle (**Fig. S23**), we can use **Eq. S11** to compute the absolute binding free energy ΔG_{bind}. Due to there being a harmonic restraint when Van der Waals and electrostatics are completely decoupled between the system and the surrounding environment on the right hand side of the cycle, but not the left side, an analytical correction ΔG_{cor} is used to account for the artificial entropy effects of the restraint according to **Eq. S12**[4]

$$P_{final} = P_{initial}\lambda \qquad \textbf{Eq. S8}$$

where P represents an electrostatic, Van der Waals parameter or harmonic spring force constant, lambda is the corresponding perturbation value.

$$U = U(\lambda, \boldsymbol{R}) \qquad \textbf{Eq. S9}$$

where U represents the potential energy, which is a function of perturbation lambda and **R** the coordinates of all atoms

$$\Delta G_{solv} + \Delta G_{bind} - \Delta G_{comp} - \Delta G_{cor} = 0 \qquad \textbf{Eq. S10}$$

where clockwise is chosen as the + direction and all the contributions on the closed cycle must sum to zero

$$\Delta G_{bind} = \Delta G_{comp} - \Delta G_{solv} + \Delta G_{cor} \qquad \textbf{Eq. S11}$$

$$\Delta\, G_{cor} = RTln(C^{\circ}\left(\frac{2\pi RT}{k}\right)^{\frac{3}{2}}) \qquad \textbf{Eq. S12}$$

$$\Delta G_{solv} = \sum_{k=1}^{k=n} \Delta G_{solv,k}\ , \Delta G_{comp} = \sum_{k=1}^{k=n} \Delta G_{comp,k} \qquad \textbf{Eq. S13, S14}$$

where ΔG_{solv} and ΔG_{comp} are computed by summing individual $\Delta G_{solv,k}$ and $\Delta G_{comp,k}$ from a total of n ΔG shown in **Fig. S22**.

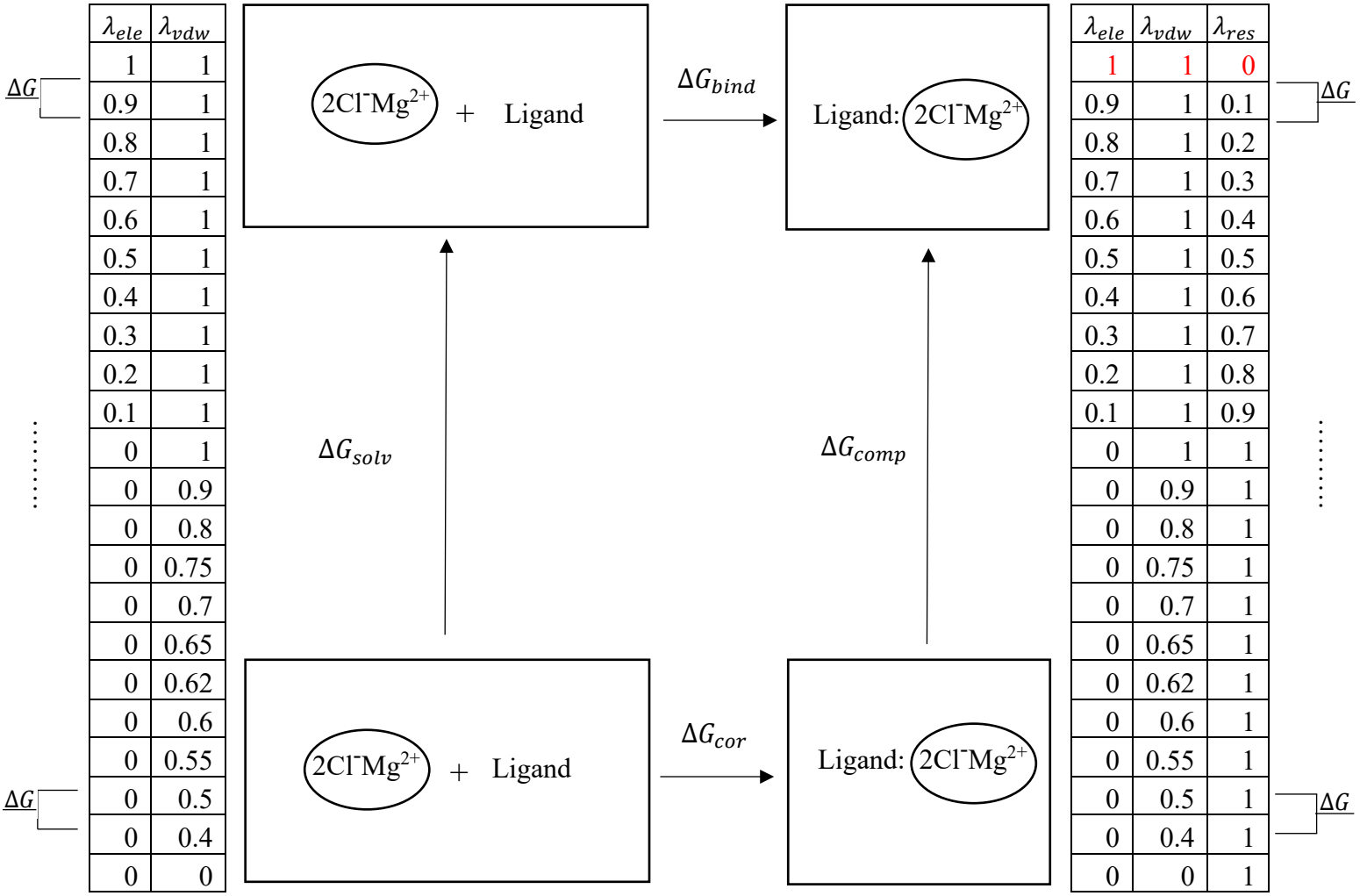

Figure S23. Thermodynamic cycle for calculating the binding free energy ΔG_{bind} for individual modes of ATP^{-4}:Mg^{2+},ATP^{-3}:Mg^{2+},ADP^{-3}: Mg^{2+} and ADP^{-2}: Mg^{2+}. The rectangle represents the periodic box and the oval represents the system, while everything else in the rectangle represents the surrounding environment. The + indicates the species are both free in solution, while the : indicates the bound complex state. The perturbation schedules for electrostatic interactions, Van der Waals interactions and the harmonic spring restraint strength ($\lambda_{ele}, \lambda_{vdw}, \lambda_{res}$) are shown on the left and right for computing solvation and complexation free energy respectively (ΔG_{solv} and ΔG_{comp}). Each combination of $\lambda_{ele}, \lambda_{vdw}, \lambda_{res}$ represents an individual dynamic simulation with perturbation lambdas according to equation **S8**. BAR is used to compute free energy changes denoted by ΔG between pairs of consecutive lambdas (**Eq. S21**). The full electrostatic and Van der Waals dynamic trajectory is highlighted in red to indicate this one was used for analysis of where Mg^{2+} tends to bind.

The free energy changes from one state to the other is thus given by **Eq. S4** and **Eq. S5**. In order to obtain free energy estimates, the Bennett acceptance ratio (BAR) method was applied.

$$G = K_B T ln(Q) = \frac{ln\,(Q)}{\beta} \qquad \textbf{Eq. S15}$$

From statistical mechanics, where Q is the configurational partition function, $\beta = \frac{1}{K_B T}$. The kinetic energy component of the partition function integrated to a constant and will cancel out $\frac{1}{N!}\left(\frac{2\pi mkT}{h^2}\right)^{3N/2}$

$$Q = \int_{\Gamma}\ e^{-\beta U(\vec{q})} d\vec{q} \qquad \textbf{Eq. S16}$$

The configurational partition function Q, depends on the potential energy $U(\vec{q})$ which is a function of all the momenta and coordinates of the system. Γ defines the phase space of momenta and positions to integrate over.

$$\Delta G_k = \Delta G_{ij} = G_i - G_j = K_B T ln(Q_i) - K_B T ln\left(Q_j\right) = K_B T ln \frac{Q_i}{Q_j} = -K_B T ln \frac{Q_j}{Q_i} \qquad \textbf{Eq. S17}$$

Manipulating **Eq. S14** and **Eq. S15,** the k[th] ΔG is computed between perturbation states i and j

$$\frac{Q_j}{Q_i} = \frac{Q_j}{Q_i}\frac{1}{1} = \frac{Q_j}{Q_i}\frac{\int \alpha(\vec{q}) e^{-U_j - U_i} d\vec{q}}{\int \alpha(\vec{q}) e^{-U_j - U_i} d\vec{q}} = \frac{Q_j}{Q_i}\frac{\int \alpha(\vec{q}) e^{\beta(-U_j - U_i)} d\vec{q}}{\int \alpha(\vec{q}) e^{\beta(-U_i - U_j)} d\vec{q}} = \frac{Q_j \alpha(\vec{q}) e^{-\beta U_i} \int e^{-\beta U_j} d\vec{q}}{Q_i \alpha(\vec{q}) e^{-\beta U_j} \int e^{-\beta U_i} d\vec{q}} \qquad \textbf{Eq. S18}$$

Multiplying by 1

$$\Delta G_{ij} = -K_B T ln \frac{\int_{\Gamma_j} e^{-\beta U_j(\vec{q})} d\vec{q}\, \alpha(\vec{q}) e^{-\beta U_i} \int e^{-\beta U_j} d\vec{q}}{\int_{\Gamma_i} e^{-\beta U_i(\vec{q})} d\vec{q}\, \alpha(\vec{q}) e^{-\beta U_j} \int e^{-\beta U_i} d\vec{q}} = \frac{\int_{\Gamma_j} \alpha(\vec{q}) e^{-\beta U_i} e^{-\beta U_j(\vec{q})} d\vec{q}}{\int_{\Gamma_i} \alpha(\vec{q}) e^{-\beta U_j} e^{-\beta U_i(\vec{q})} d\vec{q}} \qquad \textbf{Eq. S19}$$

where we used the fact that $\int e^{-\beta U_j}\, d\vec{q} = \int e^{-\beta U_i}\, d\vec{q}$

$$\Delta G_{ij} = -K_B T ln \frac{<\alpha(\boldsymbol{R}) e^{-\beta U_i}>_j}{<\alpha(\boldsymbol{R}) e^{-\beta U_j}>_i} \qquad \textbf{Eq. S20}$$

Here we take $P_j = e^{-\beta U_j(\vec{q})}\, d\vec{q}$ within phase space Γ_j and take $P_i = e^{-\beta U_j(\vec{q})}\, d\vec{q}$ within phase space Γ_i. This is the definition of average and hence **Eq. S20**.

$$\sum_{i=1}^{n_i} \frac{1}{1+e^{ln\frac{n_i}{n_j}+\beta\Delta U_{ij}-\beta\Delta G}} - \sum_{i=1}^{n_j} \frac{1}{1+e^{ln\frac{n_j}{n_i}+\beta\Delta U_{ji}-\beta\Delta G}} = 0 \qquad \textbf{Eq. S21}$$

Using the definition of variance, differential calculus can be used to minimize the variance of ΔG_{ij} in **Eq. S20** to arrive at **Eq. S21**.This expression is numerically solved to obtain ΔG_{ij}.

Total Binding Free Energy

Deriving ΔG^{total}

Here we derive the total binding free energy by considering multiple binding modes for every possible protonation state.

$$\left[X_i^j\right], j \in P = \{p_1, \ldots, p_f\} \qquad \textbf{Eq. S22}$$

X here is any species such as ATP, j represents a protonation state which exists in the set of possible protonation states P. $p_1$is the first protonation state and p_f is the final protonation state, here each protonation state $p_k < 0$ and $p_{k+1} > p_k$. The index i, represents the ith binding mode for X^j.The brackets [], represent the concentration.

$$l = \begin{Bmatrix} n_{p_1}\ if\ j = p_1 \\ \vdots \\ n_{p_f}\ if\ j = p_f \end{Bmatrix} \rightarrow \begin{Bmatrix} 1,2,\ldots,n_{p_1} \\ \vdots \\ 1,2,\ldots,n_{p_f} \end{Bmatrix} \qquad \textbf{Eq. S23}$$

The index l represents the number of binding modes for a given species with protonation state j. The braces on the right more clearly label how many binding modes exist for each species with protonation state j.

$$[Mg^{2+}] + [X] \rightarrow \left\{ \begin{array}{c} [Mg^{2+}: X_1^{p_1}] \\ \vdots \\ [Mg^{2+}: X_{n_{p_1}}^{p_1}] \\ [Mg^{2+}: X_1^{p_1+1}] \\ \vdots \\ [Mg^{2+}: X_1^{p_f}] \\ \vdots \\ [Mg^{2+}: X_{n_{p_f}}^{p_f}] \end{array} \right\} \qquad \textbf{Eq. S24}$$

Here is a system of branched reactions with various binding modes for each protonation state possible from $[Mg^{2+}] + [X]$

$$K_a = \frac{[Mg^{2+}:X]}{[Mg^{2+}][X]} = \frac{\sum_{j=p_1}^{j=p_f} \sum_{i=1}^{i=l} [Mg^{2+}:X_i^j]}{[Mg^{2+}] \sum_{j=p_1}^{j=p_f} [X^j]} \qquad \textbf{Eq. S25}$$

Here, the equilibrium constant K_a on the left-hand side of **Eq. S25** is what is measured experimentally. According to the branched system of chemical reactions (**Eq. S24**), $[Mg^{2+}: X]$ can be converted into a sum over all binding modes for a given protonation state of X. While, [X] can be converted into a sum over all possible protonation states.

$$K_a = \frac{\sum_{i=1}^{i=l} \frac{[Mg^{2+}:X_i^{p_1}]}{[Mg^{2+}][X^{p_1}]} + \sum_{j=p_1+1}^{j=p_f} \sum_{i=1}^{i=l} \frac{[Mg^{2+}:X_i^j]}{[Mg^{2+}][X^j][X^{p_1}]} \frac{[X^j]}{}}{1 + \sum_{j=p_1+1}^{j=p_f} \frac{[X^j]}{[X^{p_1}]}} \qquad \textbf{Eq. S26}$$

Here, both the numerator and denominator were divided by $[Mg^{2+}][X^{p_1}]$, then each term in the numerator is multiplied by $1 = \frac{[X^j]}{[X^j]}$

$$[X^{p_1}] + cH^+ \rightarrow [X^{p_1+c}] \qquad \textbf{Eq. S27}$$

where $p_1 < 0$, this reaction is defined to obtain an expression for $\frac{[X^j]}{[X^{p_1}]}$

$$pH = -log_{10}[H^+] \qquad \textbf{Eq. S28}$$

The pH is defined to remove reference to $[H^+]$, since pH is known from experiment.

$$K_a^{p_1+c} = \frac{[X^{p_1+c}]}{[X^{p_1}]c[H^+]} \quad \textbf{Eq. S29}$$

The equilibrium constant for **Eq. S27** is given in **Eq. S29**

$$pK_a = -log_{10}K_a \quad \textbf{Eq. S30}$$

Here pK_a which is measured experimentally is defined in terms of K_a

$$\frac{[X^{p_1+c}]}{[X^{p_1}]} = c10^{pH+pK_a^{p_1+c}} \quad \textbf{Eq. S31}$$

After manipulating **Eq. S29** and substituting **Eq. S30** and **Eq. S31** we obtain **Eq. S32**

$$c = j - p_1 \quad \textbf{Eq. S32}$$

By inspection of **Eq. S26**, c can be expressed as **Eq. S32**

$$\frac{[X^j]}{[X^{p_1}]} = (j - p_1)10^{pH+pK_a^j} \quad \textbf{Eq. S33}$$

Final expression for $\frac{[X^j]}{[X^{p_1}]}$

$$K_a = \frac{\sum_{i=1}^{i=l}\frac{[Mg^{2+}:X_i^{p_1}]}{[Mg^{2+}][X^{p_1}]} + \sum_{j=p_{1+1}}^{j=p_f}(j-p_1)10^{pH+pK_a^j}\sum_{i=1}^{i=l}\frac{[Mg^{2+}:X_i^j]}{[Mg^{2+}][X^j]}}{1+\sum_{j=p_1+1}^{j=p_f}(j-p_1)10^{pH+pK_a^j}} \quad \textbf{Eq. S34}$$

Eq. S33 substituted into **Eq. S26**

$$\Delta G = -RTlnK_a \quad \textbf{Eq. S35}$$

From statistical mechanics

$$K_{a,i}^j = e^{-\frac{\Delta G_i^j}{RT}} = \frac{[Mg^{2+}:X_i^j]}{[Mg^{2+}][X^j]} \quad \textbf{Eq. S36}$$

Here we manipulate **Eq. S35** and express in terms of free energy difference

$$K_a = \frac{\sum_{i=1}^{i=l} e^{-\frac{\Delta G_i^{p_1}}{RT}} + \sum_{j=p_{1+1}}^{j=p_f}(j-p_1)10^{pH+pK_a^j}\sum_{i=1}^{i=l} e^{-\frac{\Delta G_i^j}{RT}}}{1+\sum_{j=p_1+1}^{j=p_f}(j-p_1)10^{pH+pK_a^j}} \quad \textbf{Eq. S37}$$

Substituting **Eq. S36** into **Eq. S34**

$$\Delta G = -RTln\frac{\sum_{i=1}^{i=l} e^{-\frac{\Delta G_i^{p_1}}{RT}} + \sum_{j=p_{1+1}}^{j=p_f}(j-p_1)10^{pH+pK_a^j}\sum_{i=1}^{i=l} e^{-\frac{\Delta G_i^{j}}{RT}}}{1+\sum_{j=p_1+1}^{j=p_f}(j-p_1)10^{pH+pK_a^j}} \quad \textbf{Eq. S38}$$

Finally, ΔG expressed as ΔG_i^j from each binding mode simulation and pH, pK_awhich can be determined experimentally. If pK_a^j, which is defined relative to $[X^{p_1}]$, is not known but the pK_a between two consecutive protonation states are known, then pK_a^j can still be determined algebraically in terms of successive consecutive pK_a.

$$K_a^{i+j:i} = \frac{[X^{i+j}]}{[X^i]j[H^+]} = \frac{10^{-pH(j-1)}}{j}\prod_{l=1}^{l=j} K_a^{i+l:i+(l-1)} \quad \textbf{Eq. S39}$$

Formula for converting rate constants and hence pK_a when pK_a^j is not known.

$$K_a^{2:1} = K_a^{2:1}\frac{10^{-pH}(0)}{1} = K_a^{2:1} \quad \textbf{Eq. S40}$$

Checking the limiting case of the formula.

For the ATP^{-4} and ATP^{-3} simulations, we have $P = \{-4, -3\}$ and $l = \begin{Bmatrix} 3\ if\ j = -4 \\ 1\ if\ j = -3 \end{Bmatrix}$

$$\Delta G_{ATP} = -RTln\frac{\sum_{i=1}^{i=3} e^{-\frac{\Delta G_i^{-4}}{RT}} + \omega_{ATP}e^{-\frac{\Delta G_1^{-3}}{RT}}}{1+\omega_{ATP}} \quad \textbf{Eq. S41}$$

p_{ka} for the terminal phosphate is taken to be -6.66+/- .03 [5], where they define their equilibrium constant to be the inverse of Eq. S20, hence the negative sign. pKa measurements were taken from a range of pH data in NMR experiments. It is known that pH ranges from 7-7.4 under physiological conditions. Hence,

$$p_{ka} = -6.66, \delta p_{ka} = .03, pH = 7.2, \delta pH = .2$$

Deriving δΔG^{total}

$$A = f(X, Y, Z, \dots)$$

where A is a function of any number of variables, we want a general formula for the error δA

$$\delta A = \sqrt{(\frac{dA}{dX}\delta X)^2 + (\frac{dA}{dY}\delta Y)^2 + (\frac{dA}{dZ}\delta Z)^2 + \frac{dA}{dX}\delta X\frac{dA}{dY}\delta Y + \frac{dA}{dX}\delta X\frac{dA}{dZ}\delta Z + \frac{dA}{dY}\delta Y\frac{dA}{dZ}\delta Z + \cdots}$$

this expression works for any function, our goal is to obtain $\delta\Delta G$

$$\Delta G^j = -RTln(\sum_{i=1}^{i=l} e^{\frac{-\Delta G_i^j}{RT}})$$

we start by computing $\delta\Delta G^j$ for a single protonation state

$$S^j = \sum_{i=1}^{i=l} e^{\frac{-\Delta G_i^j}{RT}}$$

$$f_i^j = e^{\frac{-\Delta G_i^j}{RT}}$$

$$\delta\Delta G^j = \sqrt{\sum_{i=1}^{i=l} (\frac{\partial \Delta G^j}{\partial \Delta G_i^j} \delta\Delta G_i^j)^2}$$

$$\frac{\partial \Delta G^j}{\partial \Delta G_i^j} = \frac{\partial \Delta G^j}{\partial S^j} \frac{\partial S^j}{\partial \Delta G_i^j}$$

$$\frac{\partial \Delta G^j}{\partial S^j} = \frac{-RT}{S^j}$$

$$\frac{\partial S^j}{\partial \Delta G_i^j} = \sum_{i=1}^{i=l} \frac{\partial f_i^j}{\partial \Delta G_i^j} = \sum_{i=1}^{i=l} \frac{-1}{RT} e^{\frac{-\Delta G_i^j}{RT}} = \frac{-1}{RT} S^j$$

$$\frac{\partial \Delta G^j}{\partial \Delta G_i^j} = \frac{-RT}{S^j} \frac{-1}{RT} S^j = 1$$

$$\delta\Delta G^j = \sqrt{\sum_{i=1}^{i=l} (\delta\Delta G_i^j)^2}$$

now we can obtain $\delta\Delta G$ in a similar fashion

$$\Delta G(\omega^j, \{\Delta G_i^j\}) = -RTln\frac{\sum_{i=1}^{i=l} e^{-\frac{\Delta G_i^{p_1}}{RT}} + \sum_{j=p_{1+1}}^{j=p_f} \omega^j \sum_{i=1}^{i=l} e^{-\frac{\Delta G_i^j}{RT}}}{1 + \sum_{j=p_1+1}^{j=p_f} \omega^j}$$

$$\delta\,\Delta G = \sqrt{\sum_{j=p_1+1}^{j=p_f} (\frac{\partial \Delta G}{\partial \omega^j}\delta\omega^j)^2 + \sum_{j=p_1}^{j=p_f}\sum_{i=1}^{i=l} (\frac{\partial \Delta G}{\partial \Delta G_i^j}\delta\Delta G_i^j)^2}$$

we start by defining components of our expression for ΔG

$$\omega^j = \frac{[X^j]}{[X^{p_1}]} = (j - p_1)10^{pH+pK_a^j}$$

$$\frac{d\omega^j}{dp_{ka}} = \frac{d\omega^j}{dpH} = ln(10)\,(j - p_1)10^{pH+pK_a^j} = ln\,(10)\omega^j$$

$$\delta\omega^j = \omega^j ln\,(10)\sqrt{\delta {p_{ka}}^2 + \delta pH^2 + \delta p_{ka}\delta pH}$$

$$K_a = \frac{\sum_{i=1}^{i=l} e^{-\frac{\Delta G_i^{p_1}}{RT}} + \sum_{j=p_{1+1}}^{j=p_f} \omega^j \sum_{i=1}^{i=l} e^{-\frac{\Delta G_i^j}{RT}}}{1 + \sum_{j=p_1+1}^{j=p_f} \omega^j}$$

$$\frac{\partial \Delta G}{\partial \omega^j} = \frac{\partial \Delta G}{\partial K_a}\frac{\partial K_a}{\partial \omega^j}$$

$$M = 1 + \sum_{j=p_{1+1}}^{j=p_f} \omega^j$$

$$N = S^{p_1} + \sum_{j=p_{1+1}}^{j=p_f} \omega^j S^j$$

$$K_a = \frac{N}{M}$$

$$\frac{\partial K_a}{\partial \omega^j} = \frac{MS^j - S^{p_1} - N}{M^2}$$

$$\frac{\partial \Delta G}{\partial \omega^j} = \frac{-RT}{K_a}\frac{MS^j - S^{p_1} - N}{M^2}$$

$$\frac{\partial \Delta G}{\partial \Delta G_i^j} = \frac{\partial \Delta G}{\partial K_a}\frac{\partial K_a}{\partial \Delta G_i^j}$$

$$\frac{\partial K_a}{\partial \Delta G_i^j} = \frac{N}{RTM} = \frac{K_a}{RT}$$

$$\frac{\partial \Delta G}{\partial \Delta G_i^j} = \frac{-RT}{K_a}\frac{K_a}{RT} = -1$$

$$\delta\, \Delta G = \sqrt{\sum_{j=p_1+1}^{j=p_f} (\frac{\partial \Delta G}{\partial \omega^j}\delta\omega^j)^2 + \sum_{j=p_1}^{j=p_f}\sum_{i=1}^{i=l}(\delta \Delta G_i^j)^2}$$

For the ADP^{-3} and ADP^{-2} simulations, we have $P = \{-3, -2\}$ and $l = \begin{Bmatrix} 3\ if\ j = -3 \\ 3\ if\ j = -2 \end{Bmatrix}$

p_{ka} for the terminal phosphate is taken to be -6.47+/- .01 [5], where they define their equilibrium constant to be the inverse of Eq. S20, hence the negative sign. pKa measurements were taken from a range of pH data in NMR experiments. It is known that pH ranges from 7-7.4 under physiological conditions. Hence,

$$p_{ka} = -6.47, \delta p_{ka} = .01, pH = 7.2, \delta pH = .2$$

$$\Delta G_{ADP} = -RTln\frac{\sum_{i=1}^{i=3} e^{-\frac{\Delta G_i^{-4}}{RT}} + \omega_{ADP}\sum_{i=1}^{i=3} e^{-\frac{\Delta G_i^{-3}}{RT}}}{1 + \omega_{ADP}}$$

Parameters and Structures

ATP^{-4} Structure

```
43
 1  N 48.846001 39.464001 50.986000   251   10   11   15
 2  N 49.424999 41.488998 50.165001   255   11   12
 3  N 51.721001 41.568001 48.129002   253   13   41   42
 4  N 51.911999 39.273998 48.446999   257   13   14
 5  N 50.491001 38.015999 49.900002   256   14   15
 6  C 46.609001 40.422001 53.542000   324    7   25   32   33
 7  C 46.520000 38.988998 53.363998   312    6    8   26   34
 8  C 47.807999 38.874001 54.112000   318    7    9   27   35
 9  C 48.719002 38.116001 53.139000   316    8   10   28   37
10  C 48.132999 38.409000 51.721001   314    1    9   26   39
11  C 48.616001 40.841999 50.945000   248    1    2   40
12  C 50.231998 40.470001 49.664001   250    2   13   15
13  C 51.307999 40.466000 48.730999   249    3    4   12
14  C 51.493000 38.151001 49.028999   254    4    5   43
15  C 49.891998 39.252998 50.171001   247    1    5   12
16  O 45.778999 46.330002 56.051998   408   29
17  O 47.382000 44.497002 56.625999   408   29
18  O 45.972000 45.529999 58.375000   408   29
19  O 42.974998 42.722000 55.986000   410   30
20  O 43.603001 44.766998 54.678001   410   30
21  O 45.041000 44.014999 56.737999   405   29   30
22  O 46.380001 43.396000 52.787998   409   31
23  O 44.182999 42.189999 52.351002   409   31
24  O 44.917000 42.716000 54.789001   406   30   31
25  O 46.172001 41.568001 53.301998   407    6   31
26  O 46.785000 38.908001 51.948002   311    7   10
27  O 47.713001 38.356998 55.423000   346    8   36
28  O 48.632000 36.737000 53.424999   320    9   38
29  P 46.106998 45.181999 56.950001   404   16   17   18   21
30  P 43.910999 43.740002 55.654999   403   19   20   21   24
31  P 45.228001 42.668999 53.257000   401   22   23   24   25
32  H 47.666000 40.570000 53.221001   325    6
33  H 46.587002 40.459000 54.655998   325    6
34  H 45.665001 38.327000 53.639000   313    7
35  H 48.234001 39.869999 54.375000   319    8
36  H 48.532001 38.283001 55.897999   323   27
37  H 49.787998 38.422001 53.212002   317    9
38  H 49.195999 36.266998 52.821999   321   28
```

```
  39  H 48.202999 37.473999 51.117001   315    10
  40  H 47.835999 41.389999 51.499001   258    11
  41  H 52.491001 41.564999 47.459999   260     3
  42  H 51.939999 42.251999 48.852001   260     3
  43  H 52.035999 37.229000 48.758999   259    14
```

ATP^{-4} Parameters

```
atom       408   408   O    "ATP_-4_        "       8   15.999   1
atom       410   410   O    "ATP_-4_        "       8   15.999   1
atom       405   405   O    "ATP_-4_        "       8   15.999   2
atom       409   409   O    "ATP_-4_        "       8   15.999   1
atom       406   406   O    "ATP_-4_        "       8   15.999   2
atom       407   407   O    "ATP_-4_        "       8   15.999   2
atom       404   404   P    "ATP_-4_        "      15   30.974   4
atom       403   403   P    "ATP_-4_        "      15   30.974   4
atom       401   401   P    "ATP_-4_        "      15   30.974   4


multipole   401 -409 -409          1.65884
                      0.00000   0.00000  -0.16779
                      0.52438
                      0.00000  -0.18107
                      0.00000   0.00000  -0.34330
multipole   403 -410 -410          1.64959
                      0.00000   0.00000  -0.11250
                      0.32350
                      0.00000  -0.42348
                      0.00000   0.00000   0.09998
multipole   404  405    0          1.60022
                      0.00000   0.00000   0.27687
                      0.15044
                      0.00000   0.15044
                      0.00000   0.00000  -0.30087

multipole   407  324  401          -0.60147
                      0.20351   0.00000   0.45127
                     -0.12851
                      0.00000  -0.53163
                     -0.06004   0.00000   0.66014
multipole   405  403  404          -0.73555
                      0.19114   0.00000  -0.01220
                      0.22211
                      0.00000  -0.31758
                      0.05704   0.00000   0.09547
multipole   406  401  403          -0.73113
```

```
                      0.10639    0.00000   -0.02358
                      0.02209
                      0.00000   -0.23740
                     -0.00948    0.00000    0.21531


multipole   410  403  410          -0.97735
                      0.00000    0.00000    0.06641
                     -0.21878
                      0.00000   -0.08671
                      0.00000    0.00000    0.30549
multipole   408  404 -408 -408       -1.021117
                      0.00000    0.00000    0.07886
                     -0.13437
                      0.00000   -0.25646
                      0.00000    0.00000    0.39083
multipole   409  401  409          -0.98257
                      0.00000    0.00000    0.05254
                     -0.25775
                      0.00000   -0.13687
                      0.00000    0.00000    0.39462

multipole   324  325  312           0.17022
                      0.26025    0.00000    0.34835
                      0.07978
                      0.00000   -0.45645
                     -0.03790    0.00000    0.37667

multipole   325  324  407           0.01769
                     -0.00317    0.00000   -0.11654
                      0.10449
                      0.00000   -0.04493
                     -0.02925    0.00000   -0.05956



polarize    324         1.3340    0.3900 407 325
polarize    408         0.8370    0.3900 404
polarize    410         0.8370    0.3900 403
polarize    405         0.8370    0.3900 404 403
polarize    409         0.8370    0.3900 401
polarize    406         0.8370    0.3900 403 401
polarize    407         0.8370    0.3900 324 401
polarize    404         1.8280    0.3900 408 405
polarize    403         1.8280    0.3900 410 405 406
```

```
polarize     401          1.8280     0.3900 409 406 407


vdw       401  4.4500   0.3900
vdw       403  4.4500   0.3900
vdw       404  4.4500   0.3900
vdw       407  3.635    0.134
vdw       405  3.635    0.134
vdw       406  3.635    0.134
vdw       410  3.5534   0.09315
vdw       408  3.6300   0.1120
vdw       409  3.5534   0.09315
bond      72   407   465.1000    1.4275
bond      401   407   450.0000    1.7314
bond      401   406   450.0000    1.6162
bond      401   409   775.0000    1.5175
bond      403   405   450.0000    1.5911
bond      403   406   450.0000    1.7544
bond      403   410   775.0000    1.5155
bond      404   405   450.0000    1.8298
bond      404   408   775.0000    1.5499
angle     407   401   406    65.5800  100.2307
angle     407   401   409    75.8600  107.2560
angle     406   401   409    75.8600  113.6954
angle     409   401   409    89.8800  119.3235
angle     405   403   406    65.5800   96.1714
angle     405   403   410    75.8600  113.1563
angle     406   403   410    75.8600  104.3610
angle     410   403   410    89.8800  117.7377
angle     405   404   408    75.8600  104.7369
angle     408   404   408    89.8800  115.7929
angle     72   407   401    80.3000  115.0537
angle     403   405   404    80.0000  137.3775
angle     401   406   403    80.0000  144.5024
angle     66   72   407    88.0000  111.5292
angle     407   72   73    60.9900  113.1077
angle     407   72   73    60.9900  113.1077
strbnd    407   401   406    14.4000   14.4000
strbnd    407   401   409    14.4000   14.4000
strbnd    406   401   409    14.4000   14.4000
strbnd    405   403   406    14.4000   14.4000
strbnd    405   403   410    14.4000   14.4000
strbnd    406   403   410    14.4000   14.4000
strbnd    405   404   408    14.4000   14.4000
strbnd    408   404   408    14.4000   14.4000
```

```
strbnd    72   407   401    38.0000   38.0000
strbnd    403   405   404    38.0000   38.0000
strbnd    401   406   403    38.0000   38.0000
torsion 73 72 407 401 0.000 0.0 1 0.000 180.0 2 0.120 0.0 3
torsion 406 401 407 72 0.525 0.0 1 4.208 180.0 2 0.158 0.0 3
torsion 409 401 407 72 -11.673 0.0 1 6.705 180.0 2 0.158 0.0 3
torsion 407 401 406 403 -0.379 0.0 1 -1.596 180.0 2 -6.626 0.0 3
torsion 409 401 406 403 -6.626 0.0 1 -0.432 180.0 2 3.794 0.0 3
torsion 406 403 405 404 -3.253 0.0 1 -2.994 180.0 2 -3.649 0.0 3
torsion 410 403 405 404 3.279 0.0 1 -1.944 180.0 2 3.037 0.0 3
torsion 405 403 406 401 1.225 0.0 1 -2.189 180.0 2 3.859 0.0 3
torsion 410 403 406 401 3.859 0.0 1 -0.220 180.0 2 -1.321 0.0 3
torsion 408 404 405 403 0.382 0.0 1 -1.372 180.0 2 0.068 0.0 3
torsion 68 66 72 407 -0.401 0.0 1 0.496 180.0 2 2.714 0.0 3
torsion 65 66 72 407 1.333 0.0 1 -1.311 180.0 2 0.000 0.0 3
torsion 67 66 72 407 0.000 0.0 1 0.287 180.0 2 0.132 0.0 3
torsion 66 72 407 401 0.000 0.0 1 1.905 180.0 2 0.000 0.0 3
```

ADP^{-3} Structure

```
39
 1  P     5.964377   -1.636630   -0.545396   404    2    3    4    8
 2  O     6.045092   -2.405908    0.772319   408    1
 3  O     5.513452   -2.426790   -1.776554   408    1
 4  O     7.014181   -0.549889   -0.775944   408    1
 5  P     3.705822    0.508024    0.607352   401    6    7    8    9
 6  O     3.234992    0.091514    1.996929   409    5
 7  O     4.192431    1.946246    0.444407   409    5
 8  O     4.330281   -0.583185   -0.309930   406    1    5
 9  O     2.101231    0.605555   -0.285963   407    5   10
10  C     1.338100    1.543596    0.357333   324    9   11   28   29
11  C    -0.014391    1.713924   -0.290226   312   10   12   13   30
12  O    -0.811417    0.498570   -0.271838   311   11   17
13  C    -0.875972    2.764745    0.417045   318   11   14   15   31
14  O    -0.889506    4.024163   -0.280563   346   13   32
15  C    -2.311621    2.194049    0.396933   316   13   16   17   33
16  O    -3.274729    3.089575   -0.129444   320   15   34
17  C    -2.135396    0.911864   -0.445215   314   12   15   18   35
18  N    -2.973329   -0.195799    0.004854   251   17   19   27
19  C    -2.615038   -1.134970    0.941951   248   18   20   36
20  N    -3.584097   -2.007380    1.223339   255   19   21
21  C    -4.617833   -1.596160    0.417445   250   20   22   27
22  C    -5.890567   -2.138566    0.185609   249   21   23   24
23  N    -6.352464   -3.218636    0.919433   253   22   37   38
24  N    -6.700859   -1.573627   -0.719838   257   22   25
```

25	C	-6.230315	-0.487714	-1.386361	254	24	26	39
26	N	-5.047191	0.123181	-1.277847	256	25	27	
27	C	-4.266703	-0.477435	-0.358636	247	18	21	26
28	H	1.800042	2.559591	0.353167	325	10		
29	H	1.170733	1.293919	1.425076	325	10		
30	H	0.105745	2.002360	-1.348482	313	11		
31	H	-0.519766	2.920012	1.442383	319	13		
32	H	0.026407	4.154132	-0.589423	323	14		
33	H	-2.632419	1.903681	1.404585	317	15		
34	H	-2.735445	3.748168	-0.613724	321	16		
35	H	-2.404892	1.121367	-1.494198	315	17		
36	H	-1.611442	-1.146891	1.349728	258	19		
37	H	-7.058661	-3.753470	0.425827	260	23		
38	H	-5.598846	-3.783195	1.299992	260	23		
39	H	-6.918520	-0.063556	-2.116447	259	25		

ADP^{-3} Parameters

```
atom      408  408  O   "ADP_-3_      "     8   15.999   1
atom      409  409  O   "ADP_-3_      "     8   15.999   1
atom      406  406  O   "ADP_-3_      "     8   15.999   2
atom      407  407  O   "ADP_-3_      "     8   15.999   2
atom      404  404  P   "ADP_-3_      "    15   30.974   4
atom      401  401  P   "ADP_-3_      "    15   30.974   4

polarize  72       1.3340   0.3900 407 73
polarize  408      0.8370   0.3900 404
polarize  409      0.8370   0.3900 401
polarize  406      0.8370   0.3900 404 401
polarize  407      0.8370   0.3900 72 401
polarize  404      1.8280   0.3900 408 406
polarize  401      1.8280   0.3900 409 406 407


vdw     401  4.4500   0.3900
vdw     404  4.4500   0.3900
vdw     407  3.635    0.134
vdw     406  3.635    0.134
vdw     408  3.6300   0.1120
vdw     409  3.5534   0.09315
bond    72   407   465.1000   1.4275
bond    401  407   450.0000   1.7314
```

```
bond     401   406   450.0000    1.6162
bond     401   409   775.0000    1.5175
bond     404   406   450.0000    1.7544
bond     404   406   450.0000    1.8298
bond     404   408   775.0000    1.5499
angle    407   401   406    65.5800  100.2307
angle    407   401   409    75.8600  107.2560
angle    406   401   409    75.8600  113.6954
angle    409   401   409    89.8800  119.3235
angle    406   404   408    75.8600  104.7369
angle    408   404   408    89.8800  115.7929
angle    72   407   401    80.3000  115.0537
angle    401   406   404    80.0000  137.3775
angle    66   72   407    88.0000  111.5292
angle    407   72   73    60.9900  113.1077
angle    407   72   73    60.9900  113.1077
strbnd   407   401   406    14.4000   14.4000
strbnd   407   401   409    14.4000   14.4000
strbnd   406   401   409    14.4000   14.4000
strbnd   406   404   408    14.4000   14.4000
strbnd   408   404   408    14.4000   14.4000
strbnd   72   407   401    38.0000   38.0000
strbnd   401   406   404    38.0000   38.0000
torsion 73 72 407 401 2 0.0 1 -1.5 180.0 2 .89 0.0 3
torsion 406 401 407 72 .292 0.0 1 9.634 180.0 2 -5 0.0 3
torsion 409 401 407 72 -11.673 0.0 1 6.705 180.0 2 0.158 0.0 3
torsion 407 401 406 404 -.969 0.0 1 3.663 180.0 2 3.663 0.0 3
torsion 409 401 406 404 -3.663 0.0 1 3.072 180.0 2 -2.508 0.0 3
torsion 408 404 406 401 1.616 0.0 1 -1.616 180.0 2 .084 0.0 3
torsion 68 66 72 407 -0.401 0.0 1 0.496 180.0 2 2.714 0.0 3
torsion 65 66 72 407 1.333 0.0 1 -1.311 180.0 2 0.000 0.0 3
torsion 67 66 72 407 0.000 0.0 1 0.287 180.0 2 0.132 0.0 3
torsion 66 72 407 401 0.000 0.0 1 1.905 180.0 2 0.000 0.0 3

#
# Multipoles from Electrostatic Potential Fitting
#

multipole   404  406                1.60022
                           0.00000    0.00000    0.11165
                           0.13660
                           0.00000    0.13660
                           0.00000    0.00000   -0.27320
multipole   408  404 -408 -408        -1.02112
                           0.00000    0.00000    0.00641
                          -0.20971
```

```
                    0.00000   -0.17070
                    0.00000    0.00000    0.38041
multipole   401 -409 -409          1.65884
                    0.00000    0.00000   -0.26703
                    0.52475
                    0.00000   -0.19493
                    0.00000    0.00000   -0.32982
multipole   409  401  409         -0.98257
                    0.00000    0.00000    0.12264
                   -0.34301
                    0.00000   -0.23050
                    0.00000    0.00000    0.57351
multipole   406  401  404         -0.73113
                    0.18243    0.00000   -0.17650
                    0.15520
                    0.00000   -0.21086
                   -0.25394    0.00000    0.05566
multipole   407  324  401         -0.62180
                    0.21606    0.00000    0.36656
                   -0.46697
                    0.00000   -1.18459
                   -0.10116    0.00000    1.65156
multipole   324  325  312          0.14989
                    0.08925    0.00000   -0.04985
                    0.75354
                    0.00000    0.26636
                    0.36988    0.00000   -1.01990
multipole   325  324  407          0.01769
                    0.01700    0.00000   -0.06026
                    0.39170
                    0.00000   -0.15610
                   -0.05260    0.00000   -0.23560
```

ATP^{-3} Structure

```
 44
  1  P     5.672477   -2.414807   -0.898371   401    2    3    4    8
  2  O     5.937816   -3.372489    0.239965   412    1
  3  O     5.214209   -2.950802   -2.238578   412    1
  4  O     7.015494   -1.442875   -1.124316   408    1   32
  5  P     4.777097    0.058056    0.558939   402    6    7    8   12
  6  O     4.938001   -0.354427    1.995643   411    5
  7  O     5.784121    0.989885   -0.100197   411    5
  8  O     4.574133   -1.215178   -0.473923   407    1    5
  9  P     2.313727    1.881756    0.870818   403   10   11   12   13
```

10	O	2.708473	3.234145	0.315545	409	9			
11	O	1.864837	1.760985	2.309752	409	9			
12	O	3.210692	0.655255	0.338657	406	5	9		
13	O	0.920731	1.417937	-0.067602	405	9	14		
14	C	-0.094015	2.326208	0.176826	324	13	15	33	34
15	C	-1.344549	1.992891	-0.603628	312	14	16	17	35
16	O	-1.867492	0.717345	-0.245522	311	15	21		
17	C	-2.449961	2.999227	-0.263743	318	15	18	19	36
18	O	-2.564290	4.054090	-1.227840	346	17	37		
19	C	-3.753394	2.166030	-0.299330	316	17	20	21	38
20	O	-4.707437	2.650254	-1.224895	320	19	39		
21	C	-3.232615	0.753342	-0.657808	314	16	19	22	40
22	N	-3.895947	-0.316795	0.063123	251	21	23	31	
23	C	-3.513037	-0.827396	1.285017	248	22	24	41	
24	N	-4.322851	-1.778376	1.744833	255	23	25		
25	C	-5.276265	-1.881199	0.757078	250	24	26	31	
26	C	-6.375659	-2.740951	0.609005	249	25	27	28	
27	N	-6.726394	-3.630221	1.601471	253	26	42	43	
28	N	-7.137274	-2.661410	-0.492046	257	26	29		
29	C	-6.787104	-1.741216	-1.427860	254	28	30	44	
30	N	-5.768968	-0.874078	-1.426579	256	29	31		
31	C	-5.034535	-0.991729	-0.303768	247	22	25	30	
32	H	6.749586	-0.517618	-0.907500	413	4			
33	H	0.193150	3.363415	-0.102746	325	14			
34	H	-0.365901	2.350745	1.249353	325	14			
35	H	-1.150287	2.012234	-1.690060	313	15			
36	H	-2.275380	3.421005	0.734738	319	17			
37	H	-1.650142	4.342123	-1.414487	323	18			
38	H	-4.225662	2.122280	0.691106	317	19			
39	H	-4.201568	3.288306	-1.770148	321	20			
40	H	-3.368706	0.572847	-1.736745	315	21			
41	H	-2.601803	-0.483256	1.760588	258	23			
42	H	-7.273111	-4.415069	1.265373	260	27			
43	H	-5.957313	-3.874389	2.217266	260	27			
44	H	-7.429820	-1.715762	-2.307397	259	29			

ATP^{-3} Parameters

atom	412	412	O	"ATP_-3_firstopt "	8	15.999	1
atom	408	408	O	"ATP_-3_firstopt "	8	15.999	2
atom	411	411	O	"ATP_-3_firstopt "	8	15.999	1
atom	407	407	O	"ATP_-3_firstopt "	8	15.999	2
atom	409	409	O	"ATP_-3_firstopt "	8	15.999	1
atom	406	406	O	"ATP_-3_firstopt "	8	15.999	2
atom	405	405	O	"ATP_-3_firstopt "	8	15.999	2

```
atom       401  401   P    "ATP_-3_firstopt    "      15   30.974   4
atom       402  402   P    "ATP_-3_firstopt    "      15   30.974   4
atom       403  403   P    "ATP_-3_firstopt    "      15   30.974   4
atom       413  413   H     "ATP_-3_firstopt    "      1    1.008   1


polarize    412         0.8370    0.3900 401
polarize    408         0.8370    0.3900 401 413
polarize    411         0.8370    0.3900 402
polarize    407         0.8370    0.3900 401 402
polarize    409         0.8370    0.3900 403
polarize    406         0.8370    0.3900 402 403
polarize    405         0.8370    0.3900 72 403
polarize    401         1.8280    0.3900 412 408 407
polarize    402         1.8280    0.3900 411 407 406
polarize    403         1.8280    0.3900 409 406 405
polarize    413         0.4960    0.3900 408


vdw      403  4.4500   0.3900
vdw      402  4.4500   0.3900
vdw      401  4.4500   0.3900
vdw      405  3.4050   0.1100
vdw      407  3.635    0.134
vdw      408  3.62     0.08
vdw      406  3.635    0.134
vdw      428  2.8700   0.0240 0.910
vdw      412  3.635    0.08
vdw      411  3.5534   0.09315
vdw      409  3.5534   0.09315
vdw      413  2.6650   0.0150 0.910
bond     72   405   465.1000    1.4179
bond     403   405   450.0000    1.7075
bond     403   406   450.0000    1.6660
bond     403   409   775.0000    1.5074
bond     402   407   450.0000    1.6482
bond     402   406   450.0000    1.6612
bond     402   411   775.0000    1.5184
bond     401   407   450.0000    1.6772
bond     401   408   450.0000    1.6485
bond     401   412   775.0000    1.5282
bond     408   413   560.0000    0.9995
angle    405   403   406    65.5800  100.0875
angle    405   403   409    75.8600  106.3537
angle    406   403   409    75.8600  111.8154
angle    409   403   409    89.8800  123.8772
```

```
angle    407   402   406    65.5800   98.2091
angle    407   402   411    75.8600  108.5940
angle    406   402   411    75.8600  112.2672
angle    411   402   411    89.8800  119.9765
angle    407   401   408    65.5800  100.2188
angle    407   401   412    75.8600  111.5471
angle    408   401   412    75.8600  111.6206
angle    412   401   412    89.8800  119.1585
angle     72   405   403    80.3000  112.3553
angle    402   407   401    80.0000  129.7663
angle    401   408   413    60.0000  104.8737
angle    403   406   402    80.0000  134.3005
angle     66    72   405    88.0000  109.4043
angle    405    72    73    60.9900  110.9434
strbnd   405   403   406    14.4000   14.4000
strbnd   405   403   409    14.4000   14.4000
strbnd   406   403   409    14.4000   14.4000
strbnd   407   402   406    14.4000   14.4000
strbnd   407   402   411    14.4000   14.4000
strbnd   406   402   411    14.4000   14.4000
strbnd   407   401   408    14.4000   14.4000
strbnd   407   401   412    14.4000   14.4000
strbnd   408   401   412    14.4000   14.4000
strbnd    72   405   403    38.0000   38.0000
strbnd   402   407   401    38.0000   38.0000
strbnd   401   408   413    -4.5000   38.0000
strbnd   403   406   402    38.0000   38.0000
torsion 73 72 405 403 2 0.0 1 -1.5 180.0 2 .89 0.0 3
torsion 406 403 405 72 4.724 0.0 1 5.303 180.0 2 4.659 0.0 3
torsion 409 403 405 72 -2.155 0.0 1 7.602 180.0 2 -1.328 0.0 3
torsion 405 403 406 402 -1.999 0.0 1 3.795 180.0 2 -6.694 0.0 3
torsion 409 403 406 402 3.246 0.0 1 2.053 180.0 2 3.735 0.0 3
torsion 406 402 407 401 -.277 0.0 1 -.298 180.0 2 -7.506 0.0 3
torsion 411 402 407 401 -3.095 0.0 1 .326 180.0 2 1.844 0.0 3
torsion 407 402 406 403 2.034 0.0 1 4.705 180.0 2 2.705 0.0 3
torsion 411 402 406 403 1.043 0.0 1 2.635 180.0 2 -1.284 0.0 3
torsion 408 401 407 402 7.143 0.0 1 -7.143 180.0 2 -7.413 0.0 3
torsion 412 401 407 402 5.684 0.0 1 -6.188 180.0 2 4.883 0.0 3
torsion 407 401 408 413 -2 0.0 1 -1.68 180.0 2 -.8 0.0 3
torsion 412 401 408 413 -2 0.0 1 -1.68 180.0 2 -.8 0.0 3
torsion   68   66   72   405    -1.1500 0.0 1     0.0000 180.0 2     1.2800 0.0 3
torsion   65   66   72   405     2.2200 0.0 1    -1.3800 180.0 2    -1.1800 0.0 3
torsion   67   66   72   405     0.0000 0.0 1     0.0000 180.0 2     0.3000 0.0 3
torsion   66   72   405   403     0.0000 0.0 1     0.0000 180.0 2     0.0000 0.0 3
torsion   402   403   416   438    -1.3720 0.0 1     0.2320 180.0 2     0.4000 0.0 3
```

```
multipole   324  312  405            0.162195
                         0.11521    0.00000    0.15173
                         0.40225
                         0.00000   -0.32124
                         0.15284    0.00000   -0.08101

multipole   325  324  405            0.01769
                        -0.00317    0.00000   -0.11654
                         0.10449
                         0.00000   -0.04493
                        -0.02925    0.00000   -0.05956


#
# Multipoles from Electrostatic Potential Fitting
#

multipole   401 -412 -412            1.66729
                         0.00000    0.00000    0.10131
                         0.14017
                         0.00000    0.52990
                         0.00000    0.00000   -0.67007
multipole   412  401  412           -0.98202
                         0.00000    0.00000   -0.07795
                        -0.20537
                         0.00000   -0.03481
                         0.00000    0.00000    0.24018
multipole   408  401  413           -0.68650
                         0.23542    0.00000    0.04548
                         0.43290
                         0.00000   -0.40447
                         0.40132    0.00000   -0.02843
multipole   402 -411 -411            1.64139
                         0.00000    0.00000    0.03417
                         0.70341
                         0.00000   -0.36141
                         0.00000    0.00000   -0.34200
multipole   411  402  411           -0.95382
                         0.00000    0.00000   -0.07482
                        -0.28331
                         0.00000   -0.09124
                         0.00000    0.00000    0.37455
multipole   407  402  401           -0.66684
                         0.10527    0.00000    0.03797
```

```
                          1.08606
                          0.00000   -0.48190
                         -0.11713    0.00000   -0.60416
multipole   403 -409 -409            1.63400
                          0.00000    0.00000   -0.30439
                          0.24135
                          0.00000   -0.24848
                          0.00000    0.00000    0.00713
multipole   409  403  409           -0.95177
                          0.00000    0.00000    0.06439
                         -0.26691
                          0.00000   -0.36817
                          0.00000    0.00000    0.63508
multipole   406  403  402           -0.67371
                          0.24454    0.00000   -0.05151
                          0.18252
                          0.00000   -0.15574
                         -0.10601    0.00000   -0.02678
multipole   405  324  403           -0.52873
                          0.09346    0.00000    0.30704
                          0.57876
                          0.00000   -1.22241
                         -0.99158    0.00000    0.64365
multipole   413  408  401            0.25366
                          0.05887    0.00000   -0.06874
                          0.66394
                          0.00000    0.23193
                          0.52045    0.00000   -0.89587
```

ADP^{-2} Structure

```
  40
   1  P    -5.587153   -1.597173    0.448467   401    2    3    4    8
   2  O    -5.754890   -2.505808   -0.732154   412    1
   3  O    -5.015972   -2.548862    1.715137   408    1   28
   4  O    -6.679173   -0.712047    0.989585   412    1
   5  P    -3.688462    0.533441   -0.626246   403    6    7    8    9
   6  O    -3.414189    0.119342   -2.048794   409    5
   7  O    -4.350123    1.851677   -0.306407   409    5
   8  O    -4.159173   -0.692806    0.338137   406    1    5
   9  O    -2.129963    0.622724    0.150097   405    5   10
  10  C    -1.389007    1.637139   -0.449942   324    9   11   29   30
  11  C    -0.032066    1.747574    0.193539   312   10   12   13   31
  12  O     0.733891    0.535512    0.045653   311   11   17
  13  C     0.851276    2.841802   -0.413997   318   11   14   15   32
  14  O     0.797840    4.071075    0.322720   346   13   33
```

15	C	2.290098	2.276519	-0.307515	316	13	16	17	34
16	O	3.175428	3.108980	0.412669	320	15	35		
17	C	2.050614	0.907641	0.371994	314	12	15	18	36
18	N	2.918069	-0.149531	-0.117296	251	17	19	27	
19	C	2.657515	-0.989948	-1.173616	248	18	20	37	
20	N	3.646584	-1.842019	-1.436276	255	19	21		
21	C	4.593407	-1.524565	-0.490081	250	20	22	27	
22	C	5.840082	-2.095260	-0.185726	249	21	23	24	
23	N	6.382401	-3.092864	-0.968416	253	22	38	39	
24	N	6.547989	-1.623081	0.849607	257	22	25		
25	C	6.010380	-0.606025	1.568863	254	24	26	40	
26	N	4.842111	0.020963	1.399142	256	25	27		
27	C	4.166879	-0.484960	0.350997	247	18	21	26	
28	H	-4.868964	-1.916213	2.438713	413	3			
29	H	-1.883096	2.624040	-0.351901	325	10			
30	H	-1.250097	1.452693	-1.528996	325	10			
31	H	-0.145566	1.947590	1.272724	313	11			
32	H	0.572956	3.023867	-1.459478	319	13			
33	H	-0.137258	4.212175	0.557979	323	14			
34	H	2.718653	2.100734	-1.301315	317	15			
35	H	2.593326	3.747263	0.872569	321	16			
36	H	2.221344	1.002961	1.456153	315	17			
37	H	1.705415	-0.951413	-1.687047	258	19			
38	H	7.071870	-3.655857	-0.483548	260	23			
39	H	5.692415	-3.623444	-1.489805	260	23			
40	H	6.618657	-0.260480	2.403059	259	25			

ADP^{-2} Parameters

atom	412	412	O	"ADP_-2_firstopt "	8	15.999	1
atom	408	408	O	"ADP_-2_firstopt "	8	15.999	2
atom	409	409	O	"ADP_-2_firstopt "	8	15.999	1
atom	406	406	O	"ADP_-2_firstopt "	8	15.999	2
atom	405	405	O	"ADP_-2_firstopt "	8	15.999	2
atom	401	401	P	"ADP_-2_firstopt "	15	30.974	4
atom	403	403	P	"ADP_-2_firstopt "	15	30.974	4
atom	413	413	H	"ADP_-2_firstopt "	1	1.008	1

polarize	412	0.8370	0.3900 401
polarize	408	0.8370	0.3900 401 413
polarize	411	0.8370	0.3900 402
polarize	409	0.8370	0.3900 403
polarize	406	0.8370	0.3900 401 403
polarize	405	0.8370	0.3900 72 403
polarize	401	1.8280	0.3900 412 408 406

```
polarize    403         1.8280     0.3900 409 406 405
polarize    413         0.4960     0.3900 408


vdw       403  4.4500   0.3900
vdw       401  4.4500   0.3900
vdw       405  3.635    0.134
vdw       408  3.62     0.08
vdw       406  3.635    0.134
vdw       412  3.635    0.08
vdw       409  3.5534   0.09315
vdw       413  2.6650   0.0150 0.910
bond      72   405   465.1000    1.4179
bond      403   405   450.0000    1.7075
bond      403   406   450.0000    1.6660
bond      403   409   775.0000    1.5074
bond      401   406   450.0000    1.6772
bond      401   408   450.0000    1.6485
bond      401   412   775.0000    1.5282
bond      408   413   560.0000    0.9995
angle     405   403   406    65.5800  100.0875
angle     405   403   409    75.8600  106.3537
angle     406   403   409    75.8600  111.8154
angle     409   403   409    89.8800  123.8772
angle     406   401   408    65.5800  100.2188
angle     406   401   412    75.8600  111.5471
angle     408   401   412    75.8600  111.6206
angle     412   401   412    89.8800  119.1585
angle     72   405   403    80.3000  112.3553
angle     403   406   401    80.0000  129.7663
angle     401   408   413    60.0000  104.8737
angle     66   72   405    88.0000  109.4043
angle     405   72   73    60.9900  110.9434
strbnd    405   403   406    14.4000   14.4000
strbnd    405   403   409    14.4000   14.4000
strbnd    406   403   409    14.4000   14.4000
strbnd    406   401   408    14.4000   14.4000
strbnd    406   401   412    14.4000   14.4000
strbnd    408   401   412    14.4000   14.4000
strbnd    72   405   403    38.0000   38.0000
strbnd    403   406   401    38.0000   38.0000
strbnd    401   408   413    -4.5000   38.0000
torsion 73 72 405 403 0.000 0.0 1 0.000 180.0 2 0.120 0.0 3
torsion 406 403 405 72 -1.645 0.0 1 7.024 180.0 2 3.370 0.0 3
torsion 409 403 405 72 -8.877 0.0 1 8.398 180.0 2 -0.665 0.0 3
torsion 405 403 406 401 2.282 0.0 1 -3.221 180.0 2 -7.996 0.0 3
```

```
torsion 409 403 406 401 -0.714 0.0 1 -1.015 180.0 2 2.289 0.0 3
torsion 408 401 406 403 7.269 0.0 1 -7.269 180.0 2 -7.269 0.0 3
torsion 412 401 406 403 3.211 0.0 1 -5.160 180.0 2 5.226 0.0 3
torsion 406 401 408 413 -2.0000 0.0 1 -1.6800 180.0 2 -0.8000 0.0 3
torsion 412 401 408 413 -2.0000 0.0 1 -1.6800 180.0 2 -0.8000 0.0 3
torsion   68   66   72   405    -1.1500 0.0 1     0.0000 180.0 2     1.2800 0.0 3
torsion   65   66   72   405     2.2200 0.0 1    -1.3800 180.0 2    -1.1800 0.0 3
torsion   67   66   72   405     0.0000 0.0 1     0.0000 180.0 2     0.3000 0.0 3
torsion   66   72   405   403     0.0000 0.0 1     0.0000 180.0 2     0.0000 0.0 3

#
# Multipoles from Electrostatic Potential Fitting
#

multipole   401 -412 -412             1.66729
                          0.00000    0.00000    0.04808
                          0.33006
                          0.00000    0.00933
                          0.00000    0.00000   -0.33939
multipole   412  401  412            -0.98202
                          0.00000    0.00000   -0.14386
                         -0.06903
                          0.00000   -0.20917
                          0.00000    0.00000    0.27820
multipole   408  401  413            -0.68650
                          0.05468    0.00000   -0.00686
                          0.60648
                          0.00000   -0.60474
                         -0.79861    0.00000   -0.00174
multipole   403 -409 -409             1.63400
                          0.00000    0.00000   -0.23225
                          0.36132
                          0.00000   -0.50822
                          0.00000    0.00000    0.14690
multipole   409  403  409            -0.95177
                          0.00000    0.00000   -0.07762
                         -0.29123
                          0.00000    0.15075
                          0.00000    0.00000    0.14048
multipole   406  403  401            -0.67371
                          0.23593    0.00000   -0.05664
                         -0.17473
                          0.00000   -0.05279
                          0.36239    0.00000    0.22752
multipole   405  324  403            -0.47759
                          0.24549    0.00000    0.37624
```

```
                          -0.57275
                           0.00000   -1.35859
                          -0.14316    0.00000    1.93134
multipole   324  312  405             0.21334
                           0.13390    0.00000   -0.01923
                           0.67733
                           0.00000   -0.34328
                          -0.82455    0.00000   -0.33405
multipole   413  408  401             0.25366
                          -0.04961    0.00000    0.02119
                          -0.20109
                           0.00000   -0.06829
                          -0.12161    0.00000    0.26938
```

GTP^{-4} Structure

```
  44
   1  P     5.790498   -2.659318   -0.949177   404     2     3     4     5
   2  O     7.262233   -2.531069   -0.526685   408     1
   3  O     5.536152   -2.736287   -2.465725   408     1
   4  O     4.926251   -3.599865   -0.098633   408     1
   5  O     5.086785   -0.944567   -0.617522   405     1     6
   6  P     5.230997    0.150064    0.517692   403     5     7     8     9
   7  O     5.026773   -0.311535    1.941857   410     6
   8  O     6.265982    1.219872    0.220882   410     6
   9  O     3.631583    1.057190    0.090276   406     6    10
  10  P     2.671674    2.115291    0.738206   401     9    11    12    13
  11  O     2.117609    1.853151    2.131865   409    10
  12  O     2.923671    3.572095    0.356405   409    10
  13  O     1.237806    1.721645   -0.299164   407    10    14
  14  C     0.162768    2.458304    0.141008   324    13    15    33    34
  15  C    -1.053361    2.153534   -0.704107   312    14    16    17    35
  16  O    -1.456494    0.752769   -0.463056   311    15    21
  17  C    -2.284290    3.006007   -0.356040   318    15    18    19    36
  18  O    -2.724423    3.728024   -1.515769   346    17    37
  19  C    -3.351282    1.976934    0.028403   316    17    20    21    38
  20  O    -4.665256    2.372412   -0.392775   320    19    39
  21  C    -2.826528    0.689817   -0.621244   314    16    19    22    40
  22  N    -3.310920   -0.510654    0.061161   280    21    23    32
  23  C    -2.722722   -1.191051    1.104667   276    22    24    41
  24  N    -3.530789   -2.108775    1.638750   282    23    25
  25  C    -4.694725   -1.990964    0.923246   279    24    26    32
  26  C    -5.948556   -2.677717    1.066005   274    25    27    28
  27  O    -6.330626   -3.552722    1.841853   285    26
```

28	N	-6.874655	-2.177641	0.087265	277	26	29	42
29	C	-6.663953	-1.163456	-0.808278	273	28	30	31
30	N	-7.777978	-0.798112	-1.586395	278	29	43	44
31	N	-5.533028	-0.521648	-0.925823	283	29	32	
32	C	-4.584929	-0.980559	-0.040664	275	22	25	31
33	H	-0.095955	2.258370	1.199144	325	14		
34	H	0.333880	3.553798	0.058899	325	14		
35	H	-0.824360	2.255869	-1.770583	313	15		
36	H	-2.070373	3.702656	0.464236	319	17		
37	H	-3.698442	3.712072	-1.446834	323	18		
38	H	-3.340362	1.814179	1.115376	317	19		
39	H	-5.105357	1.566619	-0.729508	321	20		
40	H	-3.159025	0.622905	-1.674495	315	21		
41	H	-1.690481	-1.000132	1.378767	286	23		
42	H	-7.813859	-2.549477	0.197460	284	28		
43	H	-8.169551	-1.597959	-2.079965	287	30		
44	H	-7.470947	-0.105625	-2.266479	287	30		

GTP^{-4} Parameters

parameters /home/bdw2292/Tinker-8.4.3/params/amoebabio18.prm
fix-monopole
potential-fit 1 2 3 4 5 6 7 8 9 10 11 12 13 14 33 34

atom	408	408	O	"GTP_-4_ "	8	15.999	1
atom	410	410	O	"GTP_-4_ "	8	15.999	1
atom	405	405	O	"GTP_-4_ "	8	15.999	2
atom	409	409	O	"GTP_-4_ "	8	15.999	1
atom	406	406	O	"GTP_-4_ "	8	15.999	2
atom	407	407	O	"GTP_-4_ "	8	15.999	2
atom	404	404	P	"GTP_-4_ "	15	30.974	4
atom	403	403	P	"GTP_-4_ "	15	30.974	4
atom	401	401	P	"GTP_-4_ "	15	30.974	4

polarize	72	1.3340	0.3900 407 73
polarize	408	0.8370	0.3900 404
polarize	410	0.8370	0.3900 403
polarize	405	0.8370	0.3900 404 403
polarize	409	0.8370	0.3900 401
polarize	406	0.8370	0.3900 403 401
polarize	407	0.8370	0.3900 72 401
polarize	404	1.8280	0.3900 408 405
polarize	403	1.8280	0.3900 410 405 406
polarize	401	1.8280	0.3900 409 406 407

```
vdw      401  4.4500   0.3900
vdw      403  4.4500   0.3900
vdw      404  4.4500   0.3900
vdw      407  3.635    0.134
vdw      405  3.635    0.134
vdw      406  3.635    0.134
vdw      410  3.5534   0.09315
vdw      408  3.63     0.1120
vdw      409  3.5534   0.09315
bond     72   407   465.1000    1.4275
bond     401   407   450.0000    1.7314
bond     401   406   450.0000    1.6162
bond     401   409   775.0000    1.5175
bond     403   405   450.0000    1.5911
bond     403   406   450.0000    1.7544
bond     403   410   775.0000    1.5155
bond     404   405   450.0000    1.8298
bond     404   408   775.0000    1.5499
angle    407   401   406    65.5800  100.2307
angle    407   401   409    75.8600  107.2560
angle    406   401   409    75.8600  113.6954
angle    409   401   409    89.8800  119.3235
angle    405   403   406    65.5800   96.1714
angle    405   403   410    75.8600  113.1563
angle    406   403   410    75.8600  104.3610
angle    410   403   410    89.8800  117.7377
angle    405   404   408    75.8600  104.7369
angle    408   404   408    89.8800  115.7929
angle    72   407   401    80.3000  115.0537
angle    403   405   404    80.0000  137.3775
angle    401   406   403    80.0000  144.5024
angle    66   72   407    88.0000  111.5292
angle    407   72   73    60.9900  113.1077
angle    407   72   73    60.9900  113.1077
strbnd   407   401   406    14.4000   14.4000
strbnd   407   401   409    14.4000   14.4000
strbnd   406   401   409    14.4000   14.4000
strbnd   405   403   406    14.4000   14.4000
strbnd   405   403   410    14.4000   14.4000
strbnd   406   403   410    14.4000   14.4000
strbnd   405   404   408    14.4000   14.4000
strbnd   408   404   408    14.4000   14.4000
strbnd   72   407   401    38.0000   38.0000
strbnd   403   405   404    38.0000   38.0000
```

```
strbnd   401   406   403    38.0000   38.0000
torsion 73 72 407 401 0.000 0.0 1 0.000 180.0 2 0.120 0.0 3
torsion 406 401 407 72 0.525 0.0 1 4.208 180.0 2 0.158 0.0 3
torsion 409 401 407 72 -11.673 0.0 1 6.705 180.0 2 0.158 0.0 3
torsion 407 401 406 403 -0.379 0.0 1 -1.596 180.0 2 -6.626 0.0 3
torsion 409 401 406 403 -6.626 0.0 1 -0.432 180.0 2 3.794 0.0 3
torsion 406 403 405 404 -3.253 0.0 1 -2.994 180.0 2 -3.649 0.0 3
torsion 410 403 405 404 3.279 0.0 1 -1.944 180.0 2 3.037 0.0 3
torsion 405 403 406 401 1.225 0.0 1 -2.189 180.0 2 3.859 0.0 3
torsion 410 403 406 401 3.859 0.0 1 -0.220 180.0 2 -1.321 0.0 3
torsion 408 404 405 403 .382 0.0 1 -1.372 180.0 2 .068 0.0 3
torsion 68 66 72 407 -0.401 0.0 1 0.496 180.0 2 2.714 0.0 3
torsion 65 66 72 407 1.333 0.0 1 -1.311 180.0 2 0.000 0.0 3
torsion 67 66 72 407 0.000 0.0 1 0.287 180.0 2 0.132 0.0 3
torsion 66 72 407 401 0.000 0.0 1 1.905 180.0 2 0.000 0.0 3

#
# Multipoles from Electrostatic Potential Fitting
#

multipole   404  405                1.60022
                          0.00000    0.00000    0.22280
                          0.27904
                          0.00000    0.27904
                          0.00000    0.00000   -0.55808
multipole   408  404 -408 -408        -1.02112
                          0.00000    0.00000    0.11041
                         -0.20638
                          0.00000   -0.29000
                          0.00000    0.00000    0.49638
multipole   405  403  404            -0.73555
                          0.48552    0.00000   -0.09244
                          0.59026
                          0.00000   -0.08287
                          1.35291    0.00000   -0.50739
multipole   403 -410 -410             1.64959
                          0.00000    0.00000   -0.26487
                          0.95916
                          0.00000   -0.92206
                          0.00000    0.00000   -0.03710
multipole   410  403  410            -0.97735
                          0.00000    0.00000    0.07418
                         -0.14364
                          0.00000   -0.51008
                          0.00000    0.00000    0.65372
multipole   406  401  403            -0.73113
```

0.29809 0.00000 -0.10896
0.66145
0.00000 0.08311
0.52910 0.00000 -0.74456
multipole 401 -409 -409 1.65884
0.00000 0.00000 -0.30292
0.77144
0.00000 -0.41605
0.00000 0.00000 -0.35539
multipole 409 401 409 -0.98257
0.00000 0.00000 0.12194
-0.35377
0.00000 -0.11545
0.00000 0.00000 0.46922
multipole 407 324 401 -0.60147
0.17299 0.00000 0.34916
-0.13358
0.00000 -0.86869
0.21469 0.00000 1.00227
multipole 324 325 312 0.17022
0.22509 0.00000 0.15573
0.14095
0.00000 -0.15079
-0.04366 0.00000 0.00984
multipole 325 324 407 0.01769
0.10096 0.00000 -0.12374
0.55605
0.00000 -0.17489
0.05740 0.00000 -0.38116

GTP^{-3} Structure

45

1	P	-5.540894	-2.476544	0.935961	401	2	3	4	5
2	O	-6.861833	-2.485729	0.202682	412	1			
3	O	-5.490706	-2.947508	2.371120	412	1			
4	O	-4.395307	-3.266157	0.004157	408	1	33		
5	O	-4.807339	-0.965096	0.880930	407	1	6		
6	P	-5.048962	0.124172	-0.347093	402	5	7	8	9
7	O	-4.847121	-0.622724	-1.648402	411	6			
8	O	-6.204094	1.052731	-0.099304	411	6			
9	O	-3.608705	0.984658	0.023002	406	6	10		
10	P	-2.711984	2.079291	-0.751043	403	9	11	12	13
11	O	-2.284626	1.714392	-2.153653	409	10			
12	O	-3.083909	3.510161	-0.423095	409	10			
13	O	-1.298135	1.762225	0.235783	405	10	14		
14	C	-0.220959	2.497713	-0.244134	324	13	15	34	35
15	C	0.991808	2.219005	0.610436	312	14	16	17	36

16	O	1.382109	0.816013	0.419709	311	15	21		
17	C	2.225962	3.057740	0.238800	318	15	18	19	37
18	O	2.651966	3.810189	1.378513	346	17	38		
19	C	3.289658	2.010105	-0.107378	316	17	20	21	39
20	O	4.593383	2.422178	0.312880	320	19	40		
21	C	2.757942	0.749056	0.584919	314	16	19	22	41
22	N	3.228439	-0.477792	-0.049786	280	21	23	32	
23	C	2.635507	-1.195311	-1.066458	276	22	24	42	
24	N	3.435076	-2.137914	-1.563918	282	23	25		
25	C	4.603822	-1.994379	-0.858715	279	24	26	32	
26	C	5.854025	-2.693648	-0.978197	274	25	27	28	
27	O	6.220327	-3.608007	-1.712442	285	26			
28	N	6.790790	-2.148241	-0.033973	277	26	29	43	
29	C	6.590949	-1.092805	0.815082	273	28	30	31	
30	N	7.709282	-0.681883	1.552398	278	29	44	45	
31	N	5.459231	-0.445573	0.914887	283	29	32		
32	C	4.503342	-0.948007	0.063415	275	22	25	31	
33	H	-4.306869	-2.643408	-0.754297	413	4			
34	H	0.020980	2.251043	-1.292572	325	14			
35	H	-0.410687	3.587465	-0.198021	325	14			
36	H	0.759887	2.368135	1.670843	313	15			
37	H	2.022912	3.728870	-0.605793	319	17			
38	H	3.627401	3.796055	1.324187	323	18			
39	H	3.283165	1.810448	-1.188570	317	19			
40	H	5.054700	1.621882	0.636914	321	20			
41	H	3.080241	0.721297	1.641519	315	21			
42	H	1.605012	-1.011367	-1.347431	286	23			
43	H	7.726966	-2.531700	-0.133144	284	28			
44	H	8.168209	-1.454544	2.028802	287	30			
45	H	7.415550	0.016447	2.231251	287	30			

GTP^{-3} Parameters

atom	412	412	O	"GTP_-3_firstopt "	8	15.999	1
atom	408	408	O	"GTP_-3_firstopt "	8	15.999	2
atom	411	411	O	"GTP_-3_firstopt "	8	15.999	1
atom	407	407	O	"GTP_-3_firstopt "	8	15.999	2
atom	409	409	O	"GTP_-3_firstopt "	8	15.999	1
atom	406	406	O	"GTP_-3_firstopt "	8	15.999	2
atom	405	405	O	"GTP_-3_firstopt "	8	15.999	2
atom	401	401	P	"GTP_-3_firstopt "	15	30.974	4
atom	402	402	P	"GTP_-3_firstopt "	15	30.974	4
atom	403	403	P	"GTP_-3_firstopt "	15	30.974	4
atom	413	413	H	"GTP_-3_firstopt "	1	1.008	1

```
polarize    412         0.8370     0.3900 401
polarize    408         0.8370     0.3900 401 413
polarize    411         0.8370     0.3900 402
polarize    407         0.8370     0.3900 401 402
polarize    409         0.8370     0.3900 403
polarize    406         0.8370     0.3900 402 403
polarize    405         0.8370     0.3900 72 403
polarize    401         1.8280     0.3900 412 408 407
polarize    402         1.8280     0.3900 411 407 406
polarize    403         1.8280     0.3900 409 406 405
polarize    413         0.4960     0.3900 408


vdw      403  4.4500   0.3900
vdw      402  4.4500   0.3900
vdw      401  4.4500   0.3900
vdw      405  3.4050   0.1100
vdw      407  3.635    0.134
vdw      408  3.62     0.08
vdw      406  3.635    0.134
vdw      428  2.8700   0.0240 0.910
vdw      412  3.635    0.08
vdw      411  3.6300   0.1120
vdw      409  3.6300   0.1120
vdw      413  2.6650   0.0150 0.910
bond     72   405   465.1000    1.4179
bond     403   405   450.0000    1.7075
bond     403   406   450.0000    1.6660
bond     403   409   775.0000    1.5074
bond     402   407   450.0000    1.6482
bond     402   406   450.0000    1.6612
bond     402   411   775.0000    1.5184
bond     401   407   450.0000    1.6772
bond     401   408   450.0000    1.6485
bond     401   412   775.0000    1.5282
bond     408   413   560.0000    0.9995
angle    405   403   406    65.5800  100.0875
angle    405   403   409    75.8600  106.3537
angle    406   403   409    75.8600  111.8154
angle    409   403   409    89.8800  123.8772
angle    407   402   406    65.5800   98.2091
angle    407   402   411    75.8600  108.5940
angle    406   402   411    75.8600  112.2672
angle    411   402   411    89.8800  119.9765
```

```
angle    407   401   408    65.5800  100.2188
angle    407   401   412    75.8600  111.5471
angle    408   401   412    75.8600  111.6206
angle    412   401   412    89.8800  119.1585
angle    72   405   403    80.3000  112.3553
angle    402   407   401    80.0000  129.7663
angle    401   408   413    60.0000  104.8737
angle    403   406   402    80.0000  134.3005
angle    66   72   405    88.0000  109.4043
angle    405   72   73    60.9900  110.9434
strbnd   405   403   406    14.4000   14.4000
strbnd   405   403   409    14.4000   14.4000
strbnd   406   403   409    14.4000   14.4000
strbnd   407   402   406    14.4000   14.4000
strbnd   407   402   411    14.4000   14.4000
strbnd   406   402   411    14.4000   14.4000
strbnd   407   401   408    14.4000   14.4000
strbnd   407   401   412    14.4000   14.4000
strbnd   408   401   412    14.4000   14.4000
strbnd   72   405   403    38.0000   38.0000
strbnd   402   407   401    38.0000   38.0000
strbnd   401   408   413    -4.5000   38.0000
strbnd   403   406   402    38.0000   38.0000
torsion 73 72 405 403 2 0.0 1 -1.5 180.0 2 .89 0.0 3
torsion 406 403 405 72 4.724 0.0 1 5.303 180.0 2 4.659 0.0 3
torsion 409 403 405 72 -2.155 0.0 1 7.602 180.0 2 -1.328 0.0 3
torsion 405 403 406 402 -1.99 0.0 1 3.795 180.0 2 -6.694 0.0 3
torsion 409 403 406 402 3.246 0.0 1 2.053 180.0 2 3.735 0.0 3
torsion 406 402 407 401 -.277 0.0 1 -.298 180.0 2 -7.506 0.0 3
torsion 411 402 407 401 -3.095 0.0 1 .326 180.0 2 1.844 0.0 3
torsion 407 402 406 403 2.034 0.0 1 4.705 180.0 2 2.705 0.0 3
torsion 411 402 406 403 1.043 0.0 1 2.635 180.0 2 -1.284 0.0 3
torsion 408 401 407 402 7.143 0.0 1 -7.143 180.0 2 -7.143 0.0 3
torsion 412 401 407 402 5.684 0.0 1 -6.188 180.0 2 4.883 0.0 3
torsion 407 401 408 413 -2 0.0 1 -1.68 180.0 2 -.8 0.0 3
torsion 412 401 408 413 -2 0.0 1 -1.68 180.0 2 -.8 0.0 3
torsion   68   66   72   405    -1.1500 0.0 1     0.0000 180.0 2     1.2800 0.0 3
torsion   65   66   72   405     2.2200 0.0 1    -1.3800 180.0 2    -1.1800 0.0 3
torsion   67   66   72   405     0.0000 0.0 1     0.0000 180.0 2     0.3000 0.0 3
torsion   66   72   405   403     0.0000 0.0 1     0.0000 180.0 2     0.0000 0.0 3
torsion   402   403   416   438    -1.3720 0.0 1     0.2320 180.0 2     0.4000 0.0 3

#
# Multipoles from Electrostatic Potential Fitting
#
```

```
multipole   401 -412 -412            1.66729
                      0.00000   0.00000   -0.02156
                      0.31821
                      0.00000   -0.04624
                      0.00000   0.00000   -0.27197
multipole   412  401  412           -0.98202
                      0.00000   0.00000   -0.04252
                     -0.08067
                      0.00000   -0.11299
                      0.00000   0.00000    0.19366
multipole   408  401  413           -0.68650
                      0.24867   0.00000   -0.04616
                      0.57372
                      0.00000   -0.21081
                      0.30596   0.00000   -0.36291
multipole   407  402  401           -0.66684
                      0.13752   0.00000   -0.08868
                      0.16424
                      0.00000   -0.07683
                      0.26947   0.00000   -0.08741
multipole   402 -411 -411            1.64139
                      0.00000   0.00000   -0.00728
                      0.47720
                      0.00000   -0.51282
                      0.00000   0.00000    0.03562
multipole   411  402  411           -0.95382
                      0.00000   0.00000   -0.00361
                     -0.26137
                      0.00000   0.02643
                      0.00000   0.00000    0.23494
multipole   406  403  402           -0.67371
                      0.25954   0.00000   -0.09612
                     -0.52564
                      0.00000   -0.14680
                     -0.33224   0.00000    0.67244
multipole   403 -409 -409            1.63400
                      0.00000   0.00000   -0.33789
                      0.37356
                      0.00000   -0.39914
                      0.00000   0.00000    0.02558
multipole   409  403  409           -0.95177
                      0.00000   0.00000    0.03720
                     -0.41530
                      0.00000   0.09618
                      0.00000   0.00000    0.31912
multipole   405  324  403           -0.51104
```

0.14169 0.00000 0.39243
-0.28900
0.00000 -0.83742
0.35181 0.00000 1.12642
multipole 324 312 405 0.17988
0.15120 0.00000 0.02414
0.55333
0.00000 -0.20878
0.33591 0.00000 -0.34455
multipole 413 408 401 0.25366
-0.00152 0.00000 -0.13290
0.26419
0.00000 -0.29795
0.20254 0.00000 0.03376
0.00000 0.00000 0.00000
0.00000
0.00000 0.00000
0.00000 0.00000 0.00000

GDP^{-3} Structure

40

1	P	-5.930700	-1.549300	0.411700	404	2	3	4	5
2	O	-7.024500	-0.870300	-0.415600	408	1			
3	O	-6.147400	-1.605700	1.928800	408	1			
4	O	-5.251800	-2.771900	-0.210000	408	1			
5	O	-4.524300	-0.235600	0.388100	406	1	6		
6	P	-3.866200	0.766500	-0.614200	401	5	7	8	9
7	O	-3.348800	0.231600	-1.943800	409	6			
8	O	-4.395000	2.198200	-0.594100	409	6			
9	O	-2.313900	0.959000	0.325400	407	6	10		
10	C	-1.452600	1.742700	-0.407700	324	9	11	29	30
11	C	-0.151300	1.924800	0.340800	312	10	12	13	31
12	O	0.532600	0.618600	0.426500	311	11	17		
13	C	0.841200	2.871800	-0.350500	318	11	14	15	32
14	O	1.172700	3.950800	0.534300	346	13	33		
15	C	2.084900	2.005500	-0.573100	316	13	16	17	34
16	O	3.299000	2.751600	-0.418400	320	15	35		
17	C	1.892000	0.871600	0.442000	314	12	15	18	36
18	N	2.580900	-0.357200	0.050200	280	17	19	28	
19	C	2.089600	-1.400000	-0.703100	276	18	20	37	
20	N	3.035000	-2.276200	-1.046300	282	19	21		
21	C	4.187500	-1.751000	-0.518000	279	20	22	28	
22	C	5.543900	-2.218600	-0.596300	274	21	23	24	
23	O	6.046800	-3.207900	-1.125800	285	22			
24	N	6.402700	-1.291600	0.087500	277	22	25	38	
25	C	6.040200	-0.112200	0.682300	273	24	26	27	

26	N	7.095300	0.666300	1.182700	278	25	39	40
27	N	4.808900	0.319800	0.748500	283	25	28	
28	C	3.927700	-0.542500	0.138900	275	18	21	27
29	H	-1.218700	1.315900	-1.402600	325	10		
30	H	-1.854900	2.762600	-0.589000	325	10		
31	H	-0.335000	2.272300	1.363600	313	11		
32	H	0.436900	3.261900	-1.292900	319	13		
33	H	2.112800	4.134300	0.345000	323	14		
34	H	2.048200	1.548900	-1.572600	317	15		
35	H	3.934100	2.166200	0.039800	321	16		
36	H	2.287000	1.167300	1.432200	315	17		
37	H	1.029000	-1.477200	-0.915200	286	19		
38	H	7.390400	-1.504600	-0.022500	284	24		
39	H	7.705600	0.137200	1.801400	287	26		
40	H	6.701200	1.457400	1.686800	287	26		

GDP^{-3} Parameters

atom	408	408	O	"GDP_-3_	"	8	15.999	1
atom	409	409	O	"GDP_-3_	"	8	15.999	1
atom	406	406	O	"GDP_-3_	"	8	15.999	2
atom	407	407	O	"GDP_-3_	"	8	15.999	2
atom	404	404	P	"GDP_-3_	"	15	30.974	4
atom	401	401	P	"GDP_-3_	"	15	30.974	4

polarize	72	1.3340	0.3900 407 73
polarize	408	0.8370	0.3900 404
polarize	409	0.8370	0.3900 401
polarize	406	0.8370	0.3900 404 401
polarize	407	0.8370	0.3900 72 401
polarize	404	1.8280	0.3900 408 406
polarize	401	1.8280	0.3900 409 406 407

vdw	401	4.4500	0.3900
vdw	404	4.4500	0.3900
vdw	407	3.635	0.134
vdw	406	3.635	0.134
vdw	408	3.63	0.1120
vdw	409	3.5534	0.09315
bond	72	407	465.1000 1.4275
bond	401	407	450.0000 1.7314
bond	401	406	450.0000 1.6162
bond	401	409	775.0000 1.5175

```
bond      404   406   450.0000    1.7544
bond      404   406   450.0000    1.8298
bond      404   408   775.0000    1.5499
angle     407   401   406    65.5800  100.2307
angle     407   401   409    75.8600  107.2560
angle     406   401   409    75.8600  113.6954
angle     409   401   409    89.8800  119.3235
angle     406   404   408    75.8600  104.7369
angle     408   404   408    89.8800  115.7929
angle     72   407   401    80.3000  115.0537
angle     401   406   404    80.0000  137.3775
angle     66   72   407    88.0000  111.5292
angle     407   72   73    60.9900  113.1077
angle     407   72   73    60.9900  113.1077
strbnd    407   401   406    14.4000   14.4000
strbnd    407   401   409    14.4000   14.4000
strbnd    406   401   409    14.4000   14.4000
strbnd    406   404   408    14.4000   14.4000
strbnd    408   404   408    14.4000   14.4000
strbnd    72   407   401    38.0000   38.0000
strbnd    401   406   404    38.0000   38.0000
torsion 73 72 407 401 2 0.0 1 -1.5 180.0 2 .89 0.0 3
torsion 406 401 407 72 .292 0.0 1 9.634 180.0 2 -5 0.0 3
torsion 409 401 407 72 -10.912 0.0 1 10.912 180.0 2 2.516 0.0 3
torsion 407 401 406 404 -.969 0.0 1 3.663 180.0 2 3.663 0.0 3
torsion 409 401 406 404 3.279 0.0 1 -1.944 180.0 2 3.037 0.0 3
torsion 408 404 406 401 1.616 0.0 1 -1.616 180.0 2 .084 0.0 3
torsion 68 66 72 407 -0.401 0.0 1 0.496 180.0 2 2.714 0.0 3
torsion 65 66 72 407 1.333 0.0 1 -1.311 180.0 2 0.000 0.0 3
torsion 67 66 72 407 0.000 0.0 1 0.287 180.0 2 0.132 0.0 3
torsion 66 72 407 401 0.000 0.0 1 1.905 180.0 2 0.000 0.0 3


#
# Multipoles from Electrostatic Potential Fitting
#

multipole   404  406                1.60022
                           0.00000    0.00000    0.34417
                           0.24651
                           0.00000    0.24651
                           0.00000    0.00000   -0.49302
multipole   408  404 -408 -408        -1.02112
                           0.00000    0.00000    0.24711
                          -0.59760
                           0.00000   -0.38019
```

```
                          0.00000    0.00000    0.97779
multipole   406  401  404           -0.73113
                          1.03362    0.00000    0.03187
                          2.69650
                          0.00000   -0.05699
                          2.29507    0.00000   -2.63951
multipole   401 -409 -409            1.65884
                          0.00000    0.00000   -0.53976
                         -0.32644
                          0.00000   -2.11350
                          0.00000    0.00000    2.43994
multipole   409  401  409           -0.98257
                          0.00000    0.00000    0.26499
                         -0.14597
                          0.00000   -1.44931
                          0.00000    0.00000    1.59528
multipole   407  324  401           -0.62180
                          0.06613    0.00000    0.47703
                         -0.70331
                          0.00000    1.63463
                          1.14095    0.00000   -0.93132
multipole   324  325  312            0.14989
                          0.38186    0.00000   -0.02317
                         -0.66972
                          0.00000    0.00384
                         -0.00621    0.00000    0.66588
multipole   325  324  407            0.01769
                         -0.12813    0.00000   -0.23366
                          0.29858
                          0.00000   -0.08976
                         -0.55398    0.00000   -0.20882
```

GDP^{-2} Structure

```
   41
    1  P    -5.682200   -1.393300    0.451100   401    2    3    4    5
    2  O    -6.562900   -0.855200   -0.645600   412    1
    3  O    -6.238400   -1.768300    1.796700   412    1
    4  O    -4.724100   -2.617900   -0.157300   408    1   29
    5  O    -4.405600   -0.301200    0.736900   406    1    6
    6  P    -3.849600    0.703500   -0.417400   403    5    7    8    9
    7  O    -3.500400   -0.084900   -1.666800   409    6
    8  O    -4.492100    2.063800   -0.473400   409    6
    9  O    -2.338600    0.944500    0.402400   405    6   10
   10  C    -1.484200    1.721300   -0.383900   324    9   11   30   31
   11  C    -0.180200    1.915500    0.349500   312   10   12   13   32
   12  O     0.484200    0.615100    0.466100   311   11   17
```

13	C	0.812400	2.843300	-0.369400	318	11	14	15	33
14	O	1.138500	3.933200	0.493900	346	13	34		
15	C	2.050000	1.962000	-0.575200	316	13	16	17	35
16	O	3.253600	2.715700	-0.434500	320	15	36		
17	C	1.855200	0.857400	0.470300	314	12	15	18	37
18	N	2.525100	-0.386300	0.114200	280	17	19	28	
19	C	2.024100	-1.451000	-0.603300	276	18	20	38	
20	N	2.962200	-2.335300	-0.935000	282	19	21		
21	C	4.124000	-1.791200	-0.444700	279	20	22	28	
22	C	5.480600	-2.260500	-0.534000	274	21	23	24	
23	O	5.968400	-3.268700	-1.035700	285	22			
24	N	6.351300	-1.304800	0.094000	277	22	25	39	
25	C	5.999500	-0.105100	0.652500	273	24	26	27	
26	N	7.053500	0.701600	1.085500	278	25	40	41	
27	N	4.765300	0.324200	0.732500	283	25	28		
28	C	3.876600	-0.566900	0.180300	275	18	21	27	
29	H	-4.220100	-2.155600	-0.862800	413	4			
30	H	-1.278100	1.247800	-1.358500	325	10			
31	H	-1.909100	2.721300	-0.581500	325	10			
32	H	-0.362200	2.301900	1.358500	313	11			
33	H	0.412600	3.215200	-1.321900	319	13			
34	H	2.081600	4.114100	0.313500	323	14			
35	H	2.009400	1.480900	-1.563400	317	15			
36	H	3.915400	2.128300	-0.015100	321	16			
37	H	2.244900	1.180100	1.451600	315	17			
38	H	0.962100	-1.539200	-0.796100	286	19			
39	H	7.336800	-1.526200	-0.023100	284	24			
40	H	7.745200	0.201400	1.637000	287	26			
41	H	6.685200	1.491800	1.608100	287	26			

GDP^{-2} Parameters

atom	412	412	O	"GDP_-2_firstopt "	8	15.999	1
atom	408	408	O	"GDP_-2_firstopt "	8	15.999	2
atom	409	409	O	"GDP_-2_firstopt "	8	15.999	1
atom	406	406	O	"GDP_-2_firstopt "	8	15.999	2
atom	405	405	O	"GDP_-2_firstopt "	8	15.999	2
atom	401	401	P	"GDP_-2_firstopt "	15	30.974	4
atom	403	403	P	"GDP_-2_firstopt "	15	30.974	4
atom	413	413	H	"GDP_-2_firstopt "	1	1.008	1

polarize	412	0.8370	0.3900 401
polarize	408	0.8370	0.3900 401 413

```
polarize    411         0.8370     0.3900 402
polarize    409         0.8370     0.3900 403
polarize    406         0.8370     0.3900 401 403
polarize    405         0.8370     0.3900 72 403
polarize    401         1.8280     0.3900 412 408 406
polarize    403         1.8280     0.3900 409 406 405
polarize    413         0.4960     0.3900 408


vdw      403  4.4500   0.3900
vdw      401  4.4500   0.3900
vdw      405  3.635    0.134
vdw      408  3.62     0.08
vdw      406  3.635    0.134
vdw      412  3.635    0.08
vdw      409  3.5534   0.09315
vdw      413  2.6650   0.0150 0.910
bond     72   405   465.1000    1.4179
bond     403   405   450.0000    1.7075
bond     403   406   450.0000    1.6660
bond     403   409   775.0000    1.5074
bond     401   406   450.0000    1.6772
bond     401   408   450.0000    1.6485
bond     401   412   775.0000    1.5282
bond     408   413   560.0000    0.9995
angle    405   403   406    65.5800  100.0875
angle    405   403   409    75.8600  106.3537
angle    406   403   409    75.8600  111.8154
angle    409   403   409    89.8800  123.8772
angle    406   401   408    65.5800  100.2188
angle    406   401   412    75.8600  111.5471
angle    408   401   412    75.8600  111.6206
angle    412   401   412    89.8800  119.1585
angle    72   405   403    80.3000  112.3553
angle    403   406   401    80.0000  129.7663
angle    401   408   413    60.0000  104.8737
angle    66   72   405    88.0000  109.4043
angle    405   72   73    60.9900  110.9434
strbnd   405   403   406    14.4000   14.4000
strbnd   405   403   409    14.4000   14.4000
strbnd   406   403   409    14.4000   14.4000
strbnd   406   401   408    14.4000   14.4000
strbnd   406   401   412    14.4000   14.4000
strbnd   408   401   412    14.4000   14.4000
strbnd   72   405   403    38.0000   38.0000
strbnd   403   406   401    38.0000   38.0000
```

```
strbnd   401   408   413    -4.5000   38.0000
torsion 73 72 405 403 2 0.0 1 -1.5 180.0 2 .89 0.0 3
torsion 406 403 405 72 .08 0.0 1 -.327 180.0 2 1.533 0.0 3
torsion 409 403 405 72 .916 0.0 1 2.304 180.0 2 .5 0.0 3
torsion 405 403 406 401 6.659 0.0 1 -5.588 180.0 2 8.161 0.0 3
torsion 409 403 406 401 8.161 0.0 1 -.194 180.0 2 -4.292 0.0 3
torsion 408 401 406 403 7.269 0.0 1 -7.269 180.0 2 -7.269 0.0 3
torsion 412 401 406 403 .971 0.0 1 -3.343 180.0 2 -2.304 0.0 3
torsion 406 401 408 413 3.028 0.0 1 -5.116 180.0 2 5.116 0.0 3
torsion 412 401 408 413 -2 0.0 1 -1.68 180.0 2 -.8 0.0 3
torsion   68   66   72   405    -1.1500 0.0 1     0.0000 180.0 2     1.2800 0.0 3
torsion   65   66   72   405     2.2200 0.0 1    -1.3800 180.0 2    -1.1800 0.0 3
torsion   67   66   72   405     0.0000 0.0 1     0.0000 180.0 2     0.3000 0.0 3
torsion   66   72   405   403     0.0000 0.0 1     0.0000 180.0 2     0.0000 0.0 3

#
# Multipoles from Electrostatic Potential Fitting
#

multipole   401 -412 -412             1.66729
                          0.00000    0.00000   -0.07441
                          0.43613
                          0.00000    0.09217
                          0.00000    0.00000   -0.52830
multipole   412  401  412            -0.98202
                          0.00000    0.00000    0.00678
                         -0.14913
                          0.00000   -0.31810
                          0.00000    0.00000    0.46723
multipole   408  401  413            -0.68650
                          0.19187    0.00000   -0.04350
                          0.74235
                          0.00000   -0.18846
                         -0.13268    0.00000   -0.55389
multipole   406  403  401            -0.67371
                          0.19282    0.00000    0.01367
                         -0.28507
                          0.00000   -0.31691
                          0.02031    0.00000    0.60198
multipole   403 -409 -409             1.63400
                          0.00000    0.00000   -0.22214
                          0.33897
                          0.00000   -0.41182
                          0.00000    0.00000    0.07285
multipole   409  403  409            -0.95177
                          0.00000    0.00000   -0.03764
```

```
                    -0.30810
                     0.00000   0.24380
                     0.00000   0.00000   0.06430
multipole   405  324  403       -0.49528
                     0.20708   0.00000   0.42530
                    -0.20338
                     0.00000  -0.94027
                    -0.09808   0.00000   1.14365
multipole   324  312  405        0.19565
                     0.13090   0.00000   0.07537
                     0.15806
                     0.00000  -1.06997
                    -0.16138   0.00000   0.91191
multipole   413  408  401        0.25366
                    -0.01269   0.00000  -0.06646
                     0.63900
                     0.00000  -0.13233
                    -0.12115   0.00000  -0.50667
multipole   325  324  405        0.01769
                     0.10197   0.00000  -0.15897
                     0.40059
                     0.00000  -0.21453
                    -0.01118   0.00000  -0.18606
```


1. Wu, J. C.;Chattree, G.Ren, P., Automation of amoeba polarizable force field parameterization for small molecules. Theor Chem Acc **2012,** 131 (3), 1138.
2. Altona, C.Sundaralingam, M., Conformational analysis of the sugar ring in nucleosides and nucleotides. Improved method for the interpretation of proton magnetic resonance coupling constants. J Am Chem Soc **1973,** 95 (7), 2333-44.
3. Kobayashi, E.;Yura, K.Nagai, Y., Distinct conformation of atp molecule in solution and on protein. Biophysics (Nagoya-shi) **2013,** 9, 1-12.
4. Hamelberg, D.McCammon, J. A., Standard free energy of releasing a localized water molecule from the binding pockets of proteins: Double-decoupling method. Journal of the American Chemical Society **2004,** 126 (24), 7683-7689.
5. Swartz, M. A.;Tubergen, P. J.;Tatko, C. D.Baker, R. A., Experimental determination of pk(a) values and metal binding for biomolecular compounds using p-31 nmr spectroscopy. J Chem Educ **2018,** 95 (1), 182-185.